CERAMIC LUBRICATION: VAPOR PHASE TRIBOPOLYMERIZATION AND A NEW HIGH SPEED, HIGH LOAD PIN-ON-DISK MACHINE

By

J. Christopher Smith

Thesis submitted to the Faculty of the

Virginia Polytechnic Institute and State University

in partial fulfillment of the requirements for the degree of

MASTER OF SCIENCE
in
Mechanical Engineering

APPROVED:

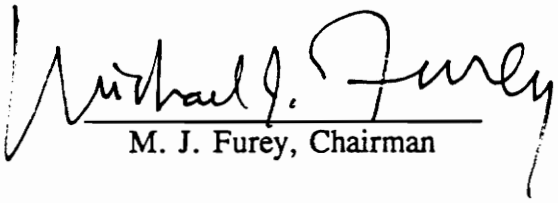

M. J. Furey, Chairman

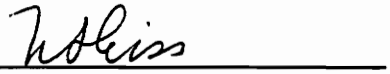

N. S. Eiss

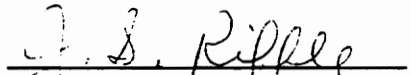

J. S. Riffle

February, 1994

Blacksburg, Virginia

CERAMIC LUBRICATION: VAPOR PHASE TRIBOPOLYMERIZATION AND A NEW HIGH SPEED, HIGH LOAD PIN-ON-DISK MACHINE

By
J. Christopher Smith
M. J. Furey, Chairman
Mechanical Engineering Program

(ABSTRACT)

An experimental study of ceramic lubrication through the concept of tribopolymerization from the vapor phase is presented. Four vinyl monomer additives were studied, i.e., vinyl acetate, diallyl phthalate, lauryl methacrylate, and vinyl octadecyl ether. The liquid additives were heated, vaporized, and delivered to an enclosed alumina-on-alumina "pin-on-disk" contact region by a stream of dry nitrogen gas.

Alumina ball wear reductions of up to 99% were observed and total wear reductions (ball and disk) of over 70% were also common. Colorful surface films visible to the naked eye were examined. Monomer concentration does not appear to have an effect over the range examined. But, higher monomer delivery temperatures have a significant beneficial effect in reducing wear. Selective FTIRM analysis shows evidence of both polymerization and monomer reactions with the alumina surface. It is believed that the surface films formed reduce adhesion and therefore decrease both wear and friction.

The development, design, and construction of a high load, high speed, high frictional heat generation pin-on-disk machine is presented. A very successful geometry has been created and recommendations for added instrumentation and its future use for both liquid and vapor phase tests are presented.

ACKNOWLEDGEMENTS

The author is grateful and wishes to express his sincere thanks to Dr. Michael J. Furey for his tremendous guidance and encouragement throughout this project. He allowed me to make mistakes and learn from them. His continued confidence in me has helped to make this project a success. Thanks are also in order for the members of my committee, Drs. Norman S. Eiss and Judy S. Riffle for their advice and assistance. Sincere gratitude is also extended to the National Science Foundation for the support of this research effort.

A special thanks is in order for Mr. Bhawani Tripathy for his tremendous insight, knowledge, and aid with SEM and FTIRM surface analytical techniques. The success of this project is due in part to his advice and suggestions.

In addition, I would like to thank the following individuals whose technical assistance, guidance, and advice are greatly appreciated:

- Dr. Czeslaw Kajdas whose insight, in part, provided the original direction of the vapor phase tribopolymerization portion of this project. His help in interpreting FTIRM spectra has been invaluable.
- Dr. A. L. Wicks for his technical assistance in the instrumentation of the new high frictional heat generation pin-on-disk apparatus.
- Dr. Roman Kempinski for his added insight and encouragement.
- Mr. Dan Hahn for his aid in performing important FTIRM analysis.
- Mr. John Cox, Mr. Jerry Lucas, and Mr. Tim Kessinger for their help in the construction of the new pin-on-disk apparatus in all of its design stages.

Finally, I would like to thank my family, especially my parents and my brother Griffin, for their love, patience, understanding, and support for the duration of this study.

TABLE OF CONTENTS

LIST OF ILLUSTRATIONS

LIST OF TABLES

1.0 INTRODUCTION

1.1 Rationale for this Study

Tribology (from the Greek "tribo", to rub) is the study of friction, wear, and lubrication [1]. Its practical importance to the science of engineering and dynamic systems is paramount. Advances in the study can reduce energy requirements, increase equipment lifetime, add increased reliability, and limit the necessity of maintenance and repairs in dynamic machinery.

Boundary lubrication is perhaps the most severe of all tribological contacts and is often experienced in practice. When reduced lubricant viscosities, low speeds, or high loads cause the breakdown of a protective hydrodynamic film, substrates come into direct contact. It is a condition in which thin films separate rubbing surfaces and is characterized by high friction, high wear, and extreme surface damage. The dominant

factor in boundary lubrication is the chemistry of the tribological system -- the contacting solids and total environment, including lubricants [2].

In recent years, an increased interest in ceramic materials for use in tribological applications has emerged. Ceramics can be used at much higher temperatures than metals, are relatively inert and resist corrosion, and are resistant to abrasive wear due to their high hardness. The low density of most ceramics compared to metals also promises energy conservation through savings in weight and inertial loads.

Applications for ceramics in industry include: ceramic engines and engine components for higher temperature operation and greater thermodynamic efficiency; advanced propulsion systems, turbomachinery, gas turbines, and aerospace bearings; cutting tools for superalloys; biomedical applications such as artificial joints; and other tribological systems requiring high temperature operation or service in abrasive or corrosive environments [3].

Conventional methods of lubrication for ceramics are limited and often ineffective. A literature/patent survey of over 150 references revealed four major categories [3]:

- Incorporation of various materials (e.g., polymers, solid lubricants) into the ceramic. [The added components can degrade the high-temperature performance of the ceramic.]

- Surface treatments and coatings (e.g., ion implantation, metallic films). [Coatings or surface films are themselves removed by wear, thus providing limited protection.]
- Dispersed solid lubricants (e.g., graphite, MoS_2) in a fluid. [This can lead to problems such as settling or filter plugging; in addition, high concentrations are often required.]
- Conventional lubricants containing soluble anti-wear additives in a carrier fluid (e.g., mineral or synthetic oils). [Since many conventional anti-wear or anti-friction additives function by chemically reacting with a metal such as steel to form a surface layer, these compounds would not be expected to act with a relatively non-reactive substrate (e.g., a ceramic).]

It is obvious that new and innovative methods of ceramic lubrication need to be explored. Effective boundary lubrication of ceramic materials will be a necessity in the development of high performance dynamic machinery in the future.

1.2 Objectives of this Study

The concept of tribopolymerization provides such a possibility. Tribopolymerization is described as the planned and intentional formation of protective

polymeric films directly and continuously on surfaces in tribological contact to reduce damage and wear [4,5]. Polymer-forming monomers can be introduced to a contact region through a variety of different carrier fluids and can reduce wear under the severe conditions of boundary lubrication. This study explores new methods of monomer delivery and develops new and more severe experimental conditions for testing the concept in the boundary lubrication of ceramics. The objectives of this study are:

1. To carry out exploratory research to test new hypotheses of tribopolymerization as a mechanism of boundary lubrication.
2. To study the vapor phase lubrication of ceramics using selected monomers or tribopolymer formers.
3. To create more realistic test regimes likely to be found in practical applications by developing a high-speed, high-load pin-on-disk machine for lubricated or vapor phase contacts.
4. To conduct basic research on the identification and characterization of surface films formed by selected monomers on ceramic surfaces in pin-on-disk tribological experiments. This includes surface profilometry, Scanning Electron Microscopy (SEM), and Fourier Transform Infrared Microspectrometry (FTIRM).

Within these objectives are two separate but related courses of research. The first is the study of vapor phase tribopolymerization and the second is the development and construction of a new high load, high speed, high frictional heat generation pin-on-disk machine capable of operation under both lubricated and vapor phase conditions. These two objectives were undertaken as parallel courses of study. Each will be presented separately, beginning with vapor phase tribopolymerization and ending with the development of the new pin-on-disk machine.

2.0 LITERATURE REVIEW

2.1 The Concept of Tribopolymerization

Tribopolymerization is described as the planned and intentional formation of protective polymeric films directly and continuously on surfaces in tribological contact to reduce damage and wear. These films are formed *in situ* or actually during the rubbing contact and are formed only in the areas where they are needed. This concept was originally proposed by Furey [4,5] and later expanded upon during collaboration with Kajdas [6,7,8]. The concept states that low concentrations of potential polymer forming materials dissolved in a carrier fluid will form protective polymeric films due to high contact temperatures, the catalytic action of freshly exposed surfaces, and exoelectron emission in regions of greatest contact. The first step in this system may be adsorption of the polymer former on the surface. In dynamic systems, these polymer

films are continuously worn away and then reformed. This built-in control is a function of the mechanism itself. As a film is formed it reduces contact and friction, thus lowering the temperature and minimizing catalytic effects in that region of contact. This slows the formation of the protective film. As this film is worn away, however, the increased contact and friction in the region will again initiate reactions that will form protective layers. The basic mechanism of wear reduction is believed to center on the reduction of adhesion and minimization of surface damaging contacts. The simplified process is shown in Figure 1.

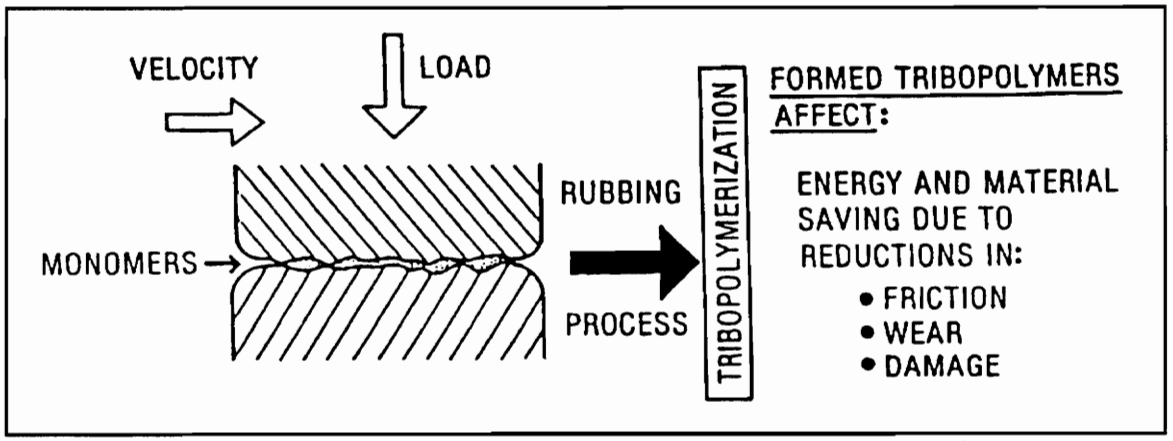

Figure 1 Tribopolymerization as a Method of Boundary Lubrication [6]

A great deal of evidence is available to support the proposed *in situ* mechanism of polymer formation. Such evidence includes the superior effectiveness of polymer forming compounds versus closely related non-polymer formers (i.e., vinyl type monomers versus their saturated relatives) [9]. Indications of localized and adherent surface films have also been found. These tenacious films have a "carry-over" effect and

wear rates remain low when additive-free lubricants replace the original. The films are easily removed by organic solvents. These effects are unique to and characteristic of the tribopolymerization concept. More recent research using FTIRM (Fourier Transform Infrared Microspectrometry) surface analysis techniques has added strong support as well [9,10]. Finally, the overall success of this approach in the selection and design of new classes of compounds for antiwear and antiscuff additives for metals and ceramics illustrates the effectiveness of the technique.

Several studies on the detailed mechanisms and actions governing the concept have been conducted. These include the synthesis of model monoester compounds [11], mechanism studies using radioactive tracers [5,11], the pronounced effects on load carrying capacity of jet fuels in Ryder Gear Tests [5,11], pin-on-disk studies with steel-on-steel systems and relevant FTIRM analysis [6], and the more recent work applying the concept to ceramic lubrication [3,9,10].

One of the earliest illustrations of tribopolymerization was found in the monoester made from a long chain C_{36} dimer acid and ethylene glycol. The monoester is believed to form a protective polyester film as follows:

$$HOOC\text{-}R\text{-}COO\text{-}C_2H_4OH \xrightarrow[Heat\text{-}Catalysis]{Rubbing\ Surfaces} HO[OC\text{-}R\text{-}COO\text{-}C_2H_4O]_nH + H_2O$$

The ability of this compound to reduce wear in a dynamic situation was shown in the Ryder Gear Machine [4]. For each test, the amount of scuffing is plotted as a percent of the tooth area scuffed versus loading pressure. Scuffing in this test is defined

as the amount of scoring, scratching, or abrasion which destroys the axial grinding marks in the teeth. Additions of only 0.1 weight percent of the monoester to a highly refined jet fuel caused an unusually large increase in scuff rating, i.e., from 350 to 5200 N/cm. Similar increases were also recorded for other carrier fluids including JP-4 jet fuel and mineral oils. The original purpose of these experiments was to evaluate additives for use in the reduction of aviation fuel pump wear. Field tests proved that large reductions in wear were indeed realized.

It is also worth noting that neither dimer acid nor glycol alone was as effective as an equimolar mixture of dimer acid/glycol or the monoester in reducing wear. In addition, the carryover effects found for the potential polymer formers did not occur for either the dimer acid or glycol alone. These experiments support the mechanism of tribopolymerization and are evidence of the extreme importance of surface chemistry and film formation in boundary lubrication.

This success led to testing of the monoester in automotive engine valve train wear experiments. Radioactive valve lifters were used to determine continuous wear rates. The results were again successful with 1 wt.% monoester/mineral oil systems showing reductions of up to 90% over mineral oil alone. This reduction is comparable to that seen with zinc dialkyldithiophosphate (ZDDP) additives which have been used for many years to limit valve train wear. A significant difference found between the behavior of the monoester and the common ZDDP additive concerned the carry-over effect. After the initial engine tests, monoester systems provided an additional three to six hours of

low wear rates in non-additive mineral oils. No beneficial carry-over effects were found with ZDDP, dimer acid, or glycol alone.

A more recent paper [6] contains examinations of these surface films using the FTIRM technique. In this study, the films from steel-on-steel experiments with monoester additive were examined. Spectral data acquired in the 1900 to 1500 cm^{-1} range is characteristic of the carbonyl stretching modes for the ester and acid functionalities of the monoester additive. A comparison of the monoester standard spectra versus the wear track spectra showed a difference in the relative levels of ester and polyester on the surface. A higher ester/acid ratio on the surface suggested that polymer formation occurred as a direct result of tribological activity. The detailed FTIRM spectra provided evidence of other reactions such as metal soap formation. Many unidentified peaks suggest that the actual mechanism is much more complex.

An oscillating aluminum-on-steel system was also studied. Contact temperatures are expected to be lower than the already low temperature steel-on-steel system due to the high thermal conductivity of aluminum (approximately three times greater than that of steel). In this system, the dimer acid/glycol monoester (a condensation type monomer) was ineffective in reducing wear. FTIRM showed evidence of metal soap formation, but not polymer formation. Styrene (an addition type monomer) on the other hand, proved to be effective in reducing wear. In addition, FTIRM provided proof of polystyrene formation on the wear tracks. These results support the main hypotheses surrounding tribopolymerization that (a) condensation-type tribopolymerization requires

relatively high surface temperatures (Furey) and (b) addition-type tribopolymerization can be initiated by effects such as exo-electron emission at much lower temperatures (Kajdas) [9,12,13].

2.2 *Tribopolymerization as a Mechanism of Ceramic Lubrication*

Since tribopolymerization is a process of deposition on a solid surface rather than reaction with a surface (as is the case with ZDDP), it appears to be an ideal method for the lubrication of ceramics. With respect to this possibility, many ceramics have high hardness (which leads to a small contact area) and low thermal conductivities. These features combined can create high contact temperatures during sliding. High temperatures are considered conducive to the formation of tribopolymers. In addition, work has shown that aluminum oxide films in atmosphere emit both positively and negatively charged particles when scratched and during microcracking [14,15]. This phenomenon as well as photon emission is also observed in other ceramics [16,17]. Particle emission is also an initiation mechanism for polymer formation according to Kajdas's negative-ion-radical action mechanism (NIRAM) [9].

In the initial exploratory study [3], alumina on alumina (Al_2O_3), zirconia on zirconia (ZrO_2), silicon nitride on silicon nitride (Si_3N_4), and sapphire on sapphire (single crystal Al_2O_3) tribological systems were investigated. A pure hydrocarbon, hexadecane,

was used as a carrier fluid for forty different chemical compounds designed, synthesized, or selected according to the tribopolymerization concept. Thirty of the compounds caused significant wear reductions, and ten of these were particularly effective -- causing wear reductions in excess of 70% at concentrations of 1 wt.% or less. In addition, compounds effective in one ceramic system were not always effective in another system. Effects on friction were generally not great, but reductions of up to 35-40% were observed.

Three main factors were cited as worthy of special note for the anti-wear mechanism. They include (a) those factors which may be involved prior to surface polymerization (i.e., structure of the molecule, adsorption on the surface, molecular orientation); (b) those controlling the process of tribopolymerization (i.e. contact temperature, catalysis, exoelectron emission, competing surface reactions); and (c) those having to do with after surface polymerization has occurred (i.e., structure of the polymer film formed, film thickness, mechanical properties, adhesion, thermal stability) [3].

Some experiments in this initial study were carried out using essentially identical molecules with differences only in the position of attached groups that were expected to either aid or interfere with the polymerization potential of the molecule. It was found that those structures expected to polymerize easily in a tribological system were effective in reducing wear while those not expected to polymerize easily were relatively ineffective.

Two classes of monomers were used in this study, i.e., addition and condensation. All of the addition type monomers have the general structure $CH_2=CXY$ while the condensation monomers have the structure HOOC-R-OH. Three-dimensional and spatial characteristics were also considered using computer generated models as shown in Figure 2. Continued research [9,10] with ceramic-on-ceramic systems has provided more evidence of the successful selection and design of these general types of additives.

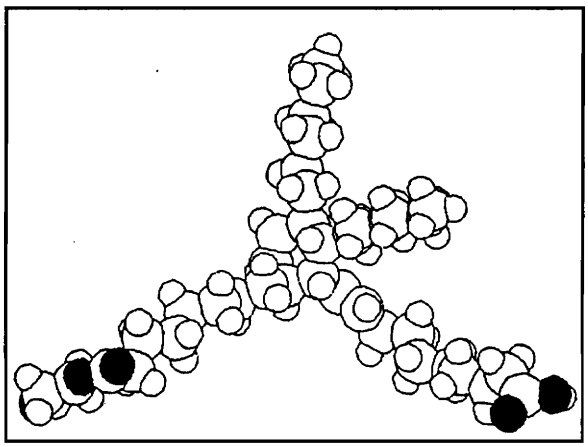

Figure 2 Three-Dimensional Model of the Monoester Compound [8]

As a final note to these tribopolymerization studies, it has been shown that the surface reactions are more complex than originally hypothesized [9,10,18,19]. Although much evidence of polymer formation has been found, indeed reactions with metal as well as with ceramic surfaces do occur under tribological conditions. The role and importance of such reactions in wear-reduction is not known.

2.3 *Other Methods of Ceramic Lubrication*

Many other studies of ceramic lubrication have been made because of the increasing interest in such materials for use in tribological systems. These have met with varying degrees of success. Fischer and Tomizawa [20] found that silicon nitride wear resistance in dry gasses was marginal and that water on the surface played a significant role. In fact, the wear rate of silicon nitride decreases in the presence of liquid water or water vapor [20,21]. The opposite is true of zirconia [22,23,24]; wear rate increases substantially in the presence of liquid water. High wear rate, for this ceramic, is blamed on stress corrosion (characteristic of oxide ceramics), while tribochemistry is used to explain this action in nonoxide ceramics [23]. Sasaki reports [24] that an increase of relative humidity in air reduces the friction coefficients of silicon nitride, alumina, zirconia, and silicon carbide. Sasaki also found that the wear rates of alumina and silicon carbide decreased with an increase in relative humidity.

Another interesting approach to the lubrication of ceramics is through the vapor phase. Though perhaps difficult to employ in a practical sense, the technique may provide insights into the tribochemical mechanisms of lubrication.

Graham and Klaus have been involved in such research for some time. Most of this research is centered around the action of tricresyl phosphate (TCP), a long used and well known additive in liquid lubrication, delivered in the vapor phase. Earlier research [25,26] was centered around the action of TCP delivered in a pure nitrogen carrier gas

at elevated temperatures on M50 hot hardness steel ball bearings in a four-ball wear tester. Although significant reductions in wear were observed, no attempt was made to characterize the chemical nature of the films that were formed. Scanning electron microscope (SEM) pictures of these films did show amorphous-like structures. Previous work suggested that polyphosphate formation resulted from the polymerization of TCP decomposition products during tribological contacts. The researchers suggested liquid-like polymer films are responsible for the anti-wear action of vapor TCP.

This research also noted differences in deposition rates and film formation on several substrate materials. These included copper, iron, stainless steel, alpha-silicon carbide, hot pressed silicon nitride, and a chromium-nickel alloy [26,27]. Knowing that physical adsorption is a reversible process and that chemisorption is irreversible, high temperature (500 - 900°C) experiments were set up to determine the mechanisms involved in film formation for some of these substrates. Results indicated that the chromium-nickel substrate provided a catalytic mechanism for chemisorption of TCP and TCP intermediates. Tenacious films were formed on the metallic substrate. On the other hand, the ceramic substrates, silicon carbide and silicon nitride, formed layers of thermally degraded TCP and TCP intermediates through physical adsorption. These layers were flaky deposits easily blown off of the substrate. As one might expect, the less chemically active ceramics did not provide for catalytic activity in film deposition.

In their most recent studies [28,29,30], the lubrication potential of these films in high temperature ceramic-on-ceramic systems was investigated. Sialon-on-sialon (silicon

nitride containing 8.3% alumina and 0.83% yttrium) reciprocating contacts were used and with marginal success. TCP vapor was able to reduce wear in this system, but only after 20 minutes of exposure to TCP vapor during the tribological contact. In the first 20 minutes, wear rates were excessive.

As shown by Makki and Graham [28], ceramic surfaces could be activated by exposure to organic solvents containing iron compounds such as ferric acetylacetonate. The procedure used formed a brown-orange iron oxide coating on the ceramic surface. This coating provided the catalytic action necessary for TCP to effectively reduce sialon wear at lower temperatures (below 400°C). At bulk temperatures of 400°C and above, it was not only necessary to have an iron oxide coating, but also to expose the coated ceramic surface to TCP vapors for six minutes prior to the start of a dynamic test; otherwise high wear was encountered immediately.

Critical test lengths were observed in these higher temperature tests. After a critical period of time, regardless of the catalytic coating on the ceramic or the TCP precoating procedures, the TCP "friction polymer" film broke down to form carbonaceous deposits, and high wear rates were again observed. The researchers speculated that under these higher temperature conditions, contact temperatures can reach 750°C and above. At such temperatures, TCP decomposes and forms a carbonaceous deposit with poor lubricating properties.

Finally, in another approach, Lauer [31,32] has shown merit in lubricating high temperature surfaces through the catalytic generation of graphitic carbonaceous deposits

from hydrocarbon gases such as ethylene, benzene, or 1-propanol vapor applied by a nitrogen carrier gas. At temperatures of 350 to 650°C, ethylene, and indeed other organic compounds, will dissociate spontaneously to form only carbon and hydrogen in the presence of the proper catalyst such as nickel or a nickel-containing alloy. This drawback is one of the method's limiting features with respect to ceramics. Alumina ceramics must be coated with 100 nm thick layers of nickel oxide in order to have any beneficial effect. Once a surface coating is worn away, so is the ability of the vapor to minimize wear. Although the method appears to work with uncoated silicon carbide and silicon nitride surfaces, with low wear and low coefficients of friction observed, initial run-in periods were necessary before positive benefits were experienced. High wear and high coefficients of friction characterized these run-in periods.

Critical speeds of operation were also found due to the rate of diffusion of the hydrocarbon and/or the decomposition products to the surface. This type of behavior limits a system's dynamic range of operation.

These studies raise the interesting question of tribopolymerization in the vapor phase. Can this method be applied to high temperature "dry" contacts? Although the practical applications of this approach are unknown, it is possible that studies of vapor phase tribopolymerization may add insight to the mechanisms by eliminating other possible surface reactions (i.e., with hydrocarbon carrier fluids or oxygen). This type of knowledge may aid the ability to scientifically select compounds that will reduce wear in dynamic ceramic systems. In theory, the elimination of a carrier fluid would also

allow for increased concentration of triboemitted charged particles thus aiding monomer activation according to the NIRAM concept. Without the mass of the lubricant to absorb these emissions, more charged particles should be available in the critical contact region.

3.0 EXPERIMENTAL TECHNIQUE

3.1 Apparatus Overview

Vapor phase tribopolymerization experiments were performed using a "pin-on-disk" type machine. The basic contact geometry and diagram of the test apparatus is shown in Figure 3. This setup consists of a fixed spherical test specimen or "ball" loaded against a rotating disk. Each of the specimens is held by two-part (top and bottom) threaded stainless steel holders. When the top and bottom parts are screwed together with a specimen between them, the specimen is clamped into place. Two spacer rings are included with the stainless steel disk holder. The first of these is a 1.0 mm thick, 21.0 mm I.D., 25.0 mm O.D. nylon ring used to elevate the disk specimen and prevent contact of fresh test surface (or previous wear tracks) with the disk holder base. The second of these spacer rings is a 2.0 mm thick, 26.0 mm I.D., 30.0 mm O.D.

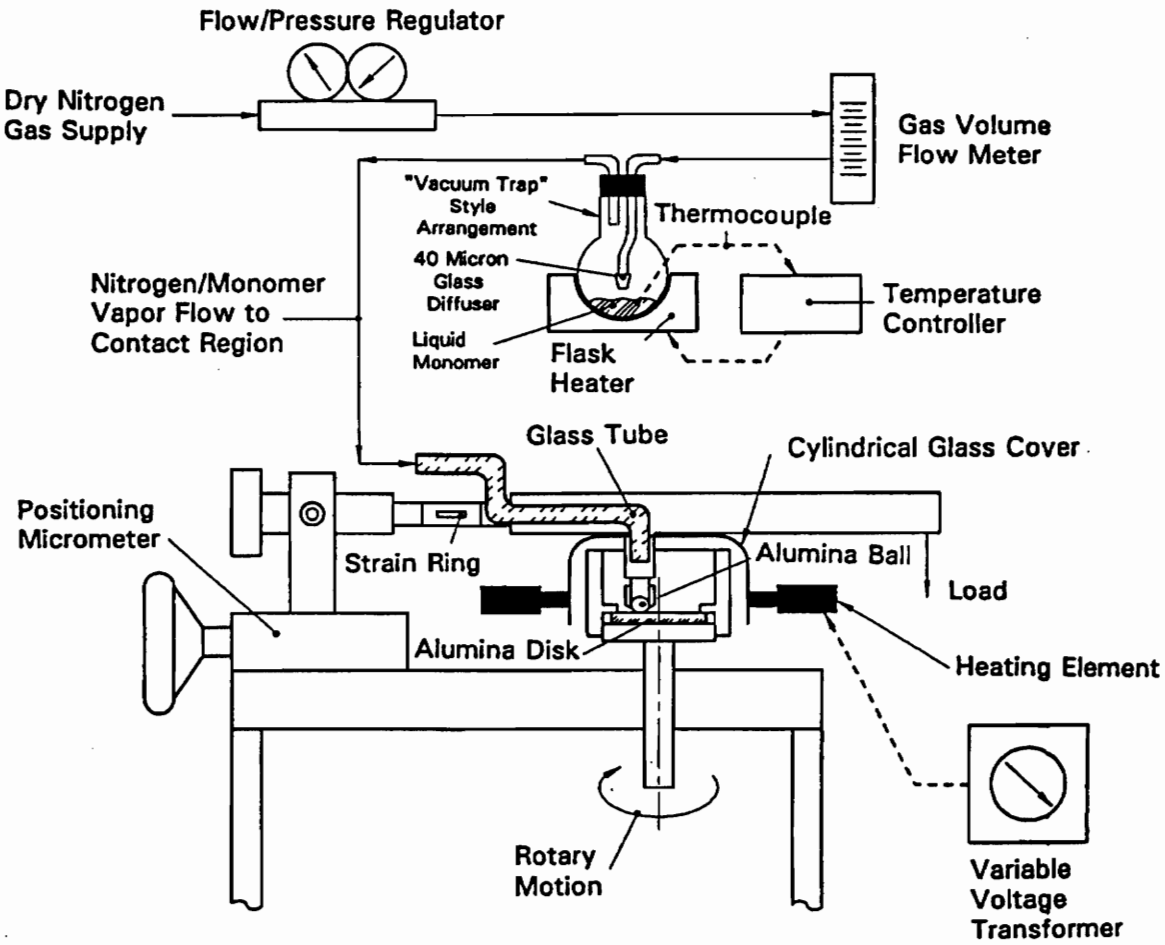

Figure 3 Basic Contact Geometry and Diagram of Experimental Vapor Phase Apparatus

centering ring used to center the disk specimen in the oversized holder.

Normal loads were applied by dead weights hung from the end of the load arm. An aluminum strain ring containing a full bridge arrangement of foil strain gages attached to this load arm was used in conjunction with a Micro-Measurements P-3500 portable strain indicator and an Astro-Med Incorporated Dash II Model MT chart recorder to continuously measure and record friction force.

The chart recorder was used in the peak-to-peak mode with an internal 10 Hz filter activated. In all experiments, the x-axis of the recorder represented time with recording speed set to 15 mm/min (i.e., 15 millimeters of chart paper per minute of test time). The y-axis in these dry experiments was set to 10 mV/div (i.e., 10 millivolts of strain gage output per division on chart paper axis) and proved adequate for all experiments.

Dry nitrogen gas was used as the carrier fluid for the additives tested. One quarter inch diameter Tygon tubing was used for all flexible gas connections. Gas flow was controlled by a Veriflo Corporation Model P/N pressure regulator in conjunction with a Dwyer Series VFB Visi-Float (1000 ml/min maximum) in-line flow meter.

Additive monomers were vaporized using a vacuum trap type arrangement. A ground glass stopper with only one inlet and one exit was used in conjunction with a 100 ml Kimax 24/40 boiling flask. The inlet nitrogen gas flow was dispersed into the boiling flask through a 40 micron glass diffuser.

Monomers in the boiling flask were heated in order to increase vapor pressure and

thus concentration in the nitrogen carrier gas. Temperatures were raised and controlled using an Electrothermal Unimantle 100 ml boiling flask heater in conjunction with an Omega temperature controller and a standard chromel/alumel thermocouple immersed in the fluid additive. The nitrogen/monomer gas mixture exited through the exit tube in the top of the stopper and was then delivered directly to the dynamic contact region.

Monomers were weighed inside the boiling flask before and after each experiment to determine weight loss and thus average concentration in the carrier fluid. Weight measurement was performed using a Mettler Type HS balance with a range of 0 - 160 grams and with accuracy to 0.0001 gram.

The contact region was enclosed with a glassware cover. Two different covers were made to allow for two different contact radii. Since the load arm is positioned (and thus the radius of the disk wear scar determined) using a micrometer positioning dial located at the end of the arm, two different covers were made in order to minimize the clearance between the rotating disk holder and the stationary glassware cover. Minimizing this clearance was necessary in order to insure a positive flow of nitrogen/monomer gas out of the contact region. Since a given volume of fluid will flow at lower velocity through a large cross-sectional area, minimal clearance provides for maximum fluid velocity leaving the contact region. Too large a clearance could lead to contamination of the intended enclosed testing region by atmospheric gasses stirred by vortices and/or other flow disturbances created by rotating parts (i.e., the disk and the disk holder).

These covers were rigidly fixed to the load arm by fine steel wires wrapped around glass hooks on the sides of the covers. The load arm was then re-balanced by repositioning the counterweight. The larger of the two holes on top of the glassware cover allows the ball and ball holder to fit into the enclosed space. The smaller of the two holes is sized to allow a glass applicator tube to be positioned directly above and behind the experimental contact region; this way, the additives entered the contact region just above the rotating disk surface just before contact with the ball.

Since two tests were performed on one side of a disk test specimen, the rotational speed of the disk was altered according to the radii of the contact to maintain constant sliding speed during all tests. The variable speed motor on the pin-on-disk machine allowed rotational speeds to calibrated with a General Radio Company Type 1531 strobotac with care taken to insure that frequency aliasing was not experienced.

In many experiments, the bulk temperature of the contact region was raised in order to prevent additive condensation on the surface of the test specimens. This was accomplished using a flat ring-shaped resistance heater and a variable voltage transformer or "Variac". Bulk temperatures attained with this setup were calibrated according to the dial gage rotation of the Variac as described in Appendix A.

3.2 *Materials*

Alumina (Al_2O_3) balls and disks were used for the tribological contacts described in this study. The disks were 25.0 mm in diameter and 3.2 mm thick and were obtained from 99.5% isostatically pressed alumina as supplied by LSP Industrial Ceramics, Incorporated. Disk surfaces were ground to a 0.5-0.65 micrometer average surface roughness. Grade 5 alumina balls, 99.5% pure and 3.2 mm (1/8 inch) in diameter were obtained from Sapphire Engineering, Incorporated.

3.3 *Lubricants*

In all of the tests conducted, pure dry nitrogen gas obtained from Industrial Gas Supply was used as a carrier fluid for the monomer additives tested. Dry nitrogen was selected for its inertness with respect to alumina as well as the monomers themselves. In addition, it is known that alumina surfaces are reactive with water [33] while oxygen has been shown to have an effect on the rate of thin film deposition on some surfaces [24]. Because of this, it was decided to eliminate water vapor as well as gaseous oxygen from the enclosed contact region. Nitrogen/monomer vapor was introduced into the enclosure at 1000 ml/min to provide a controlled atmosphere in the contact region and insure a positive pressure flow out of the enclosure.

The compounds selected for this study consisted of four oxygen-containing addition type monomers. Specifically these were vinyl acetate, diallyl phthalate, lauryl methacrylate, and vinyl octadecyl ether. Their structures are shown in Table I.

Table I [9]

VINYL MONOMERS USED IN THIS STUDY			
Chemistry of the Monomers	**Molecular Weight**	**No. of Vinyl Groups/Molecule**	**Polymerization Mechanism**
Vinyl Acetate 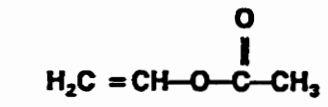	86.1	1	Radical
Lauryl Methacrylate 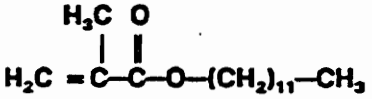	254.4	1	Anionic and Radical
Diallyl Phthalate 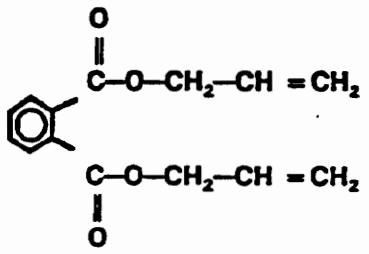	246.3	2	Radical
Vinyl Octadecyl Ether 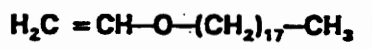	296.5	1	Cationic

3.4 Experimental Procedure

The test conditions used in this phase of the research are summarized in Table II. These conditions were selected for a number of reasons. The system geometry, sliding speed, and sliding distance are identical to those used in previous liquid-phase work with tribopolymerization. These conditions were selected in order to provide a standardized method for comparison of results. A 5 N load was chosen based on previous experience with dry alumina-on-alumina sliding contacts. In previous pilot tests, higher loads caused the alumina ball to loosen in its holder and spin. The holder

Table II Vapor Phase Experimental Setup and Test Conditions

System:	Alumina-on-Alumina
Geometry:	Sphere on Flat (Fixed Ball on Rotating Disk)
Specimen Size:	3.2 mm (1/8 in.) Ball on 25 mm (1 in.) Diameter Disk
Lubricants:	Vapor of Selected Vinyl Monomers in Dry Nitrogen Gas
Lubricant Delivery Temperature:	Variable
Applied Load:	5 N
Sliding Velocity:	0.25 m/s
Sliding Distance:	500 m
Ambient Temperature:	20°C
Bulk Temperature:	Variable (20 - 145°C)
Relative Humidity:	0% (Dry Nitrogen)

can be tightened sufficiently to prevent ball spinning with a 5 N load.

All alumina disks and alumina balls were cleaned prior to use in an experiment. Several samples were cleaned simultaneously in successive 20 minute ultrasonic baths of hexane, methanol, and deionized water. Samples were then placed in a new, clean (hexane rinsed) petri dish and dried in a vacuum oven at 150°C for two hours. Disks and balls were stored separately in a desiccator until use.

To begin a test, the radius of the contact was set using the micrometer dial load arm positioning mechanism. In order to insure a constant 0.25 m/s sliding speed, the rotational speed was set according to the radius of the contact using the strobotac. The desired 500 meter sliding distance would be reached in a test duration of 33 min 20 s.

The disk test specimen was then loaded into place using both spacing rings; the top part of the disk holder was screwed into place and tightened with a wrench. Next, due to space requirements, the glassware cover corresponding to the proper radius of contact was loaded on top of the disk holder but not yet fixed to the load arm. The ball holder was fit into place and rigidly fixed using a set screw in the load arm. The glassware cover was then positioned and tied with a fine steel wire to the load arm. The load arm was then re-balanced using the counterweight.

The 100 ml boiling flask was filled with a small amount of a monomer and weighed. The minimum weight of a monomer additive placed in the flask prior to an experiment was approximately 12 grams. This was calculated using vapor pressure data found in the CRC Handbook of Chemistry and Physics [34] for the lowest molecular

weight and most volatile monomer additive tested, vinyl acetate. The procedure is outlined in Appendix B. After weighing, the flask was put into place.

For tests conducted at elevated bulk temperature and elevated monomer temperature, heating was started. Since monomer temperature typically rises faster than bulk temperature in the configuration described, the bulk heater was started first and took approximately 12 to 15 minutes to reach constant temperature. After 10 minutes of bulk heating, heating of the additive commenced. As soon as the additive reached its desired temperature (usually in 3 to 5 minutes), preparations for the test continued.

Elevated bulk temperatures were necessary for this work primarily due to the high molecular weights and low volatilities of the monomer additives tested. In order to create significant concentrations in the carrier fluid, the monomers had to be heated to temperatures approaching their boiling points. Experience showed that condensation formed rapidly on test surfaces as well as on the surrounding structures when high temperature monomer vapors were introduced to an ambient bulk temperature environment. Elevated bulk temperatures were necessary to eliminate condensation and insure vapor delivery of the monomers. Indeed, this was the case; no physical evidence of condensation was found during any of the experiments.

The next step was to tighten the ball holder while it was hot. Heating of the bulk region causes the stainless steel holders to expand and loosen. The disk holder did not need to be re-tightened at the elevated temperature. It was found through experience that if this step was not performed, the ball would frequently loosen in its holder and spin,

causing rolling contact and failure of the test.

Finally, the friction measuring strain gages on the load arm were balanced and the chart recorder was checked for proper settings and started. Nitrogen/monomer gas flow was turned on. No nitrogen flow was allowed to occur during the monomer heating process, so that a small excess of vapor built up inside the flask and the connecting tubes. This excess was allowed to clear itself to the surroundings prior to introduction of the vapors to the enclosed test region.

After clearing the excess, nitrogen/monomer gas was allowed to purge the contact region for 10 to 15 seconds prior to ball/disk contact. After this purge, the motor was started and the ball was loaded against the rotating disk. The tests were timed using a digital stopwatch for the 33 minutes and 20 seconds necessary to reach the standard 500m sliding distance at a sliding speed of 0.25 m/s. Any particularly interesting or unusual observations were noted.

3.5 Sample Analysis

After a test, it was necessary to allow the test region to cool for 15 to 20 minutes before the specimens could be handled and removed. During this time the additive flask was removed and reweighed in order to determine the mass lost in vapor. The average vapor concentration was calculated from the mass of additive transported in the vapor and

the volume of nitrogen gas (33⅓ l) allowed to pass through the contact region (1000 ml/min for 33 min 20 s).

Worn surfaces were examined using a Leitz-Wild Photomacroscope. This device utilizes a binocular tube and a photographic tube. The binocular tube is used to view the sample while the photographic tube is used for producing photographic or video images. The device has a maximum magnification of 80X using the phototube.

After the materials had cooled enough to be removed, the ball specimen was examined first. The flat, nearly circular wear scar was measured across its major and minor diameters under the photomacroscope at an appropriate magnification and then averaged to give an approximate scar diameter. Wear volume lost from the ball was calculated using a simple mathematical expression for the volume of a spherical segment. Any interesting visual observations were noted. Balls were carefully removed from the holder and stored for later inspection or analysis. Pictures of worn disk surfaces were also taken.

Worn disk surface profiles were studied and recorded using a Taylor-Hobson Talysurf 4 profilometer. Charts of various magnifications were recorded in order to determine disk wear volume. Four separate traces across different sections of the wear scar were taken and their magnifications noted. Disk wear volume could be determined by integrating and determining the area between each curve (wear scar profile) and the zero plane (original unworn plane of the disk surface). Averaging these wear scar cross-sectional areas, the total volume of material removed or worn was calculated by

multiplying the area and the track length (circumference).

Selected surfaces were then examined using a Nicolet 6000 Fourier Transform Infrared Microspectrometer (FTIRM) coupled with a Spectra-Tech IR-Plan sampling microscope with a 15X Cassegrain objective to inspect the wear tracks. FTIRM spectra were taken in order to determine the chemical composition of surface films left on the wear scar. Wear scar samples were scraped using the edge of a glass microscope slide to remove surface films. Removed material was deposited on a gold mirror and examined under the FTIRM microscope in the reflectance mode. Absorption spectra were recorded and printed for further examination.

Selected surfaces were also inspected using Scanning Electron Microscopy (SEM) to view any interesting surface characteristics present.

Disks were stored in a desiccator for later inspection or analysis. The Kimax boiling flask was rinsed with hexane after every test and allowed to dry thoroughly before adding fresh monomer, of the same type as the original, for another test. If a new monomer was to be tested, a new boiling flask was used and the other glassware, as well as the holders and other exposed parts, was cleaned in successive ultrasonic baths of acetone, hexane, and methanol for 20 minutes each.

4.0 RESULTS AND DISCUSSION

4.1 Low Temperature Experiments

Ball wear results for the alumina-on-alumina ambient (20°C) bulk temperature systems tested are summarized in Figure 4 and Table III. Monomer temperatures were raised to the temperatures indicated in the figure for the duration of the experiments and each bar represents a single experimental result. Scatter in the ball wear data for this initial study is greater than one would like, particularly for the dry nitrogen and diallyl phthalate (DP) tests. However, it does appear that vinyl acetate (VA) at the higher monomer delivery temperature (60°C) caused a significant reduction in wear. This was encouraging.

At the 80% confidence level, a statistically significant reduction in wear over the nitrogen standard occurs for the vinyl acetate 60°C treatment. This is according to

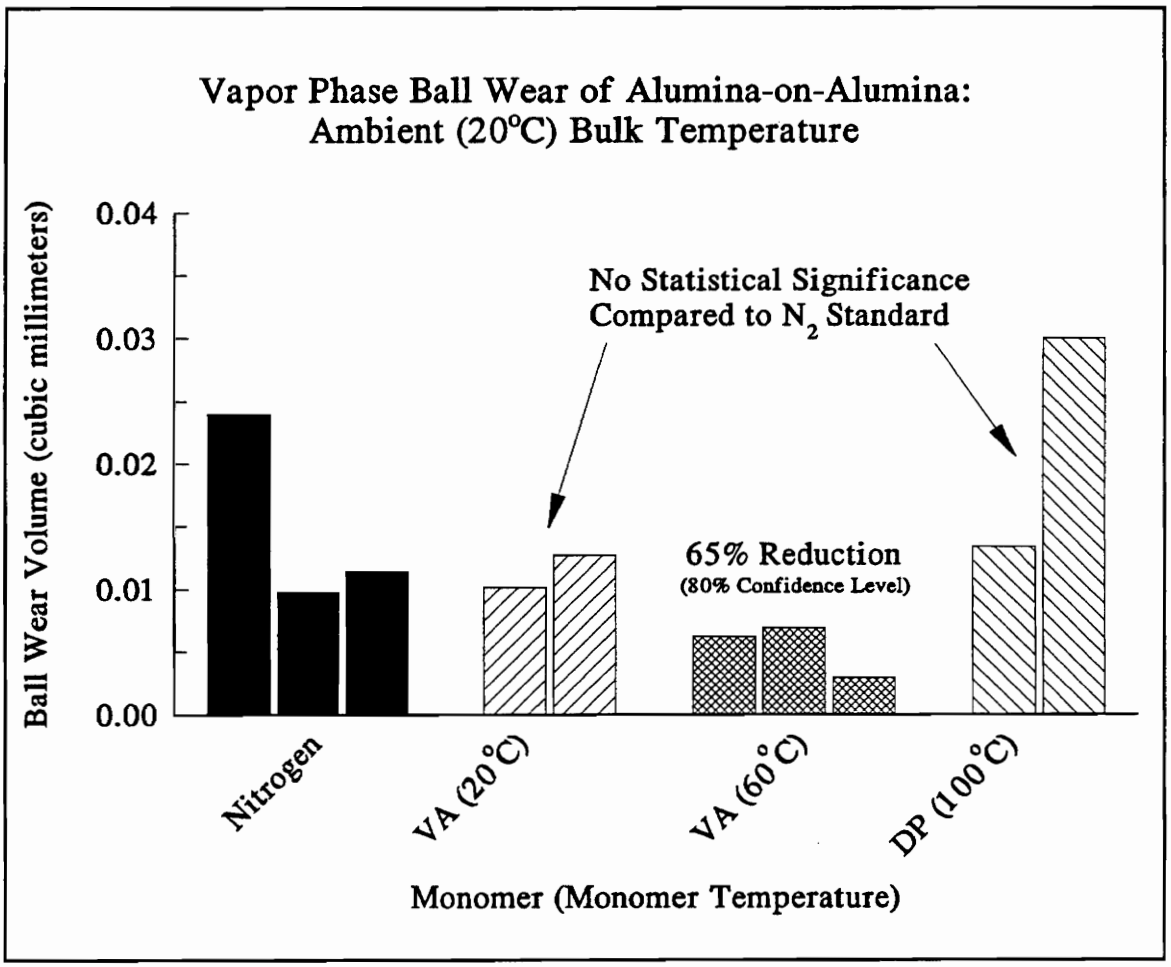

Figure 4 Vapor Phase Wear Results for Alumina-on-Alumina: Bulk 20°C

Fisher's Least Significant Difference (LSD) method of comparison. Details of this technique are given in Appendix C and tabled data is given in Appendix D.

The results for vinyl acetate wear reduction suggest a temperature dependent path. With an increase in monomer delivery temperature from 20°C (ambient) to 60°C, numerical (but not statistical) wear reductions increase from 24% to 65%. This trend is shown in Figure 5.

Statistically speaking, the 80% confidence level governing this difference is

Table III Vapor Phase Ball Wear Results of Alumina-on-Alumina: Bulk 20°C

Vapor Treatment	Vapor Delivery Temperature	Average Ball Wear Volume (mm^3)	Apparent Effect	Statistical Significance (80% Confidence Level)
N_2-Standard	-----	0.0150	------	------
Vinyl Acetate	Ambient (20°C)	0.0114	24% Reduction	NO
Vinyl Acetate	60°C	0.0053	65% Reduction	YES
Diallyl Phthalate	100°C	0.0217	44% Increase	NO

admittedly low. Higher confidence levels show that all treatments are statistically equivalent. However, the aim of this initial exploratory study was to see if any effects could be observed under these conditions. Additional repeat tests would be needed to improve the statistical treatment.

It was quite interesting that a very pale yellow tint in the wear track can be seen for vinyl acetate 60°C experiment. This is evidence of film formation in the wear track.

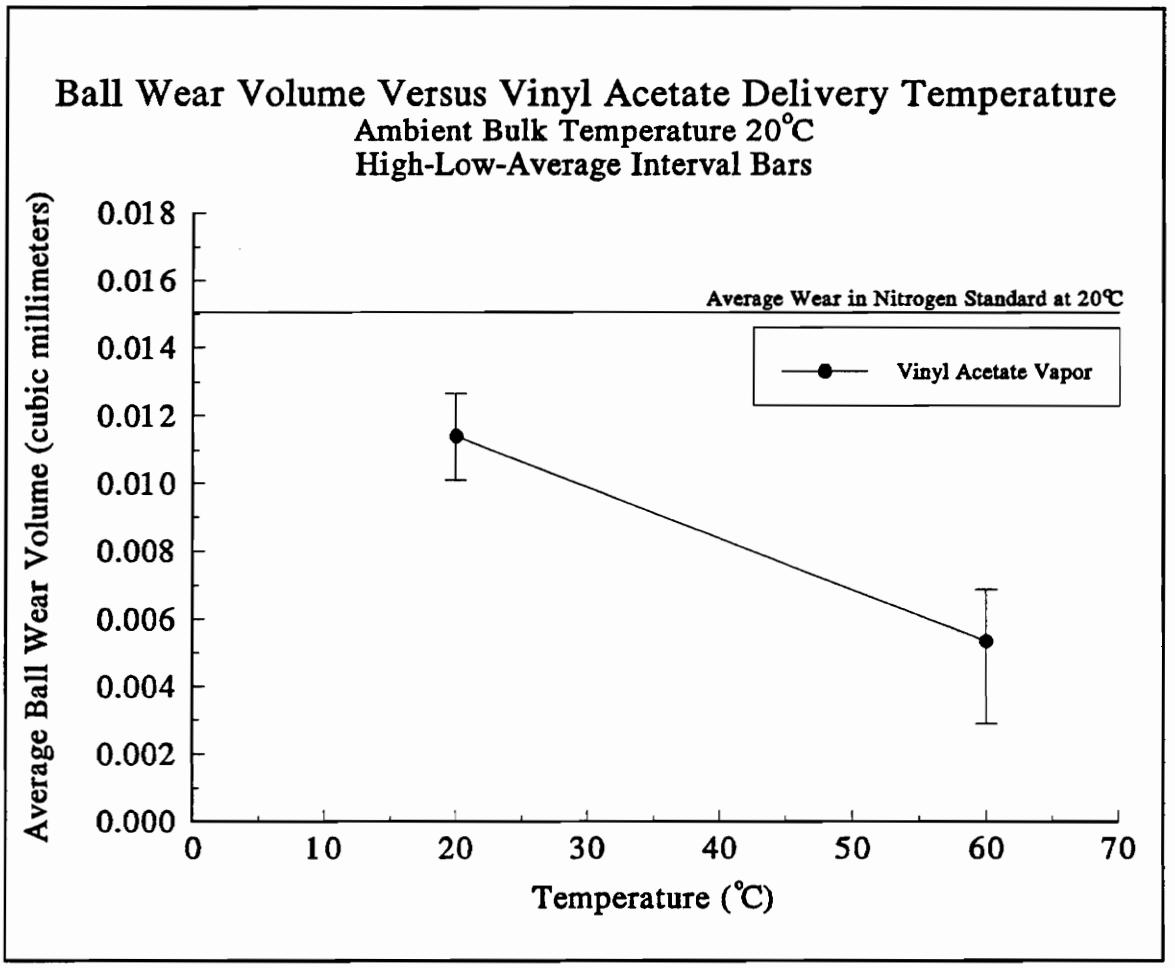

Figure 5 Average Ball Wear Volume Versus Monomer Delivery Temperature

No coloring or film was observable in the wear track of either the vinyl acetate 20°C test or the diallyl phthalate 100°C treatment. This is a clear indication or proof that it is indeed possible to reduce ceramic wear in the vapor phase by using a particular, selected monomer. It also suggested additional experiments described in the next section.

4.2 *High Temperature Experiments*

Ball wear results for the alumina-on-alumina elevated bulk temperature (145°C) treatments are summarized in Figures 6, 7, and 8. Monomer temperatures were raised to the temperatures indicated in each figure for the duration of the experiments and each bar represents a single experimental result. These figures show large reductions in wear for various treatments when compared to the nitrogen standard.

Dramatic reductions in wear occur particularly for those monomers delivered at the highest temperatures. Percentage wear-reductions range from 35% to as high as 99%. Furthermore, all reductions are statistically significant when compared with the

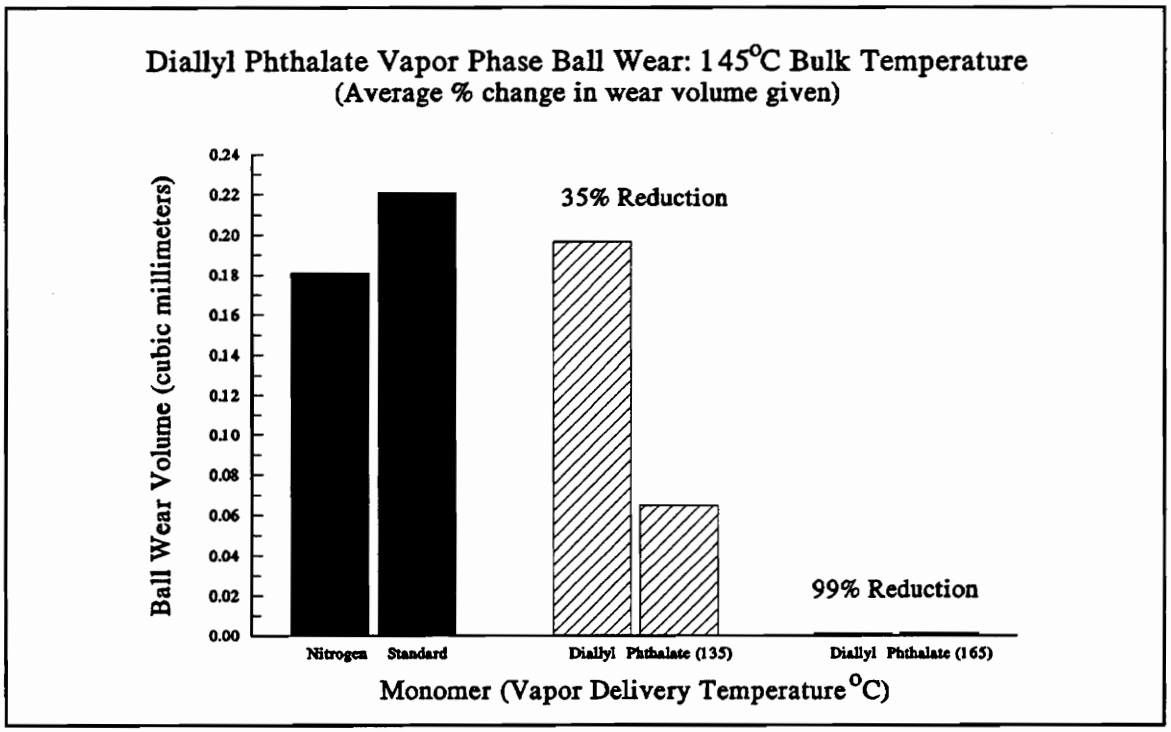

Figure 6 Diallyl Phthalate Vapor Phase Ball Wear: 145°C Bulk Temperature

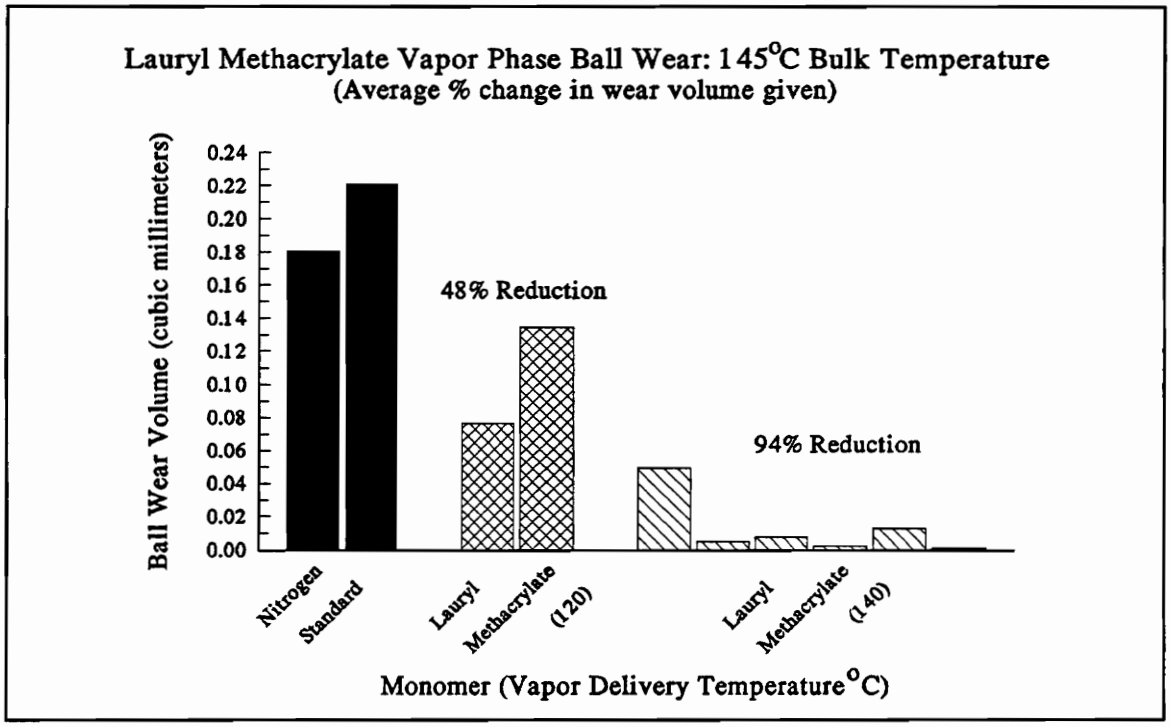

Figure 7 Lauryl Methacrylate Vapor Phase Ball Wear: 145°C Bulk Temperature

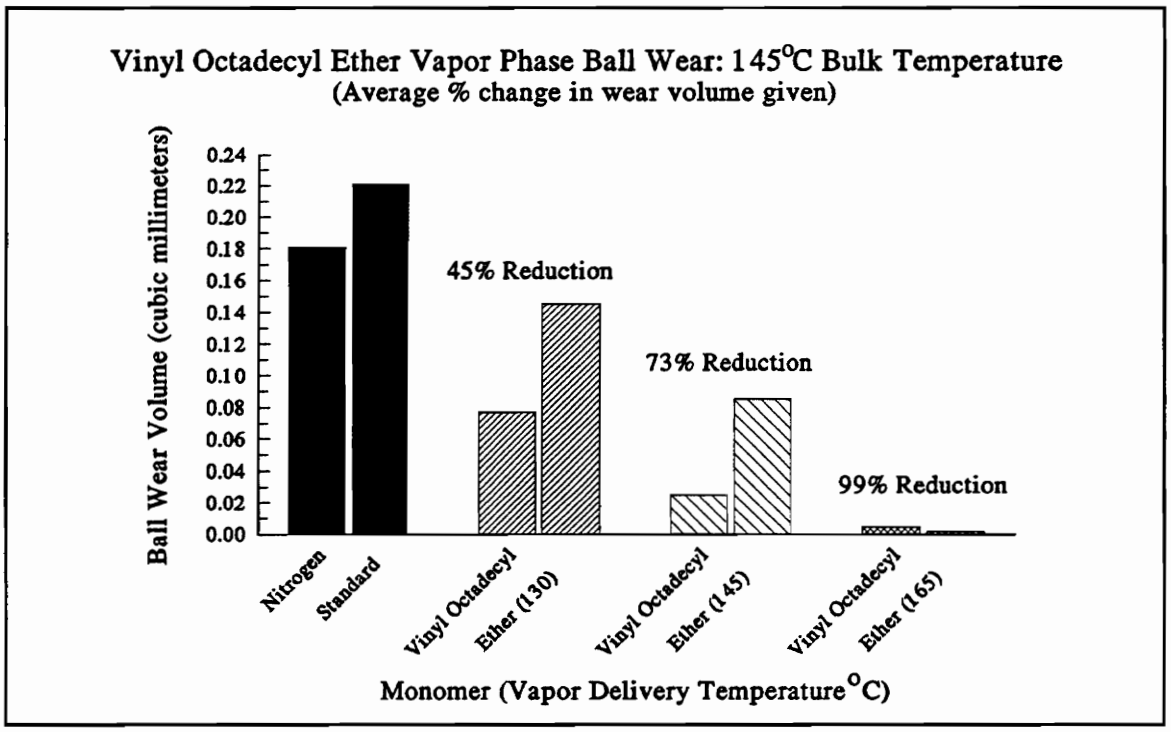

Figure 8 Vinyl Octadecyl Ether Vapor Phase Ball Wear: 145°C Bulk Temperature

nitrogen standard at the 95% confidence level according to Fisher's LSD method.

Each increase in monomer delivery temperature is followed by a reduction in wear. This trend was suggested in ambient bulk temperature tests as illustrated previously in Figure 5. The trend reappears quite clearly under 145°C bulk conditions as shown in Figure 9. This pattern of behavior occurred for the three monomers tested.

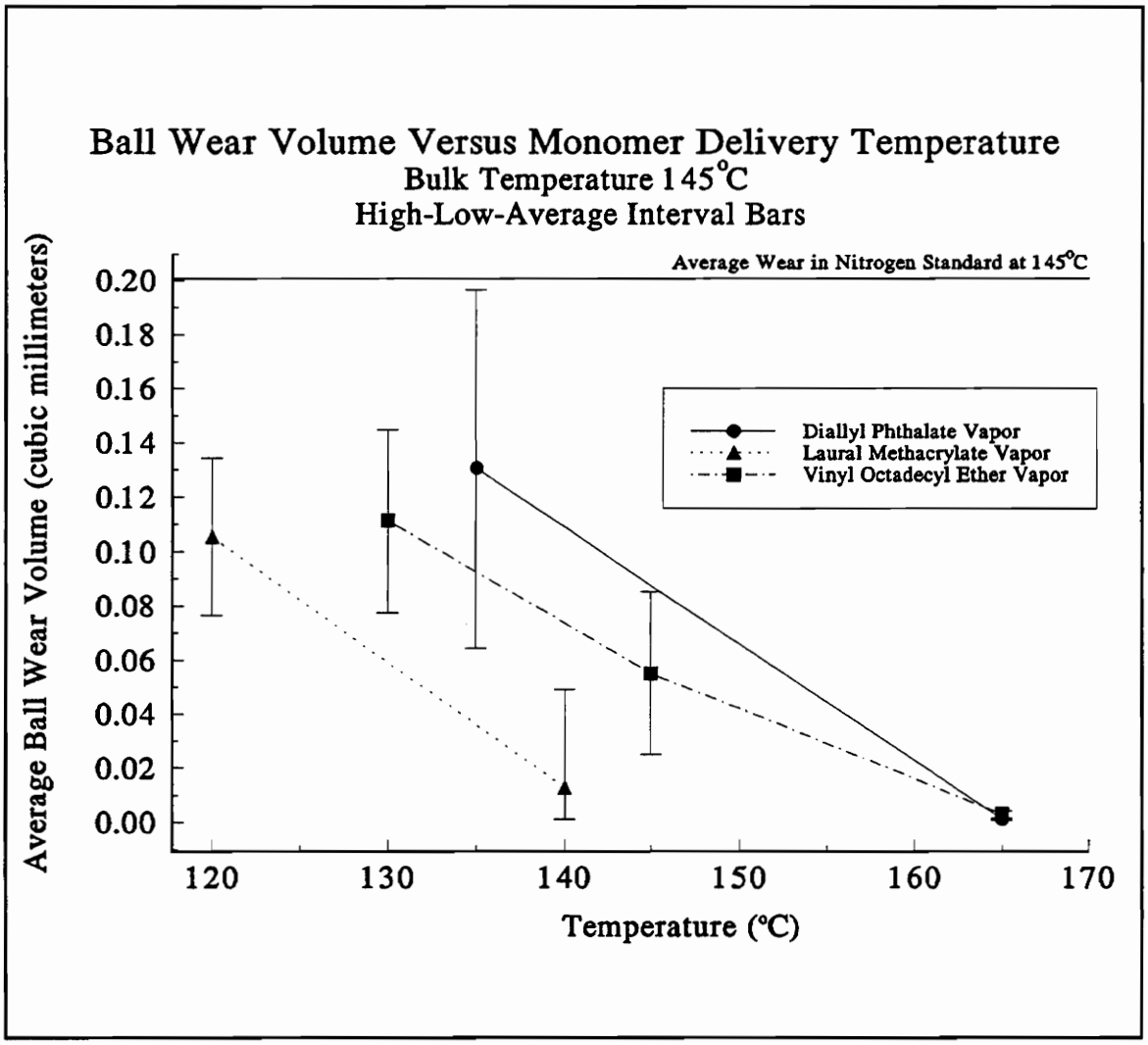

Figure 9 Average Ball Wear Volume Versus Monomer Delivery Temperature

At the 95% confidence level, the following are true concerning vapor phase treatments (monomer delivery temperatures shown) with ">" indicating "better" or "more effective" in terms of wear volume reductions:

a) All monomers	>	Nitrogen (Standard)
b) Diallyl Phthalate-165°C	>	Diallyl Phthalate-135°C
c) Lauryl Methacrylate-140°C	>	Lauryl Methacrylate-120°C
d) Vinyl Octadecyl Ether-165°C	>	Vinyl Octadecyl Ether-130°C

The vinyl octadecyl ether-145°C treatment was statistically equivalent to both the 130°C and 165°C vinyl octadecyl ether treatments. So with the exception of vinyl octadecyl ether, all increases in monomer delivery temperature cause statistically significant additional reductions in wear according to Fisher's LSD procedure.

For completeness, the following can also be said at the 95% confidence level:

e) DP 135°C = LM 120°C = VOE 130°C = VOE 145°C

f) DP 165°C = LM 140°C = VOE 145°C = VOE 165°C

Because of these statistics, it is not possible to say that one additive is better than another at reducing wear under the given conditions. However, all are better than the no-additive nitrogen standard. Lauryl methacrylate provides the highest reduction in wear (94%) at the lowest possible temperature. An additional 25°C temperature increase is needed for either diallyl phthalate or vinyl octadecyl ether to equal the performance of lauryl methacrylate at 140°C.

4.3 Total Wear

As shown, the statistical analysis of ball wear volumes provide solid evidence that the monomers tested reduce wear. Disk wear is more difficult to measure. Some selected monomer treatment disk wear volumes were, however, calculated and total wear volumes of these experiments were computed. Figure 10 illustrates the effectiveness of the selected monomer additives in total wear reduction. This figure clearly shows that indeed, the selected monomers do reduce total (ball and disk) ceramic wear with reductions ranging from 74 to 92%.

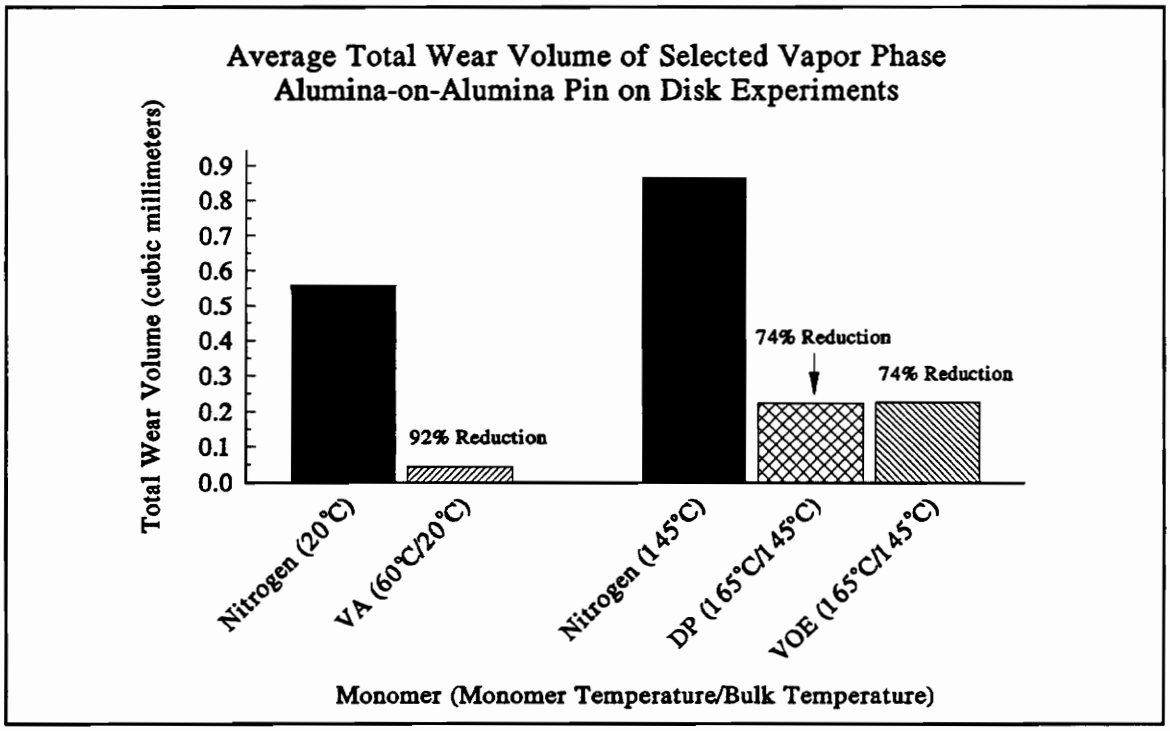

Figure 10 Average Total Wear Volume of Selected Vapor Phase Experiments

4.4 Monomer Vapor Concentration Effects

The next four figures (Figures 11-14) are presented together and summarize the results of alumina ball wear versus monomer concentration for the vapor phase experiments performed. Trends common to all of these additives become clearest when these results are reviewed collectively. Each point on a graph represents a single experimentally observed result.

In Figure 11, it appears that for vinyl acetate vapor delivered at 60°C, increasing

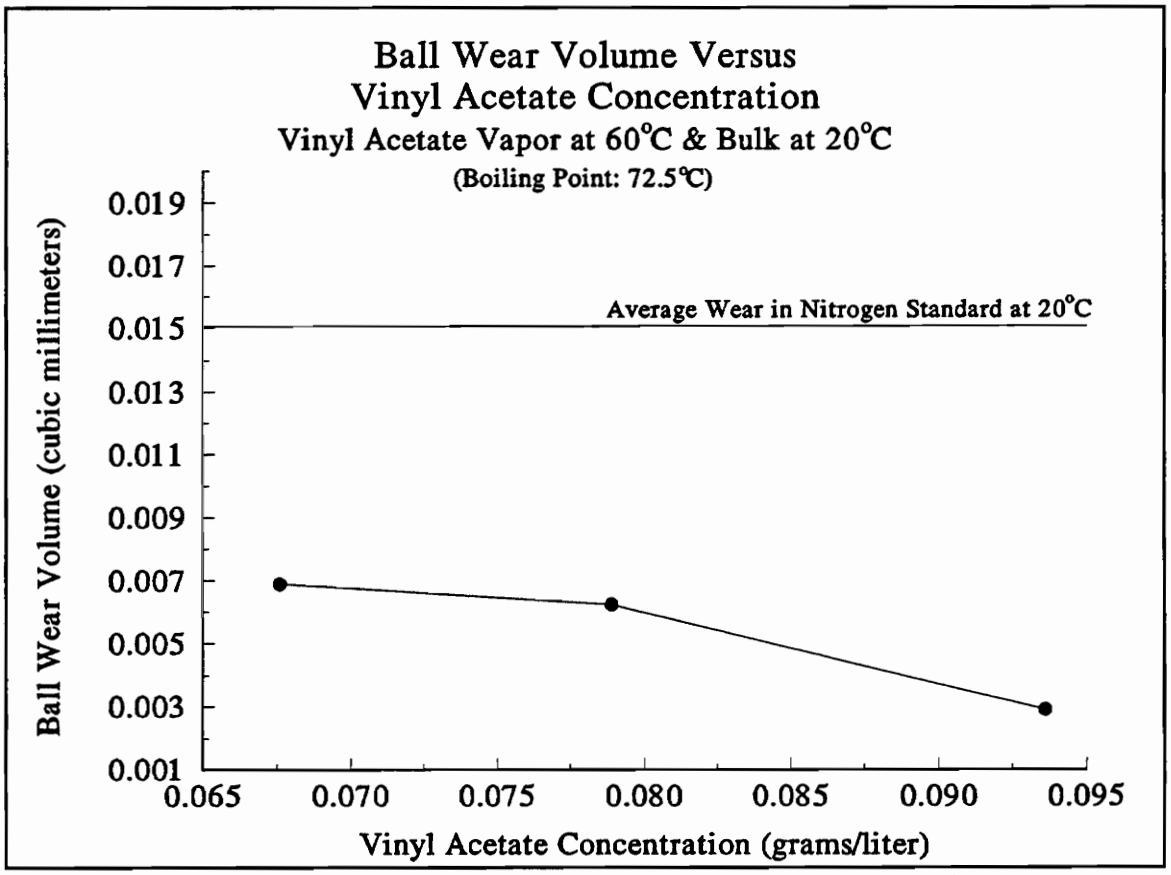

Figure 11 Ball Wear Volume Versus Vinyl Acetate Vapor Concentration

vapor concentration leads to lower wear. If this relationship is true, then according to the figure, a 50% increase in concentration is followed by a 50% reduction in wear. This may be proven or disproved with repeated experiments.

In Figure 12, this trend is evident again for diallyl phthalate vapor at 100°C as well as at 165°C. At the intermediate 135°C delivery temperature, though the concentrations of vapor in the two experiments are similar, a much larger variation in wear data was found; the reason for this is not known.

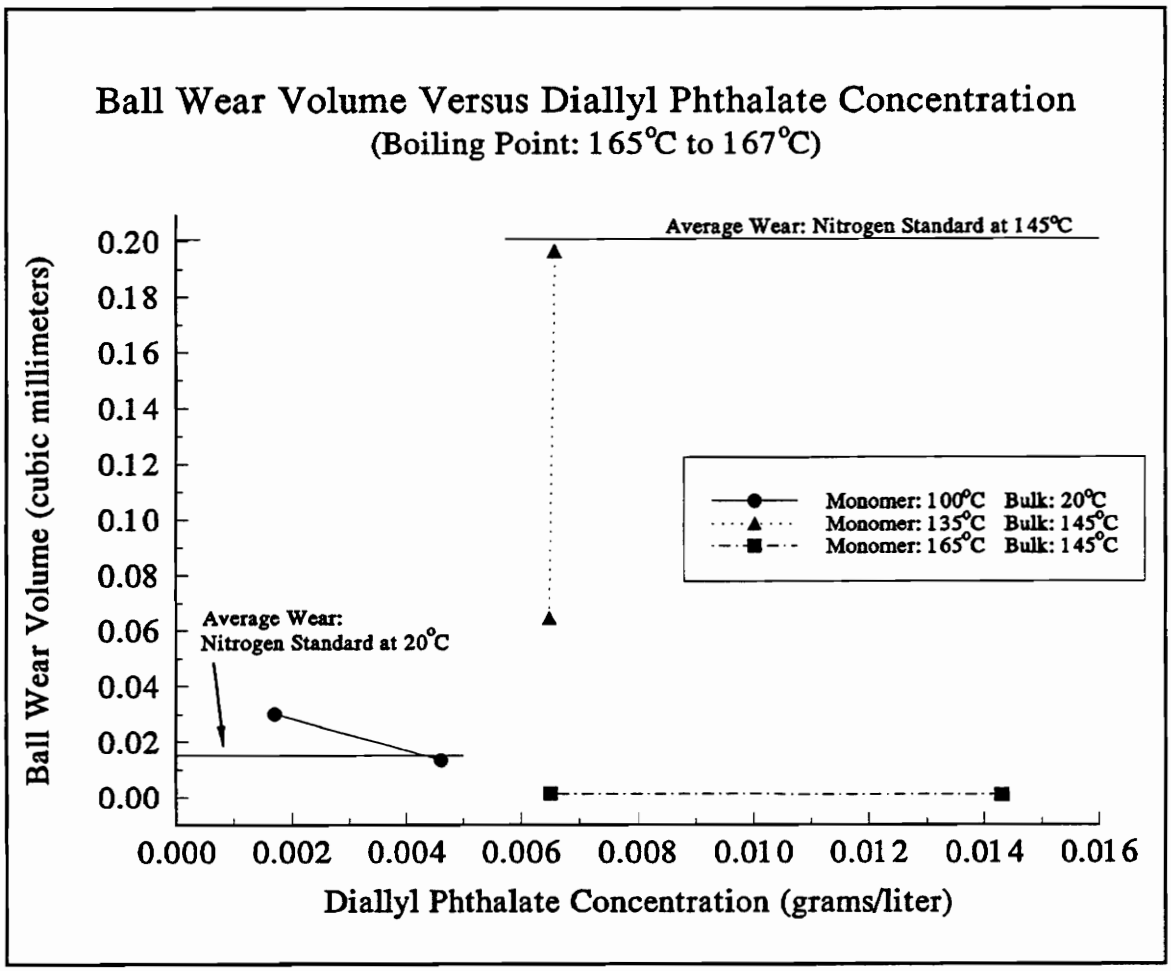

Figure 12 Ball Wear Volume Versus Diallyl Phthalate Vapor Concentration

Figure 13 shows that lauryl methacrylate, at the lower temperature of 120°C, exhibits some variation in wear volume, although again the concentrations are similar. At the higher monomer delivery temperature of 140°C, wear is reduced to a much lower value with less variation in the wear volume data. Here, no apparent benefits are found with concentrations beyond 0.006 g/l.

Figure 14 shows similar trends again for the concentration characteristics as related to vinyl octadecyl ether vapor. At lower temperatures (130°C and 145°C) a large

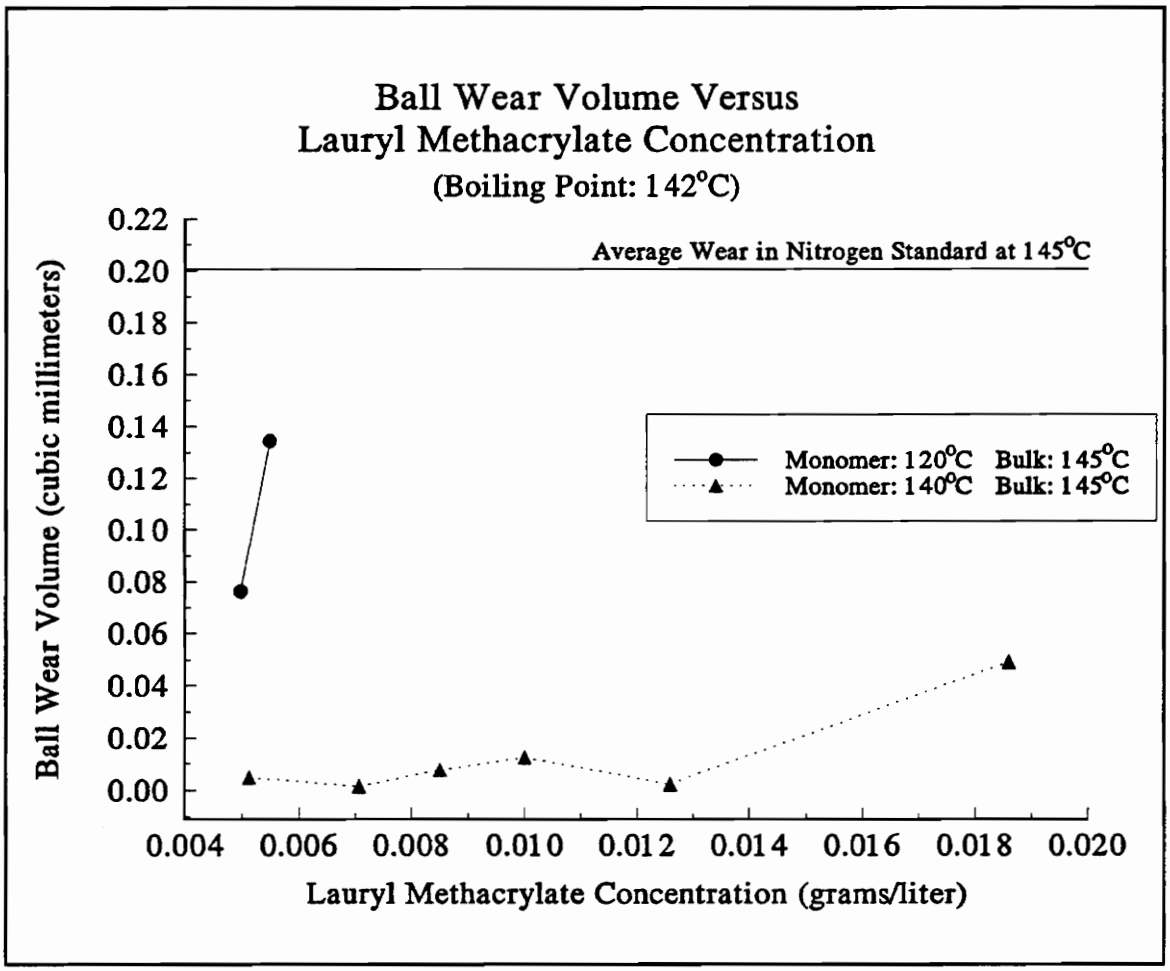

Figure 13 Ball Wear Volume Versus Lauryl Methacrylate Vapor Concentration

variation appears in the wear data for similar vapor concentrations. At the highest and most effective delivery temperature, 165°C, additional reduction appears unlikely for even a large increase in vapor concentration.

Further examination reveals other interesting and common observations. As each monomer approaches its boiling point, it becomes successively more effective in reducing wear. It would appear that this increased effectiveness **is not** the result of higher concentrations of monomer in vapor. Though as a general rule, as would be expected,

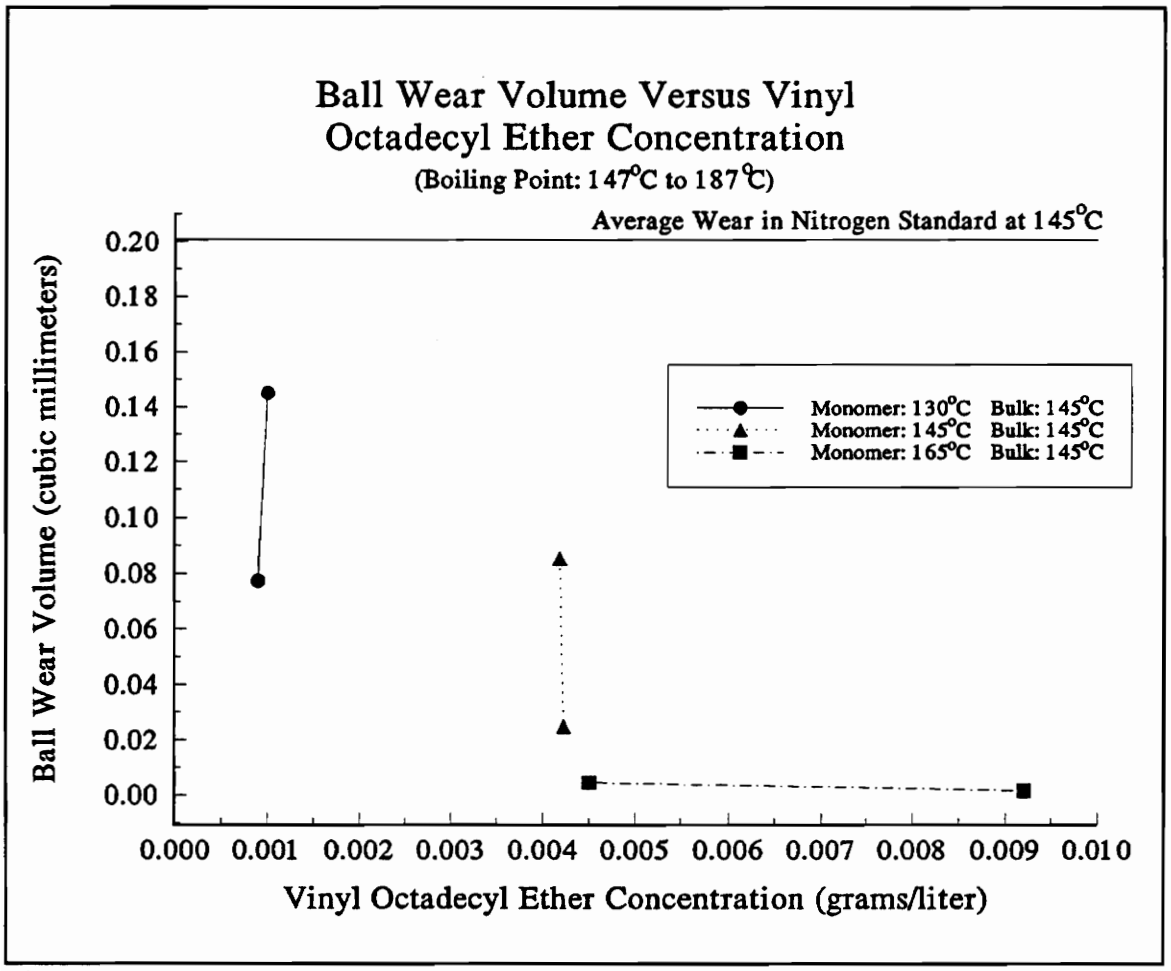

Figure 14 Ball Wear Volume Versus Vinyl Octadecyl Ether Vapor Concentration

higher temperatures did produce slightly higher concentrations, viewing Figures 12, 13, and 14 shows that similar concentrations are observed for different monomer delivery temperatures. This suggests that **monomer delivery temperature** and not concentration is the dominant factor in increased effectiveness in reducing wear.

It is interesting to note the temperatures at which these observations are made. Boiling points specified by the manufacturer (Aldrich Chemical Company) of each monomer are given in the individual figures directly beneath the title. The most effective delivery temperature is within 2°C of the boiling point for both diallyl phthalate and lauryl methacrylate. It is difficult to determine this with respect to vinyl octadecyl ether using the manufacturer's specifications, but 165°C is obviously within the range given. Vinyl acetate appears to be effective and consistent when delivered at approximately 12°C below its boiling point. Erratic wear data begins to appear when monomer delivery temperatures drop to between 10°C and 20°C below the boiling point regardless of concentration.

The widest variations in concentration for a given test treatment were found at the highest and most effective delivery temperatures. In each case (with the exception of lauryl methacrylate 140°C), much higher concentrations of vapor provide relatively little additional wear reduction. Very low concentrations of monomer vapor provide substantial reductions in wear. Any additional benefit resulting from higher monomer concentration is small. The rise in wear seen for a high concentration of lauryl methacrylate at 140°C may simply be a statistical outlier or may be a real trend showing that above a certain

level, wear may actually increase.

Due to heating monomer additives during testing, some polymerization apparently occurred in the flask. This phenomenon was most evident after experiments in which monomer delivery temperatures were highest. Since monomer vapor concentrations were not controlled directly, polymerization in the flask may be one of the sources of variation in monomer vapor concentration. This may also have had the effect of reducing absolute vapor concentration over time. One might expect that an increasing degree of polymerization would result in a continually decreasing value of monomer concentration with time over the course of an experiment.

Two physical characteristics of the post-experiment monomers are cited for reaching this conclusion: color and viscosity. Vinyl acetate was an exception, showing no noticeable changes. Diallyl phthalate, a clear liquid, turned an off-yellow color at 165°C and experienced a small increase in viscosity. Lauryl methacrylate, another clear liquid, stayed the same color but became noticeably more viscous at 140°C. Vinyl octadecyl ether first heated to 165°C, then cooled to room temperature, changed appearance. At room temperature, monomer vinyl octadecyl ether is a clear translucent wax. After an experiment, it became noticeably more opaque and white in color.

These results suggest that new ways to deliver monomers in future vapor phase studies are needed.

4.5 Friction

Results regarding the frictional characteristics of vapor phase tribopolymerization show consistent trends as seen in Figures 15 and 16. At ambient bulk temperature (20°C), monomers do not have any effect on the coefficient of friction of alumina. This is illustrated in Figure 15. The coefficient of friction is approximately 0.4 for all

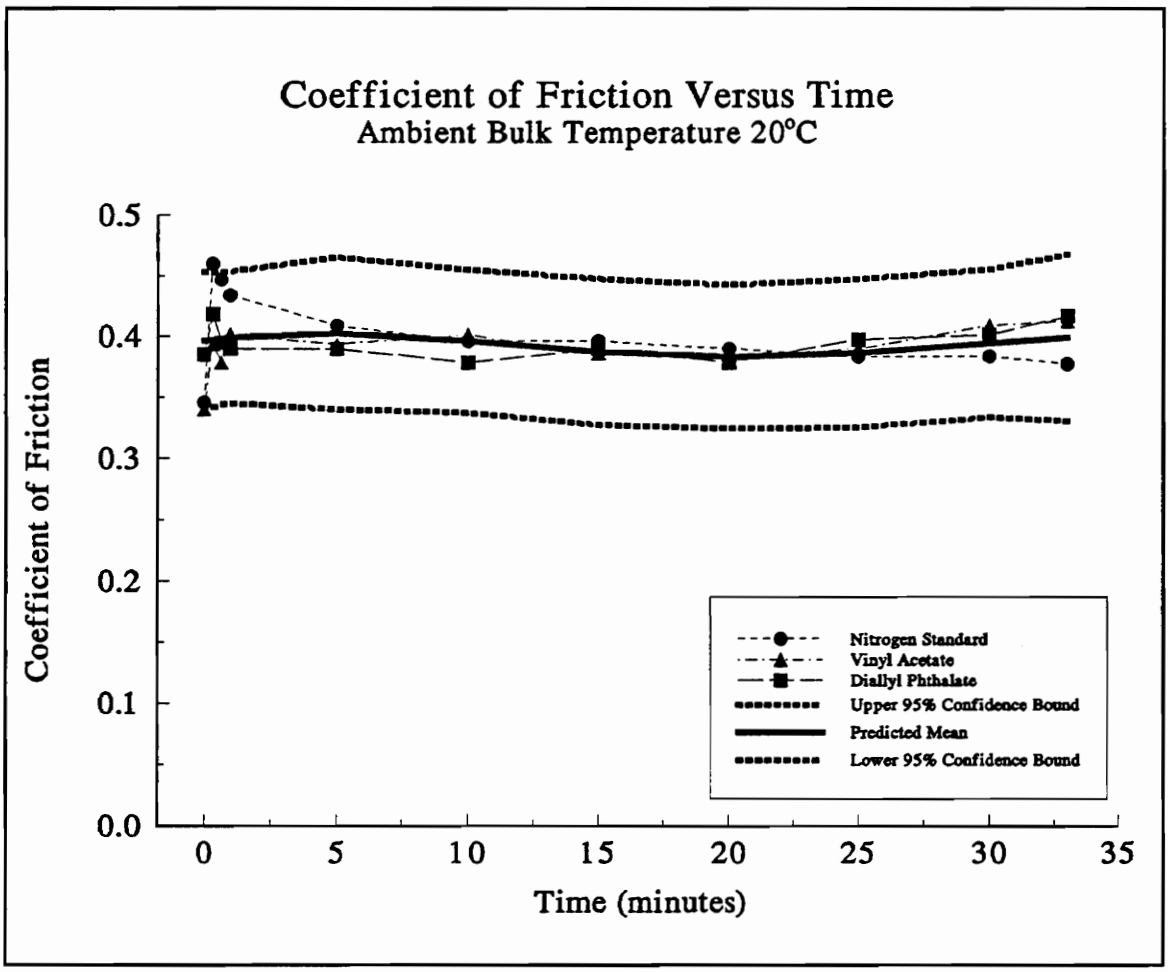

Figure 15 Ambient Bulk Temperature (20°C) Friction Data

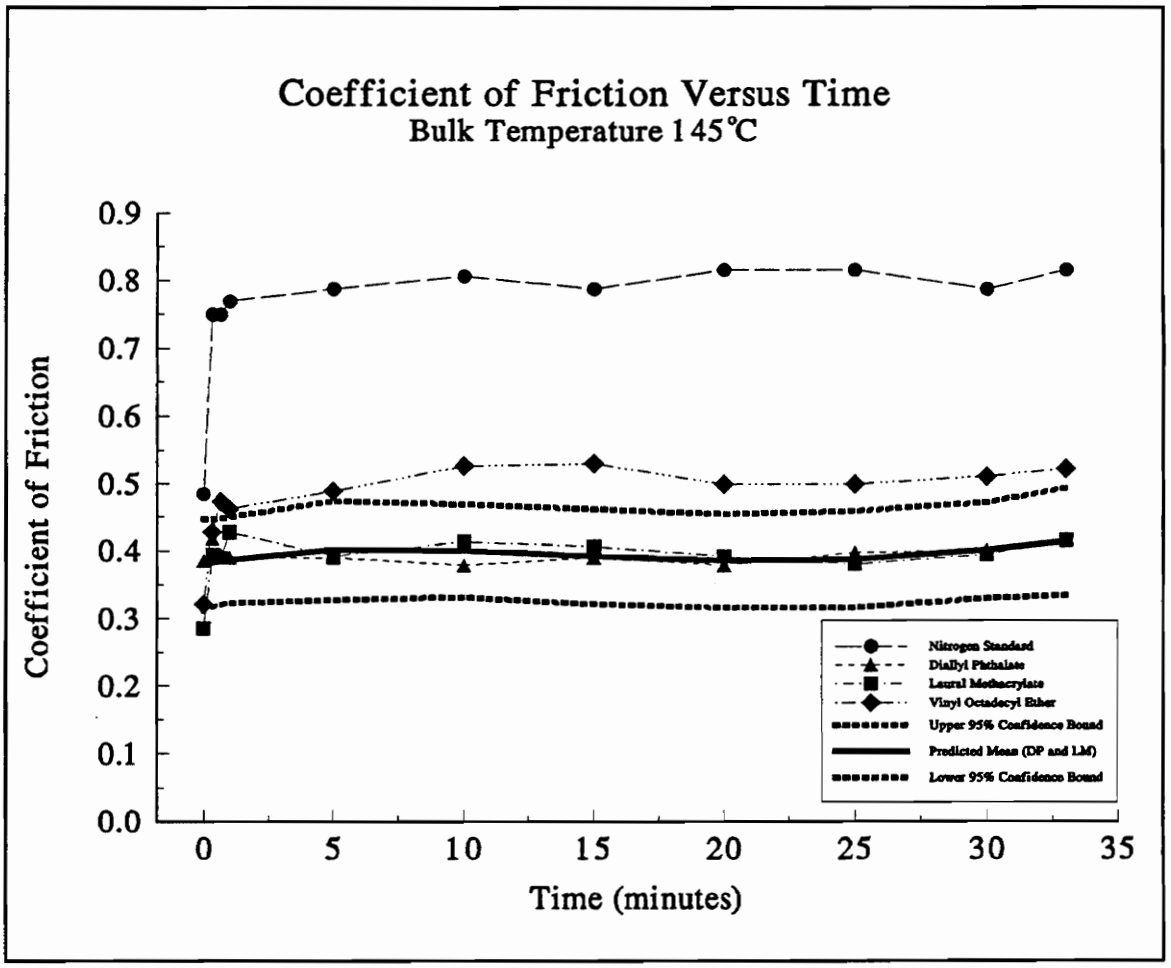

Figure 16 Elevated Bulk Temperature (145°C) Friction Data

experiments, including the nitrogen standard.

At 145°C, the coefficient of friction for the nitrogen standard is around 0.8 as shown in Figure 16. Under these conditions, vinyl octadecyl ether reduces friction coefficients to 0.5 while both diallyl phthalate and lauryl methacrylate reduce friction coefficients to 0.4. This shows that monomers reduce friction by roughly a factor of 2.

The friction coefficients observed for monomer vapors at elevated bulk temperatures are the same as those observed at ambient temperatures where adsorbed

layers of water and other molecules are expected to play a role [24,33] in friction mechanisms. Similarly, adsorbed layers of monomer additives tested in the high bulk temperature regime may reduce friction by providing a low shear strength film of chemical reaction products in the interface. This may reduce adhesive forces believed responsible for friction. These films were often visible to the naked eye.

4.6 Visual Inspection of 145°C Bulk Temperature Wear Surfaces

The surface characteristics of the 145°C nitrogen standard ball wear scar are difficult to examine. The area around the wear scar is clean without any type of buildup. The scar itself is, however, covered with a powdery material which, when examined more closely, appears to be flake-like in nature. These features can be seen in SEM photos of Figures 17 and 18. The lack of severe physical markings such as grooves may suggest that ploughing and other forms of mechanical wear do not play important roles in friction and wear under these test conditions.

Visual inspection of wear scars resulting from monomer vapor treatments showed clear, obvious, and unusual deposits. They will be described in the following paragraphs.

Wear scars from experiments with diallyl phthalate vapor delivered at 135°C were characterized by the formation of a small quantity of a brown powdery film that was

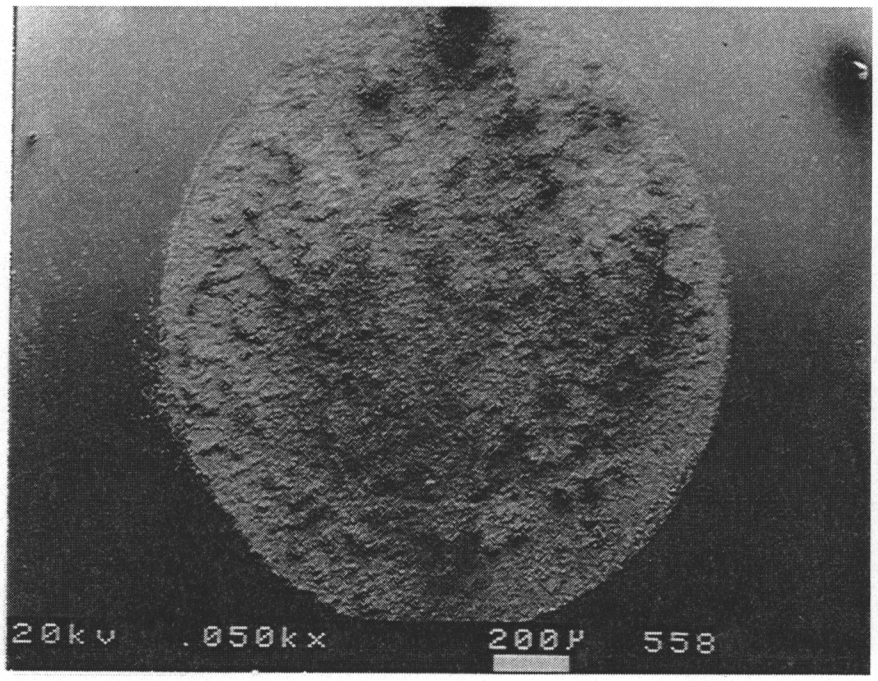

Figure 17 SEM of Nitrogen Standard Ball Wear Scar

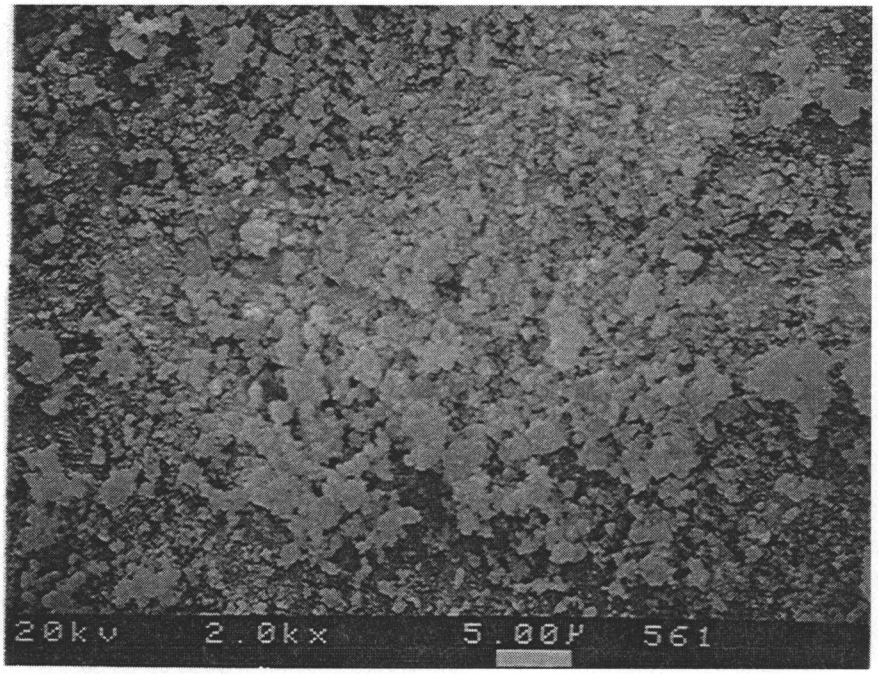

Figure 18 SEM of Flake-Like Wear Particles on Nitrogen Standard Ball Wear Scar

easily blown away. Figure 19 shows the film left by diallyl phthalate vapor delivered at 165°C. The film consists of a thick, black, wet, powdery material, like an oily graphitic substance. This figure is primarily intended to illustrate color As this film was pushed out of the contact region, it left large deposits on the edges of the disk wear scar. The Talysurf profile of the disk surface in Figure 20 illustrates the relative size of the deposits left. The ball wear scar, as well as the ball holder, was similarly covered with this black deposit. These large buildups can be seen in the SEM photograph in Figure 21. It is worth noting that this black deposit was visibly observed forming on the disk

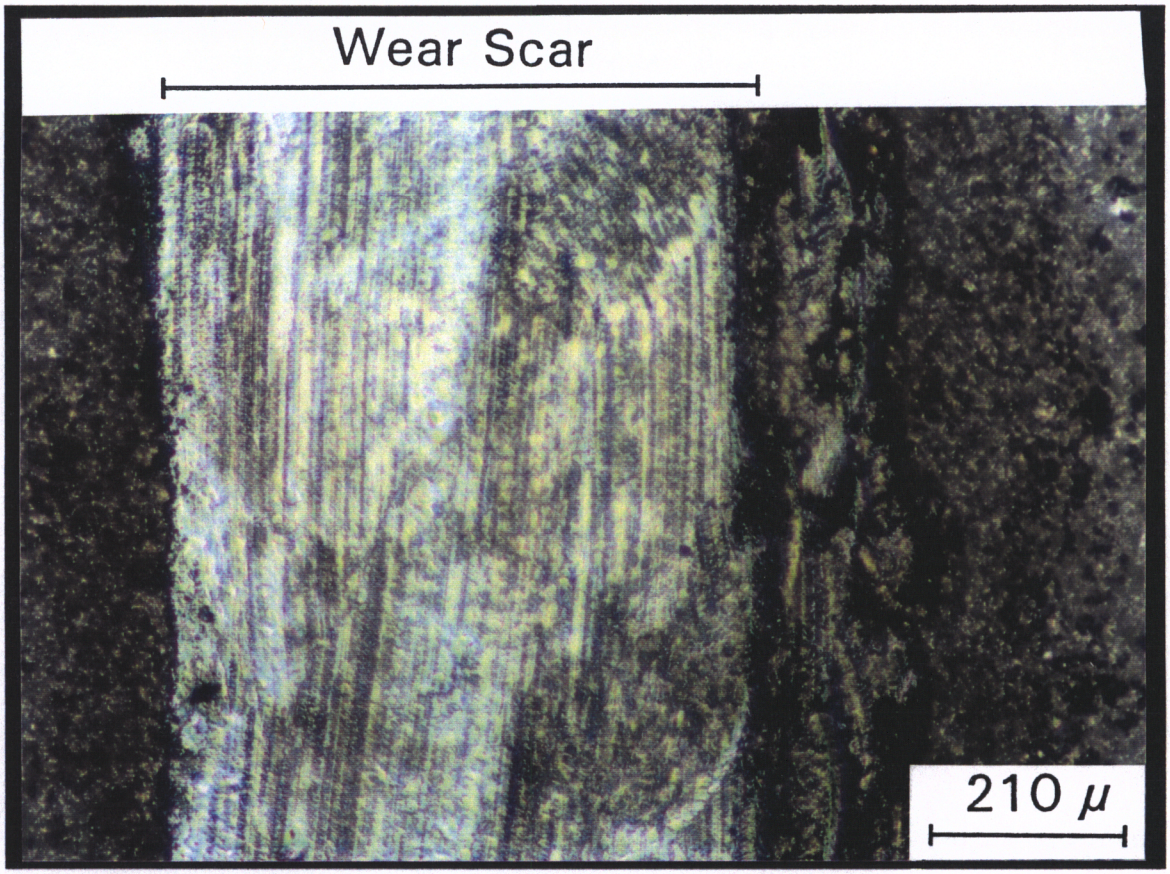

Figure 19 Photomacrograph of a Diallyl Phthalate Disk Wear Scar

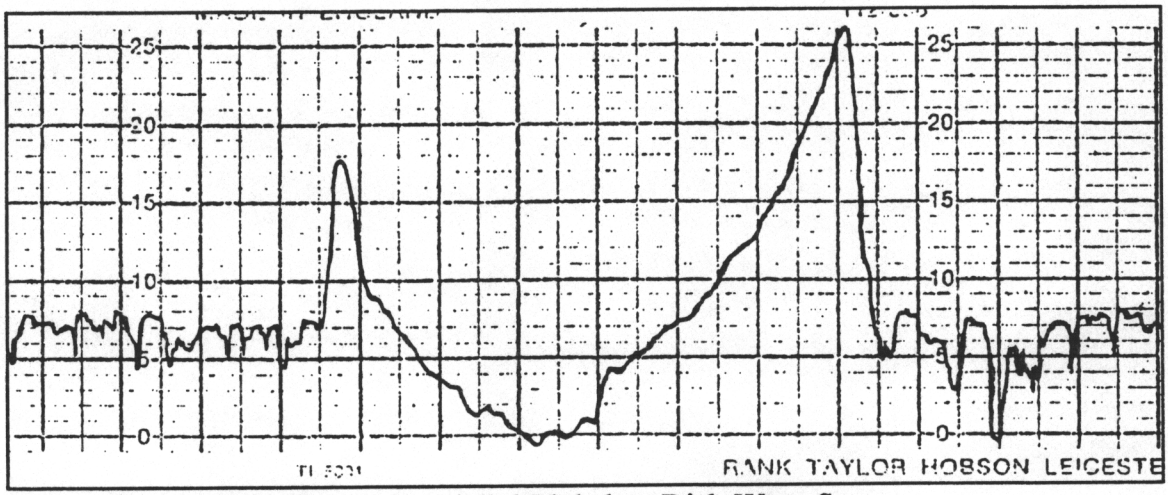

Figure 20 Talysurf Trace of a Diallyl Phthalate Disk Wear Scar;
Scale: X - 100x; Y - 10,000x

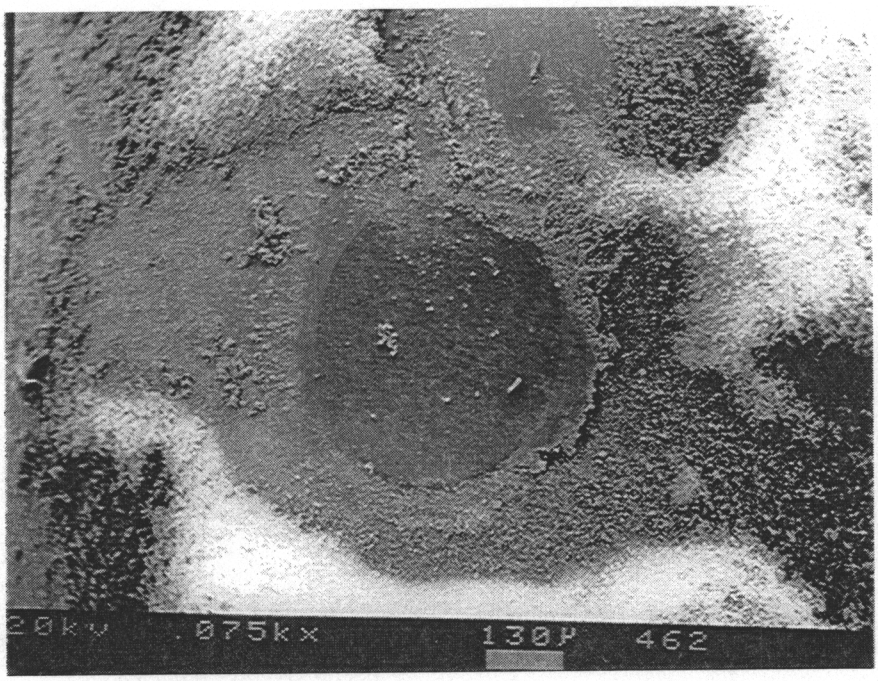

Figure 21 SEM of Diallyl Phthalate Ball Wear Scar

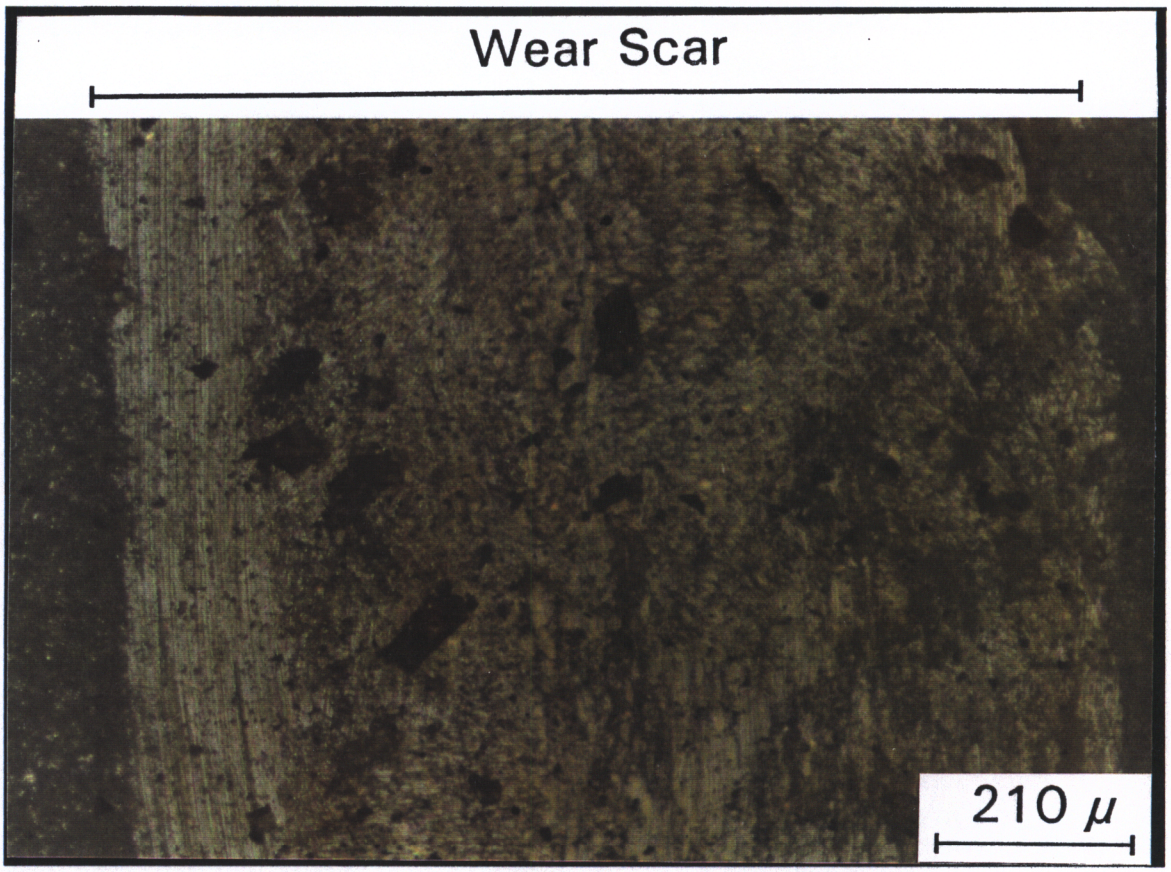

Figure 22 Photomacrograph of Lauryl Methacrylate Disk Wear Scar

surface within the first 30 seconds of an experiment.

Lauryl methacrylate vapor delivered at 120°C left no visible films. When vapor was delivered at 140°C, however, a very adherent yellow/brown film formed on the wear track. This is seen in the photomacrograph of Figure 22 which is primarily intended to show color. The ball scars were covered with the same yellow/brown film and characterized by buildups of a powdery yellow/brown material all over of the scar, as shown by the SEM photo of Figure 23.

Vinyl octadecyl ether vapor delivered at 130°C and 145°C showed little visible

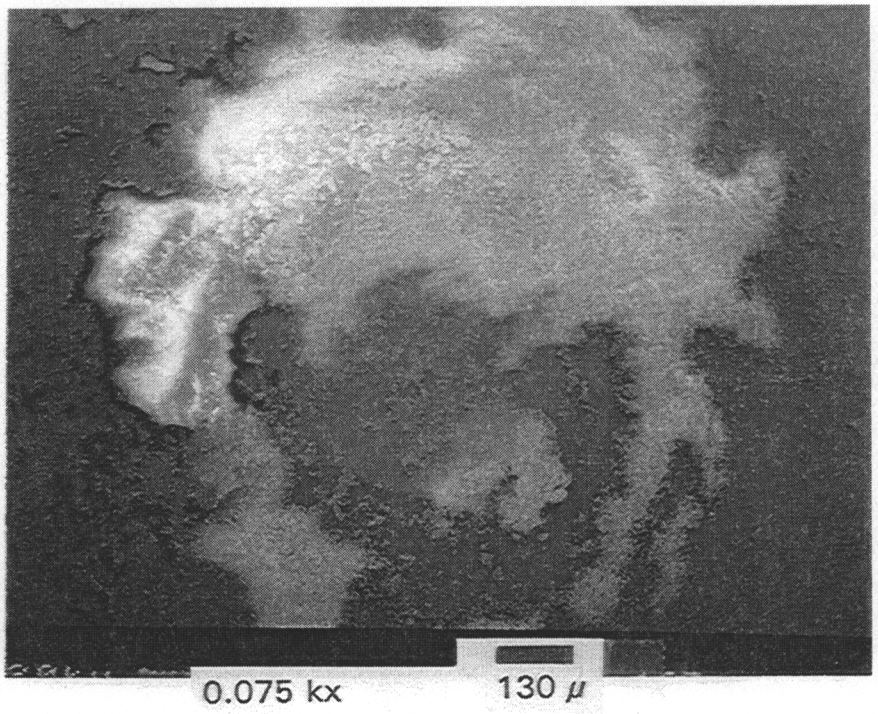

Figure 23 SEM of Lauryl Methacrylate Ball Wear Scar

film formation in the disk wear tracks themselves. Removal of these disks after a set of experiments showed an unusual type of deposit formation. It appeared that whatever films were being formed at the contact region were so loosely adhered to the surface that the centrifugal force of the spinning disk caused deposits to be thrown from the actual contact region. Large deposits of yellow tinted material built up around the perimeter of the disk holder.

Vinyl octadecyl ether vapor delivered at 165°C left a more adherent film similar to that observed with lauryl methacrylate vapor at 140°C. The yellow/brown film can be seen on the disk surface in the photomacroscope image of Figure 24, intended again to show only color. Ball wear scars under this treatment appeared very clean with large

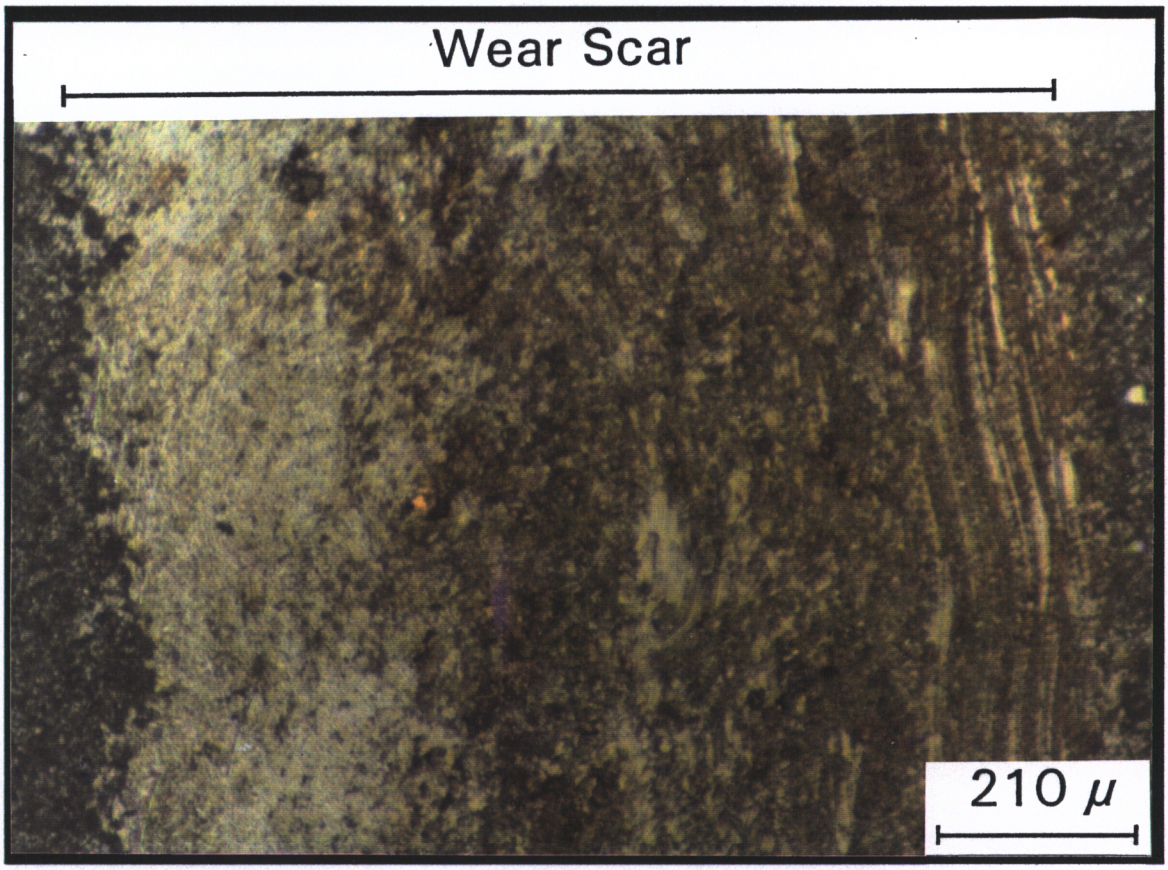

Figure 24 Photomacrograph of a Vinyl Octadecyl Ether Disk Wear Scar

buildups of powdery material around the perimeter of the scar. This feature is shown in the SEM photo of Figure 25.

Finally, one trend is consistent with respect to the SEM analyses of the wear surfaces. In all cases in which monomers were delivered in the vapor phase, microcracking occurred perpendicular to the direction of sliding. These microcracks are probably the result of tensile stresses created at the material surface due to friction. It is believed that through repeated stressing, the microcracks propagate and small flake-like wear particles are formed. This does not appear to be the severe wear condition of flake

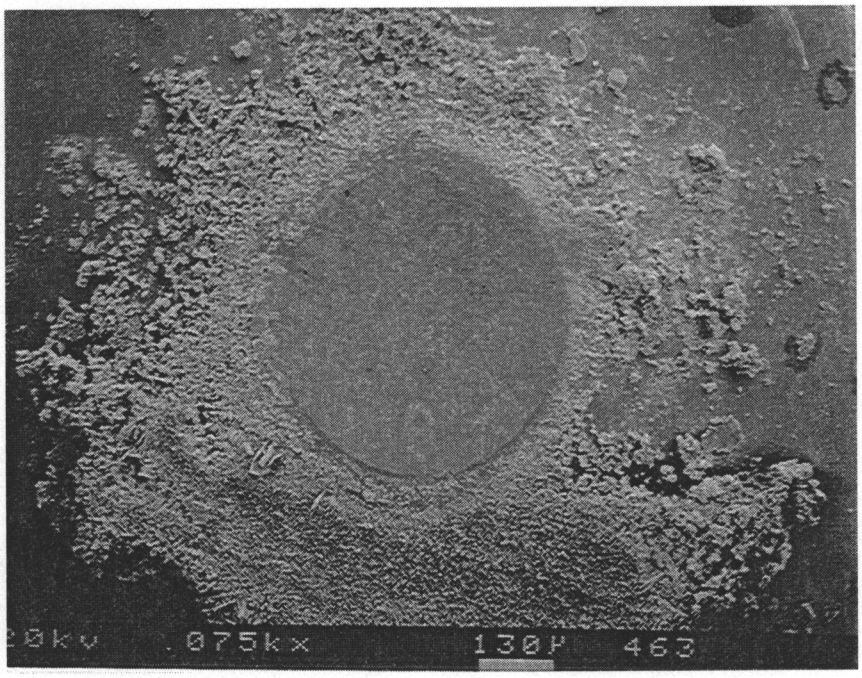

Figure 25 SEM of Vinyl Octadecyl Ether Vapor Ball Wear Scar

formation referred to by Hokkirigawa [35] and others where flake size is on the order of the apparent area of contact. Rather, these flakes are much smaller and appear to be no more than 5 to 10 microns in length. Wear scars in these experiments were typically on the order of 500 or 1000 microns in diameter.

Buckley and Miyoshi [36] describe microcracking as indicative of adhesion during sliding. Brittle fracture of the ceramic occurs due to the high surface tensile forces created by the adhesive mechanism. Given that all of the monomer treated wear surfaces observed were in general very smooth (as opposed to a rough and grooved

surface characteristic of ploughing), adhesion is believed to be the primary mechanism responsible for both friction and wear.

The surface of the nitrogen standard wear scar cannot be seen due to worn material covering the scar and therefore, whether or not microcracking has occurred cannot be determined. Closer examination of this material reveals that the wear particles formed are flake-like in nature and are of similar size to those observed on monomer treated wear surfaces. This may indicate that similar mechanisms are responsible for friction and wear under both additive and additive-free conditions.

Characteristic microcracking can be seen in the SEM photos of Figures 26 and 27. Figure 26 shows the edge of a ball wear scar from a diallyl phthalate vapor

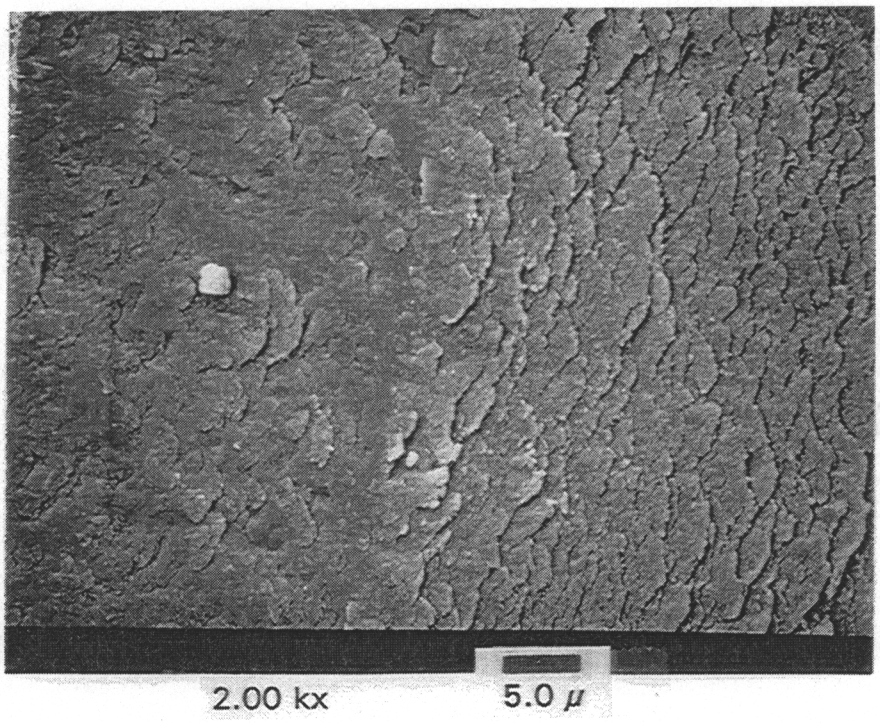

Figure 26 SEM of Diallyl Phthalate Ball Wear Scar Edge

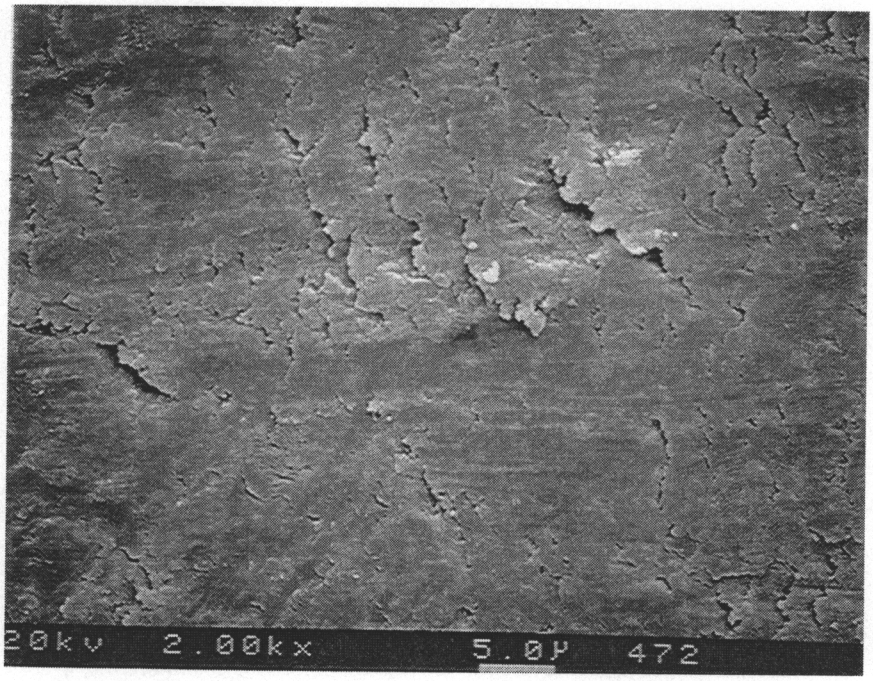

Figure 27 SEM of Diallyl Phthalate Disk Wear Scar

experiment (165°C vapor, 145°C bulk). Figure 27 shows a central portion of the disk wear scar from the same experiment. In each case, the microcracking perpendicular to the direction of sliding is evident.

4.7 FTIRM Surface Analysis

Fourier transform infrared microspectrometry (FTIRM) spectra of selected test specimens can aid the chemical characterization of surface films formed during tribological contact. Figures 28 through 31 show FTIRM spectra obtained from the surfaces of the most effective monomer treatments: vinyl acetate vapor delivered at 60°C and ambient bulk; diallyl phthalate vapor delivered at 165°C with 145°C bulk; lauryl methacrylate vapor delivered at 140°C with 145°C bulk; and vinyl octadecyl ether vapor delivered at 165°C with 145°C bulk. Each of these is presented along with its corresponding standard spectra obtained from pure monomer. Plots are given versus wavenumber which by convention has units of cm^{-1}.

Ranges of wavenumbers are often given with respect to a certain type of bond. Often specific peaks appear at different wavenumbers that correspond to the nature of the particular chemical bonding present. For instance, the C-H vibrations corresponding to a methyl group (CH_3) will appear at a slightly different wavenumber than a saturated C-H vibration found in the backbone of a long chain hydrocarbon (CH_2). In addition, the specific wavenumber where the C-H vibrations appear is also affected by the electronegativity and electronic nature of the group to which it is attached. The wavenumber at which a certain group appears may shift 10 or even 50 wavenumbers up or down due to such effects. Since these effects are relatively small, a range of wavenumbers often corresponds to a particular general type of bonding.

The y-axis, absorbance, is not shown in these figures. It provides little useful means for spectra comparisons due primarily to low signal to noise ratios and the ability of alumina to absorb infrared radiation. Noise is typically the erratic signal seen riding the contours of the main spectral signal. Often, noise is as strong as the signal one would hope to measure, therefore, the signal itself becomes lost in the noise making spectral interpretation difficult. Note also that the x-axes scales are not all identical and must be read individually.

The first and most striking observation is that each of the spectra obtained from wear products is very different from the standards. In addition, the signal to noise ratio for the products spectra is not especially good. There is, however, enough of a signal in each case to analyze and use in drawing some general conclusions.

The spectrum for vinyl acetate shown in Figure 28 provides strong evidence of a surface reaction with alumina. The intense peaks seen around 1600 and 1400 cm^{-1} are characteristic of the carboxylates. They correspond to the asymmetric and symmetric bending vibrations of the C=O bond respectively. It is hypothesized that the bonds forming ester groups in the vinyl acetate monomer were broken and new products were formed. It is believed that these peaks are the result of a monomer/alumina reaction to form alumina soaps.

Polymerization as a method of wear reduction for the vinyl acetate system can neither be proven nor ruled out. In the standard spectrum, C-H stretching vibrations appear at 3089 cm^{-1} for unsaturated groups and between 2937 and 2994 cm^{-1} for saturated

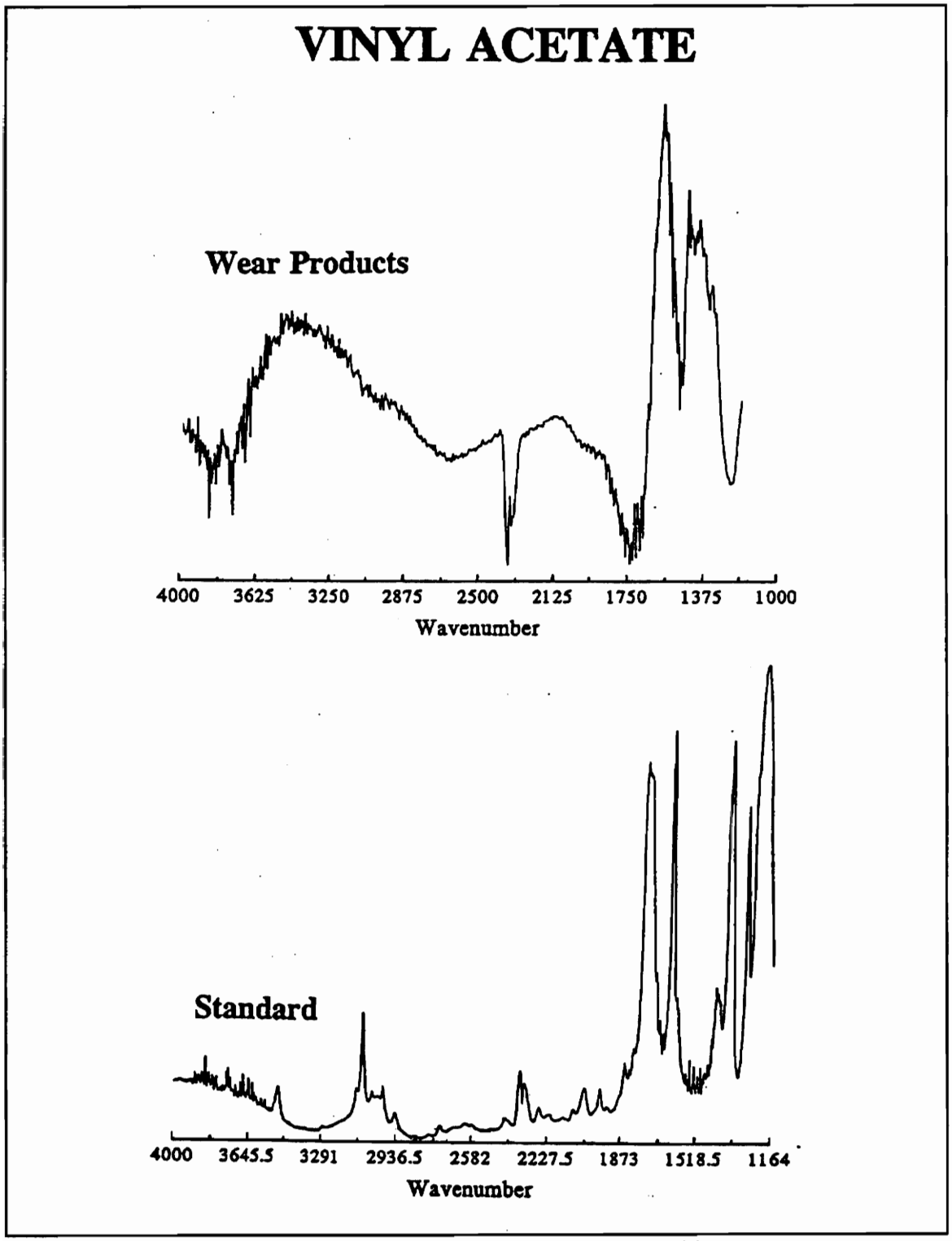

Figure 28 FTIRM Spectra: Vinyl Acetate Vapor 60°C; Bulk 20°C

groups. This is typical of most vinyl type monomers as saturated bonds generally appear at frequencies below 3000 cm^{-1}, and unsaturated bonds appear above 3000 cm^{-1}. In the wear products spectrum, neither of these peaks appears, probably due to noise. Therefore, polymerization cannot be proven nor can it be ruled it out.

Figure 29 shows the FTIRM spectra for diallyl phthalate. This spectra provides strong evidence for the polymerization mechanism of diallyl phthalate. The standard spectrum shows peaks in the region from 2880 to 3080 cm^{-1} which again correspond to C-H stretching vibrations. Several peaks appear in this region due not only to saturated and unsaturated bonds, but to aromatic bonds as well. In the wear products spectrum, the peaks above 3000 cm^{-1}, characteristic of C-H stretching in the aromatic ring, are missing. A strong peak, however, appears at about 2900 cm^{-1} and no peaks responsible for unsaturations are seen above 3000 cm^{-1}. Although the signal to noise ratio is poor, this suggests a disappearance of or a decrease in the number of double bonds present in the wear products on the surface. The intensity of this saturated C-H stretching peak in the products spectrum is over four times greater than that in the standard. This suggests an increased concentration of CH_2 saturated groups. This can only be explained by a polymerization reaction in which the double bonds of diallyl phthalate molecules are broken to form oligomers/polymer.

The strong peaks at 1725 and 1280 cm^{-1}, common to C=O and C-O-C stretching vibrations in diallyl phthalate monomer, are eliminated in the products spectrum. Instead, four intense peaks are seen between 1730 and 1245 cm^{-1}. The first two peaks

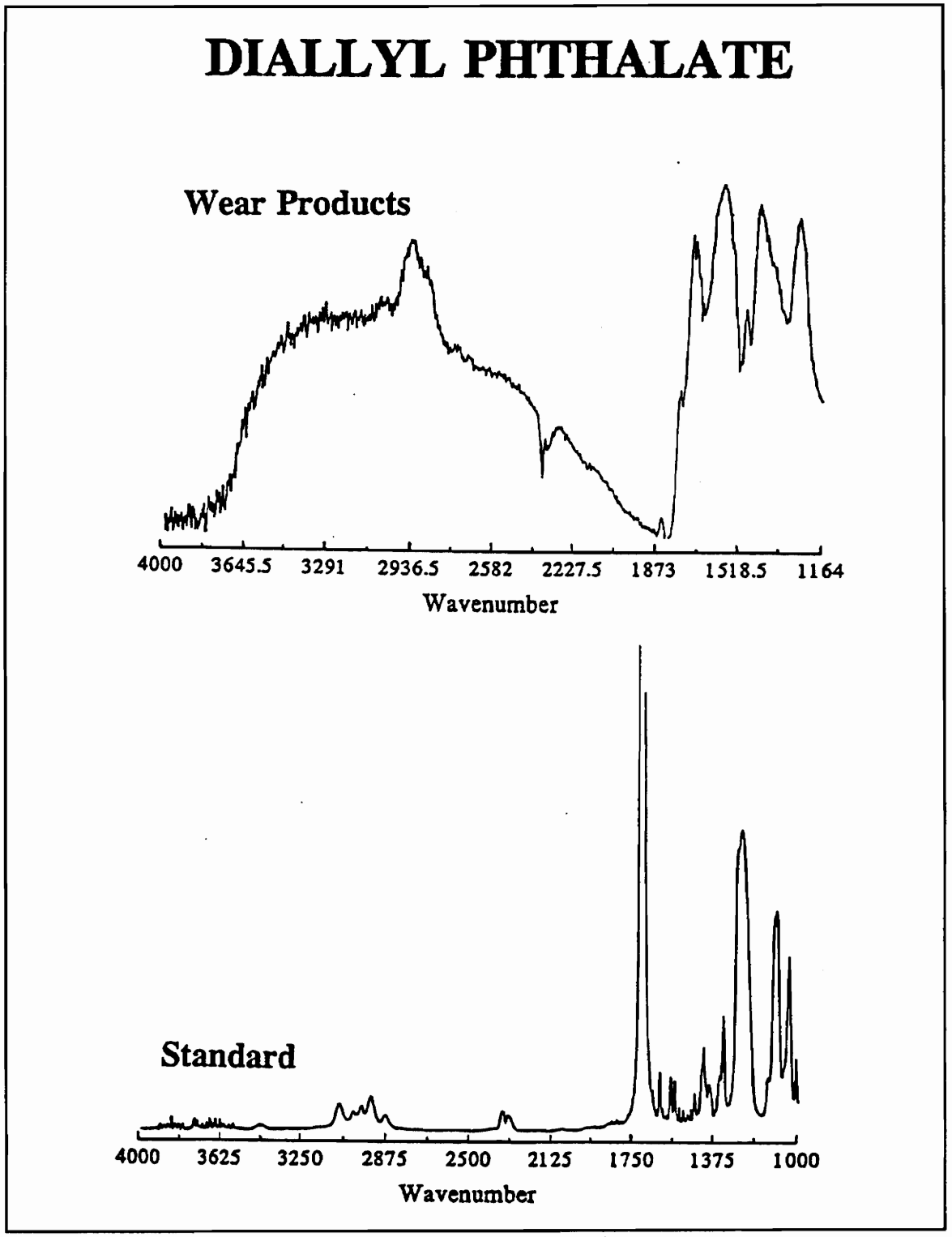

Figure 29 FTIRM Spectra: Diallyl Phthalate Vapor 165°C; Bulk 145°C

between 1730 and 1530 cm^{-1} may have been the result of the asymmetric stretching of C=O bonds in carboxylates commonly found in the region of 1610-1560 cm^{-1}. The second two peaks in the lower region of 1435-1245 cm^{-1} may also be due to the carboxylates as the common region of C=O symmetric stretching is between 1400 and 1300 cm^{-1}. These peaks again suggest a reaction between diallyl phthalate and alumina to form alumina soaps.

Spectra for the wear products of lauryl methacrylate and vinyl octadecyl ether are shown in Figures 30 and 31. In each case, peaks above 3000 cm^{-1} corresponding to unsaturation in the monomer standards cannot be seen. This is likely due to the low ratio of unsaturated C=C bond to saturated C-C bonds for these two monomers. The saturated C-H stretching peaks, seen in the standards below 3000 cm^{-1}, do, however, reappear in the wear products spectra for both monomers. Evidence of polymerization, therefore, cannot be found for either. Though the NIRAM concept would eliminate the possibility of vinyl octadecyl ether polymerization, it is believed that polymerization of either or both of these monomers cannot be conclusively ruled out.

Both of these spectra do include the now characteristic peaks near 1600 and 1400 cm^{-1}, supporting the hypothesized monomer/alumina reactions. As a final note, two saturated C-H stretching peaks appear in the vinyl octadecyl standard with the peak at 1840 cm^{-1} higher than the peaks around 1900 cm^{-1}. In the wear products spectrum, this relationship is reversed. The significance of this and other undiscussed peaks, in all of the analyzed spectra, is not known.

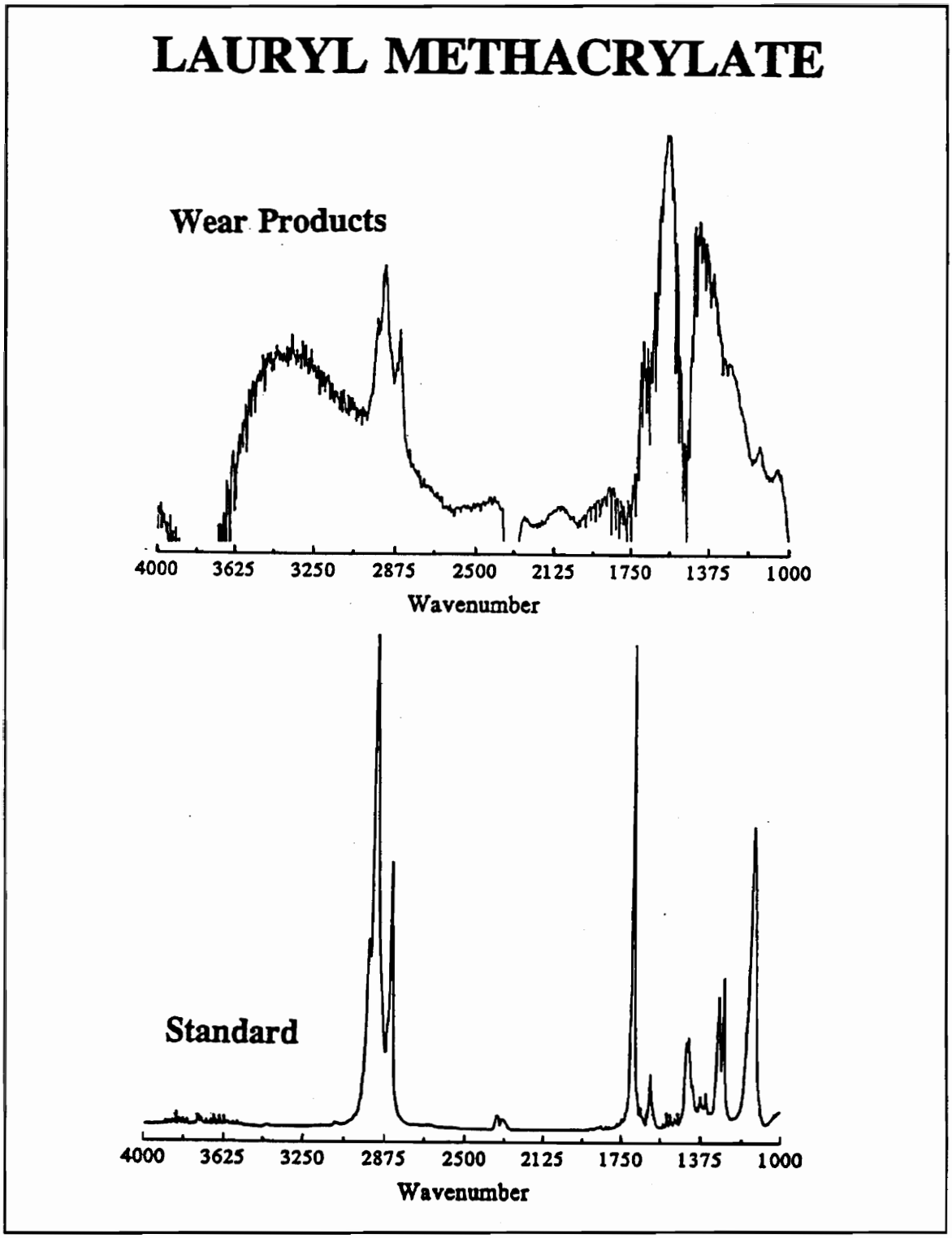

Figure 30 FTIRM Spectra: Lauryl Methacrylate Vapor 140°C; Bulk 145°C

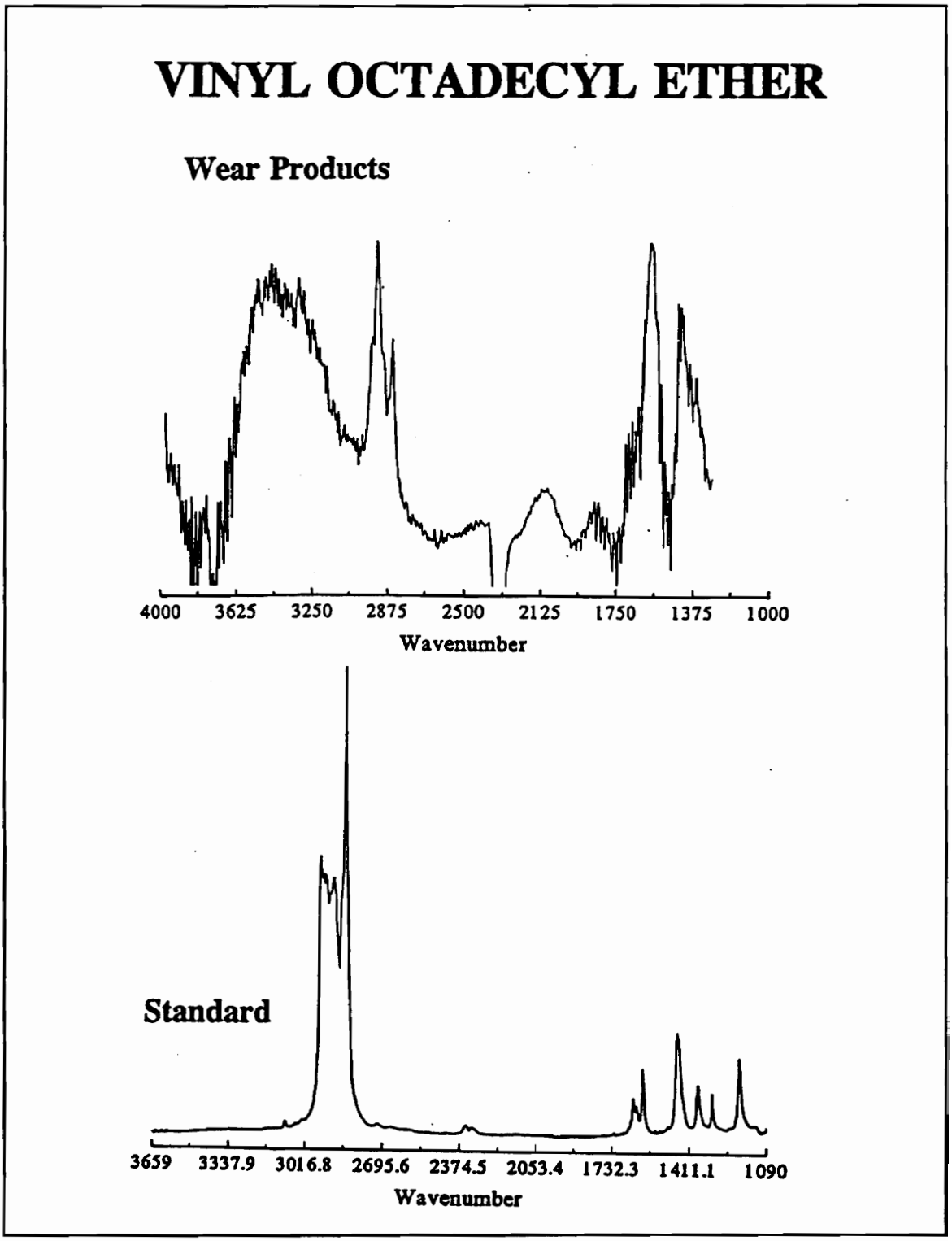

Figure 31 FTIRM Spectra: Vinyl Octadecyl Ether Vapor 165°C; Bulk 145°C

It becomes obvious that the picture is very complex. The analysis presented is very general in nature. The detailed analysis is more difficult to prepare and requires a great level of expertise which the author does not possess. Dr. C. Kajdas provided such expertise in the past (Spring/Summer 1993) and his assistance has been invaluable to the author in learning the basics of the technique. This general analysis does, however, provide some new insights.

Earlier FTIRM work performed on the wear products of hexadecane and hexadecane/monomer tests provided results that were difficult to decipher. It was hypothesized [9] that during hexadecane/monomer lubricated contact, ester groups within the monomer molecules decomposed under tribological conditions form soaps with the alumina surface. It was also shown [10] that soaps could also be formed by the oxidation of hexadecane to form carboxylic acids, which react with aluminum hydroxides. The separation of these hypothesized reactions from one another in a single spectrum is difficult since both are independent and are not mutually exclusive. Having found evidence of alumina soaps in the absence of hexadecane, it can be said conclusively that monomer/alumina reactions do occur and can result in soap and perhaps other chemical product formation.

4.8 Wear Reducing Reaction Mechanisms

A few notes on the difference in wear volumes observed between the nitrogen standard at ambient bulk conditions (20°C) and that of the nitrogen standard at 145°C bulk conditions are in order. It is known that alumina surfaces are highly reactive with water and water vapor [24,33,37] and it would be expected that, in standard atmosphere and at room temperature, an adsorbed surface layer would be present on the surface of an alumina specimen which would include, among other things, adsorbed water vapor. At elevated temperatures, this adsorbed surface layer would be expected to change; water and other molecules would be revaporized and driven off.

This may explain the increase in wear observed for the nitrogen standards at higher bulk temperatures. The effects of water and water vapor on the wear rates of ceramics has been shown in many reports [20,21,23,24,33,36]. Sasaki [24] found that the wear rate of alumina decreased with an increase in relative humidity. This behavior is believed to be due to the formation of wear reducing aluminum hydroxide films [33]. Since samples were exposed to atmospheric air after cleaning for extended periods of time, an adsorbed surface layer of water vapor would have undoubtedly been present. At elevated bulk temperatures, where one would expect adsorbed water molecules to be driven off, wear rates would be expected to increase. This was the case as the average value of ball wear volume for the 145°C nitrogen standard is thirteen times greater than that seen in the ambient standard.

Without adsorbed water vapor, protective aluminum hydroxide films [33] will not form. Without these films, more tribochemically reactive surfaces will be exposed and more adhesion may occur. These mechanisms could be involved in promoting the observed increased friction and wear at high bulk temperatures. It is not known how the presence or absence of aluminum hydroxides affects the mechanism of tribopolymerization.

Tribopolymerization, under all conditions, is expected to be initiated through one of, or a combination of, three factors. Those factors are contact temperature, exoelectron emission, and catalytic effects [9]. Contact temperatures in dry conditions are higher than in lubricated conditions for two reasons -- higher friction and no liquid lubricant to absorb heat.

Nakayama, Hashimoto and others [14-17] have shown that several materials including aluminum oxide films and alumina emit both positively and negatively charged particles during tribological contact in vacuum and in atmosphere. Kadjas [9] has hypothesized that this particle emission may also play an important role in tribopolymerization. Of the additives tested, vinyl acetate and diallyl phthalate polymerize exclusively through the free radical mechanism, lauryl methacrylate polymerizes through anionic or free radical mechanisms, and vinyl octadecyl ether polymerizes through only cationic polymerization [9].

According to Kadjas's negative-ion radical action mechanism (NIRAM), electrons emitted in the contact region are responsible for the creation of active radical and anion

species and thus the initiation of polymerization. Positively charged particles emitted are not considered in this theory and therefore cationic mechanisms of polymerization are not believed to be initiated. By this account, vinyl octadecyl ether should not polymerize and should be ineffective in reducing wear. Previous results in lubricated experiments with alumina-on-alumina [9] have supported this theory. Results presented here, however, do not agree with the NIRAM concept.

It is conceivable that polymerization of vinyl octadecyl ether may be initiated in unlubricated contacts by positively charged particle emission. In lubricated contact, much more mass (i.e., hexadecane) is present in the contact region than in a "dry" vapor phase contact. This additional mass may absorb large portions of charged emissions.

Nakayama, Hashimoto, and Fukuda [15] have shown that the intensity of negative particle emissions from aluminum oxide films is greater than that of positive particles. Having fewer positive than negative particles available, and with much of both being absorbed in the mass of an oil based lubricant system, relatively few charged particles would be available to initiate polymerization. Cationic initiation may not be effective under lubricated tribological conditions simply because the concentration of positively charged particles capable of an initiation reaction is too low.

The effects of adsorbed water vapor on particle emission were also investigated. After drying aluminum oxide films at 150°C, experiments showed marked increases in emissions of both positive and negative particles. Therefore, under dry 145°C bulk temperature conditions where adsorbed water layers would not be present, many more

positively charged particles would be expected in the contact region than under ambient bulk temperature lubricated conditions. These particles may be able to initiate cationic polymerization.

On the other hand, if the NIRAM concept is valid, other catalytic reactions and/or tribochemical reactions may be responsible for the antiwear action of vinyl octadecyl ether vapor in dry contacts. Reactions between vinyl octadecyl ether and the alumina surface have been confirmed by this study; such reactions, rather than tribopolymerization, could be responsible for the anti-wear effects.

One might also consider that both temperature and concentration are the two most important factors governing polymerization. Higher temperatures, such as those found when heating the monomer and the bulk, are conducive to polymerization. Higher concentrations of initiator molecules, such as those believed emitted from the alumina surface under elevated bulk temperatures (versus ambient bulk temperatures), are also conducive to polymerization. Though results show that monomer vapor concentration does not appear to play a role, these other two conditions found at higher temperatures indicate that the probability of polymerization is better at higher monomer/bulk temperatures than at lower monomer/bulk temperatures. The results support this view. An increase in polymerization rate and volume is expected to be more effective at reducing wear. Monomers are more effective in reducing wear in high temperature experiments than in low temperature experiments. This indicates that at higher temperatures (monomer and bulk), potential polymer formers are better at reducing wear.

5.0 CONCLUSIONS: VAPOR PHASE STUDY

1. An existing pin-on-disk machine was adapted for use in exploring the potential of vapor phase tribopolymerization as a method of wear reduction for ceramic-on-ceramic tribological systems.

2. Vinyl monomers selected on the basis of the tribopolymerization concept can cause significant reductions in alumina-on-alumina wear in the vapor phase. Diallyl phthalate vapor and vinyl octadecyl ether vapor reduce alumina ball wear by 99% at elevated temperatures. Lauryl methacrylate vapor and vinyl acetate vapor reduce alumina ball wear by 94% and 65% respectively.

3. Monomer delivery temperatures have a direct and significant effect on wear reduction. Monomers become successively more effective in wear reduction as delivery temperatures increase. The most effective performance is observed when

the monomer delivery temperature is within a few degrees of its boiling point.

4. Over the range observed, monomer concentration does not have a significant effect on wear reduction. Although some weak trends are evident favoring greater wear reduction with higher concentration, large increases in concentration do not necessarily provide additional benefit.

5. At elevated bulk temperatures, monomers in the vapor phase can reduce friction coefficients by as much as half, from 0.8 to 0.4.

6. FTIRM analysis provides strong evidence that reactions between the studied vinyl monomers and alumina occur. The effects of these reactions on wear are not completely understood.

7. FTIRM analysis provides evidence to support the mechanism of tribopolymerization for diallyl phthalate monomer. Although polymerization is not proven in other wear products spectra, it cannot be ruled out.

8. Monomers in the vapor phase can cause large reductions in wear in the absence of any prior surface treatment or added catalytic film to promote a reaction (i.e. as necessary for vapor delivered TCP [28] or hydrocarbon gasses [31,32]).

6.0 RECOMMENDATIONS: VAPOR PHASE STUDY

1. A more controlled atmospheric enclosure needs to be found. Though flow rates were high to ensure a flooded contact region, the absolute elimination of contaminant oxygen, water vapor, or other gasses was not guaranteed.

2. Greater control over monomer concentration needs to be exercised. To do this, a method other than batch heating of a monomer needs to be used for vaporization. A vacuum vaporization or other similar method may be in order.

3. Repeats of some experiments need to be performed, particularly for dry nitrogen and some monomers at ambient bulk temperature conditions. Possible sources of error need to be examined carefully.

4. A better understanding is needed of both positive and negative particle emissions, their intensities, and the catalytic potential of alumina and other ceramic wear surfaces.

7.0 HIGH SPEED, HIGH LOAD PIN-ON-DISK MACHINE

7.1 Introduction

In research at Virginia Polytechnic Institute and State University, experiments have been carried out under primarily low load, low speed conditions such as those listed in Table IV. The contact pressures are high in these experiments but frictional heat generation and contact temperatures are relatively low considering where ceramics will find application (i.e., turbomachinery, automotive engine components, etc.). Questions arise concerning the effectiveness of tribopolymerization under the more severe conditions of high load, high speed, high contact temperature conditions that may be seen in practice. It is then of interest to provide bench test conditions that more closely reflect real world conditions under which ceramics and tribopolymerization will find application. In order to provide such test conditions, a new pin-on-disk machine has been designed and built.

Table IV Currently Used Pin-on-Disk Test Conditions at V.P.I. & S.U.

System:	Material A-on-Material A or Material A-on Material B etc.
Geometry:	Sphere-on-Flat: Fixed Ball on Rotating Disk
Specimen Size:	3.2 mm (1/8 in.) Ball on 25 mm (1 in.) Diameter Disk
Lubricants:	Hexadecane + Selected Monomers
Applied Load:	5 N to 40 N (Maximum)
Sliding Velocity:	0.25 m/s
Sliding Distance:	500 m (Variable)
Ambient Temperature:	20°C to 23°C
Relative Humidity:	Uncontrolled Atmospheric Conditions: 35% to 45%

7.2 Review of Ceramic Tribology and Design Development

Ceramic tribology is a relatively new area where applications consist of journal bearings, bushings, cutting tools, diesel engine parts, and gas turbine parts to name a few [38,39,40,41]. Data collected on ceramic tribology is often limited, however, to qualitative analyses or just a few data points [40].

Cranmer [40] provides a comprehensive review of the basic theory and

mechanisms behind the science of ceramic tribology. An outline of the conventional mechanical models and equations for theoretical prediction of friction and wear is given. A critical look at common pitfalls in experimental work is presented, including the frequent exclusion of tribochemical considerations and lack of material characterization. Cranmer notes that ceramic materials often exhibit different mechanical properties from lot-to-lot if not from piece-to-piece. Without good material characterization, properties can vary widely and results in seemingly identical tests can confuse or distort otherwise valuable scientific research.

Theoretical fracture and abrasion models of mechanical wear, rather than adhesion, are often applied to high normal load conditions and tend to agree with observations [33,35,40]. Mechanical wear of ceramics increases in severity from ploughing, to powder formation, to large flake formation (on the order of the apparent area of contact) with increasing normal load. Wear mode maps that correspond to such mechanisms have been suggested by experiment [35,41]. Although adhesion must certainly still occur under high normal load conditions, its effects are overshadowed by the brittleness of ceramics. Fracture mechanics, rather than adhesion or tribochemical reactions, dominates high normal load ceramic friction and wear.

These more severe mechanisms of ceramic wear are likely to be encountered in practice where high demands will be placed on such materials. The need for a higher speed, higher load, higher contact temperature tribological bench test becomes evident.

7.3 Specification Goals

The design of this new apparatus needed to be versatile for use in dry, lubricated, or vapor phase environments. Ideally the device would also be capable of high sliding speeds, high loads, and high frictional heat generation under environmentally controlled conditions (i.e., high bulk temperatures and controlled atmosphere). Although other geometries are available, the pin-on-disk configuration is one of the simplest. It allows for constant sliding speeds, constant loads, easy analysis, and is more easily aligned than many other geometries. The specifications in Table V were outlined as goals that meet

Table V Minimum System Specification Goals

System:	Solid A-on Solid A or B
Geometry:	Sphere-on-Flat (Fixed Ball on Rotating Disk)
Specimen Size:	1/8 in. Ball (or Larger) on 1 in. Diameter Disk
Specimen Materials:	Alloy Steels and Other Metals.; Ceramics
Applied Load:	1 N to 50 N
Sliding Velocity:	0.1 m/s to 5 m/s
Sliding Distance:	Variable (500 m, 10,000 m, etc.)
Measurements:	Ball and Disk Wear, Friction, Metallic Contact, Surface Damage, Film Formation
Specimen Temperature:	20°C to 500°C
Environment:	Controllable (Air, Nitrogen, Monomers, etc.)

or exceed present state of the art limits in tribological experimentation. These goals were set as ideals with the expectation that a suitable machine meeting such ambitious limits would likely be the product of several iterations and modifications.

7.4 Design Procedure

First and foremost of considerations is the specific geometry of a high load, high speed pin-on-disk apparatus. Most machines of this geometry are characterized by a rotating disk driven from beneath and a fixed pin attached to a cantilever beam and loaded from above. The deflection of this beam is generally used for the measurement of friction and is determined either through displacement transducers or strain gages as illustrated earlier in Figure 3. Loads are generally applied through dead weight.

The combination of dead weight and an elastic element such as the traditional load arm can cause vibrations. In severe contacts such as dry sliding, large vibrational motions can be excited in a standard load arm/cantilever beam arrangement due to the high deflections caused by high friction. When heavier loads (which increase the absolute value of the friction force) or higher coefficients of friction are found, large deflections promote high amplitude forced vibrations. If the force of these vibrations is high enough, dead weight loads may start to swing. As the dead weight moves in reaction to these forced vibrations, inertial forces are built up and the weight swings.

This swing also contains a normal component of force (normal to the contact).

The combined effect of these vibrations is a contact that is no longer a constant load geometry but rather a fluctuating load system. Such behavior has been experienced during dry vapor phase experiments with one of the existing pin-on-disk machines and is easily observed through sight and sound.

Larger moment/loading arms can be used to control large forced vibrations. The tradeoff is lower accuracy in measurements taken with low load, low friction coefficient systems due to smaller deflections. This type of solution may seem reasonable, but other specifics of this type of design make high load arrangements difficult. For instance, if a dead weight system is designed, high loads can be difficult to work with. A 250 N load would require greater than 50 pounds of dead weight. A dead weight of this size is difficult to manipulate. In addition, the supporting structures and load arm would have to be bulky to accommodate such a load.

In addition, disks and other flat rotating specimens are often cemented, bolted, or clamped to a rotating drive surface and the pin specimen is loaded onto this surface from above. High speed dry contacts can accommodate this geometry, but lubricated high speed contacts pose a problem. If a cup to hold lubricant is fixed to the same rotating base as the flat specimen, high speeds will throw the lubricant away from the contact region due to centrifugal force. The presently used system (illustrated earlier in Figure 3) is of this type and performs adequately within its low speed regime. If instead the cup is fixed and the flat rotating specimen is located inside the cup, a rotating seal

must be employed. Such a seal would have to be readily accessible for cleaning or replacement between experiments to eliminate contamination.

These obstacles considered together led to the first design pursued shown in Figure 32. This design consisted of a fixed disk loaded from beneath by a pneumatic actuation system against a pin revolving around the disk's center line in a fixed plane. The design was a modification to a standard milling machine selected for its high speed drive capability and its ability to withstand very high loads. A "pin bit" was designed

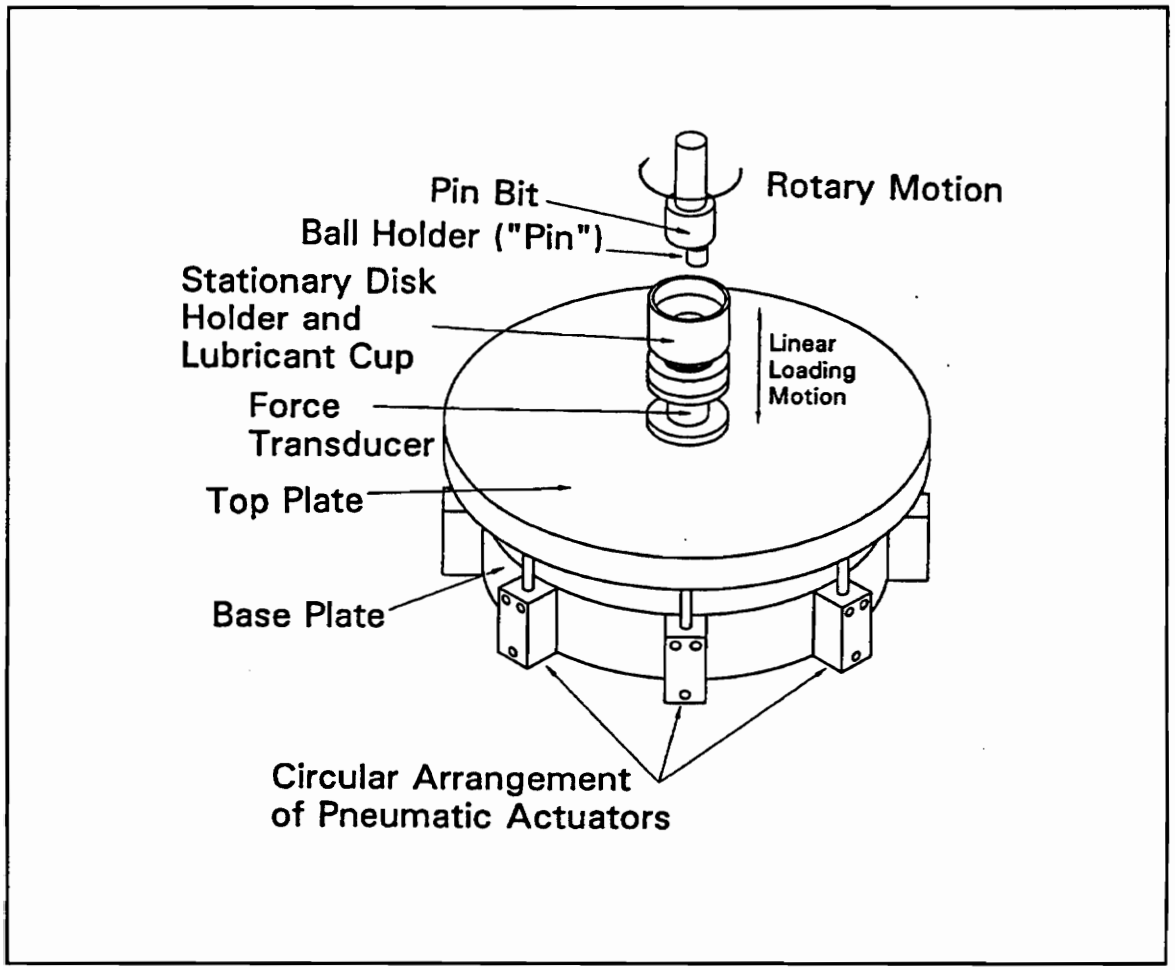

Figure 32 First Design - Circular Arrangement of Actuators

to be inserted into a standard tool holder. A pneumatic loading system provided for high loads while avoiding large, dead weights. The absence of a load/moment arm in the design was expected to eliminate unwanted excess vibrations found in severe contacts. The use of a fixed disk, rotating pin configuration was chosen to change the reference frame of motion only, and to eliminate rotating seals or high speed centrifugal forces on the lubricant.

Alignment in this first design was to be accomplished through the interconnection of the actuators to a single pressure source and the subsequent equilibration of force exerted by each. The top plate was designed in this fashion and expected to tilt in order to accommodate the plane in which the pin was spinning.

Figure 33 illustrates the vibrational characteristics expected to be of concern.

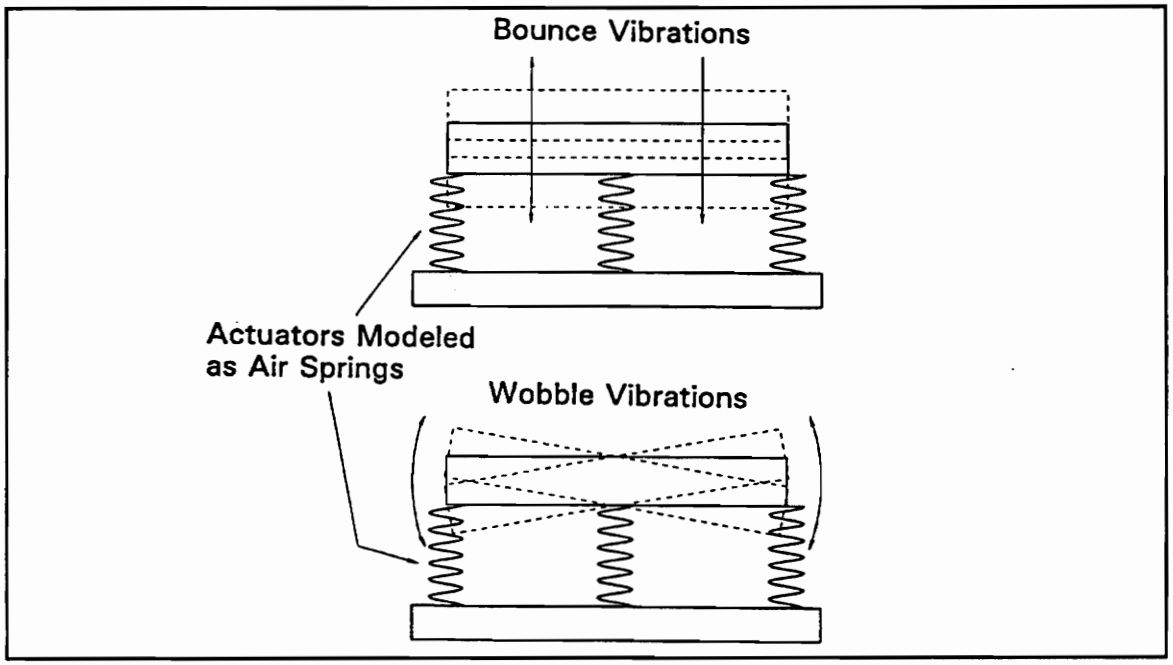

Figure 33 Vibrational Modes of Concern

These included a three dimensional wobble vibration induced by the pin rotation and a bounce vibration normal to the contact examined in Appendix E.

After this analysis, a major design change was made in the loading mechanism. The series of interconnected actuators was replaced by a Firestone Air Spring as shown in Figure 34. This proved to be a mistake. The airspring was expected to operate similarly to what was expected for the series of actuators. Although wobble and bounce vibrational characteristics were expected to be factors, an acceptable model for the

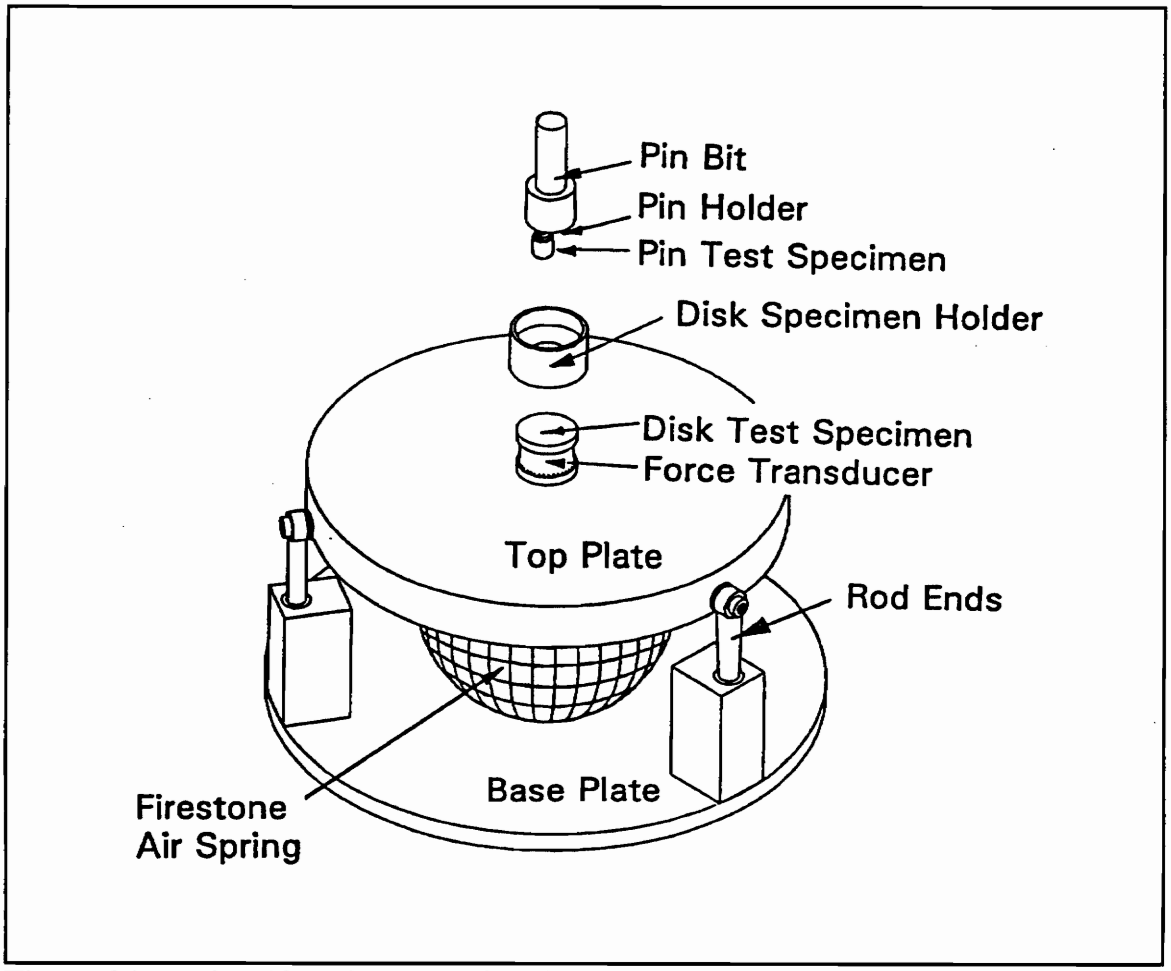

Figure 34 Design #2 - Firestone Airspring

wobble characteristic was not available.

A model for the bounce mode of vibration was given with the literature describing the performance of the air spring. In addition, though theory predicted low natural frequencies for the actuator arrangement, actual natural frequencies were expected to be much higher due to relatively high friction and stiffness in actuator piston/cylinder seals.

Theory predicts very low natural frequencies for the Firestone Airspring arrangement. The Airspring's spring constant, and thus natural frequency, could be driven even lower by increasing loads. In order to do this, a 40 pound steel plate was used to preload the Airspring. This increase in mass is also lowers the natural frequency of the system. This was another mistake contradicting the already known desire to avoid dead weights whose inertial effects can cause vibration difficulties. It was expected that a very low natural frequency system would be as effective as a high natural frequency system as long as the known danger frequencies were avoided.

In the theoretical evaluation of the actuator model, wobble natural frequencies and bounce natural frequencies were close to one another. It was similarly felt that if the bounce characteristics of the Firestone Airspring were sufficiently low, so would wobble vibrations. These unknown wobble vibrations were considered most dangerous to the design as a possible point of difficulty. Bounce vibration was never thought to be of concern. Also, since inherent to the design of the Airspring is its ability to move through an angle, alignment with the plane of the pin rotation was expected to be automatic.

This system was built and, in practice, performed as it was designed to. At low speeds, wobble vibration was indeed a factor. Wobble natural frequencies were close to the rotational speeds intended for low sliding speed experiments. This effect was magnified due to an unconsidered excessive moment arm and an extremely elastic element in the system. The stiffness of a Firestone Airspring is very low and the distance between the point where the friction force was applied and the base of the air spring was almost seven inches. This moment arm allowed low speed wobble to be greatly magnified, thus eliminating the ability to run low speed experiments.

High speed operation proved to be well enough above the system's wobble natural frequency. Low load, high speed performance of the design was good since operation well above natural frequency eliminated dangerous wobble vibration. Preliminary high load tests, however, showed that the system failed in the primary area in which it was designed to operate.

The more severe wear modes encountered under high load induced unexpected bounce vibrations in the system. This caused the pin and disk to bounce against one another and come into and out of contact. The force of this bounce motion was great due in large part to the inertia of the now bouncing 40 pound dead weight on top of the Airspring. As is a well known fact, the impact strength of ceramics is very low. The motions described can be likened to hitting the test specimens with a hammer. As proof, disk specimens in every high load test were broken into several pie shaped pieces. The center of an impact was identified by the point at which the tips of the pie shaped pieces

converged.

The failure of this first design and the lessons learned have been translated into the second design shown in Figures 35 and 36. Photographs of this new device are shown in Figures 37-39. This is again a modification to a milling machine and many of the parts used in the original design are again used here. This time, the standard fixed pin on rotating disk geometry is reintroduced but upside-down with the rotating disk above the pin which is loaded from below. The base, which contains the pin and loading mechanism, is fixed to the milling machine's x-y-z table and the disk is clamped onto a shaft that fits into a standard tool holder.

In the already available low speed pin-on-disk setup, the cup for holding the

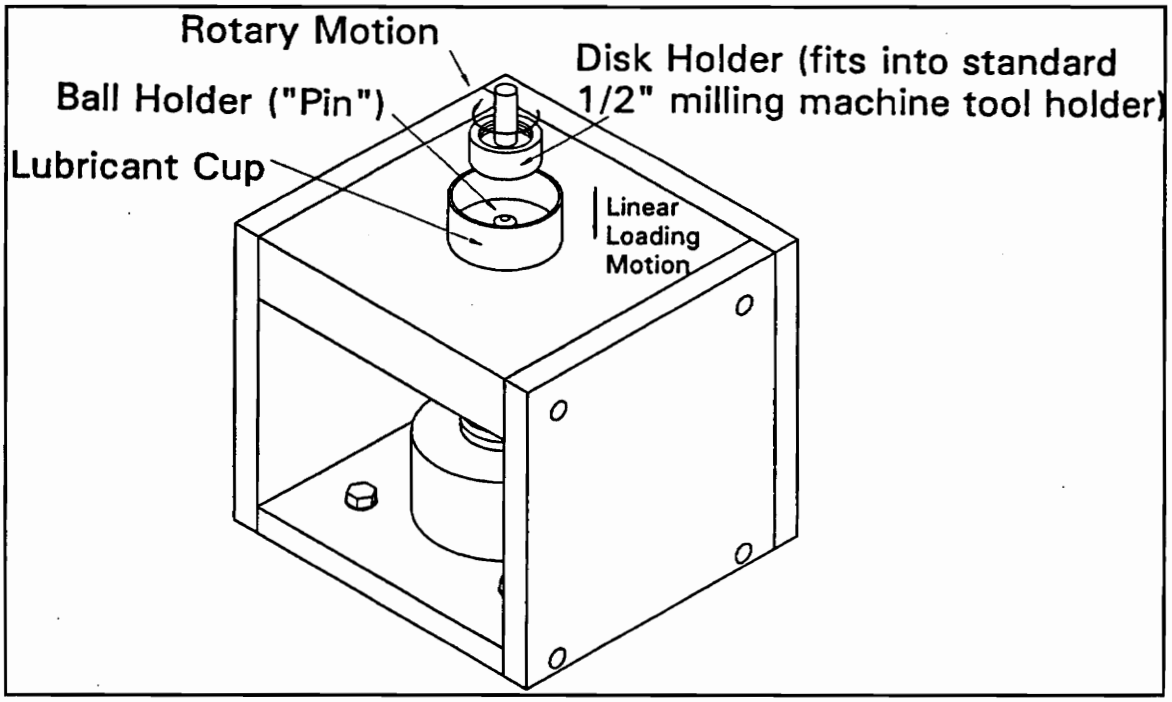

Figure 35 Design #3 - Isometric Solid View

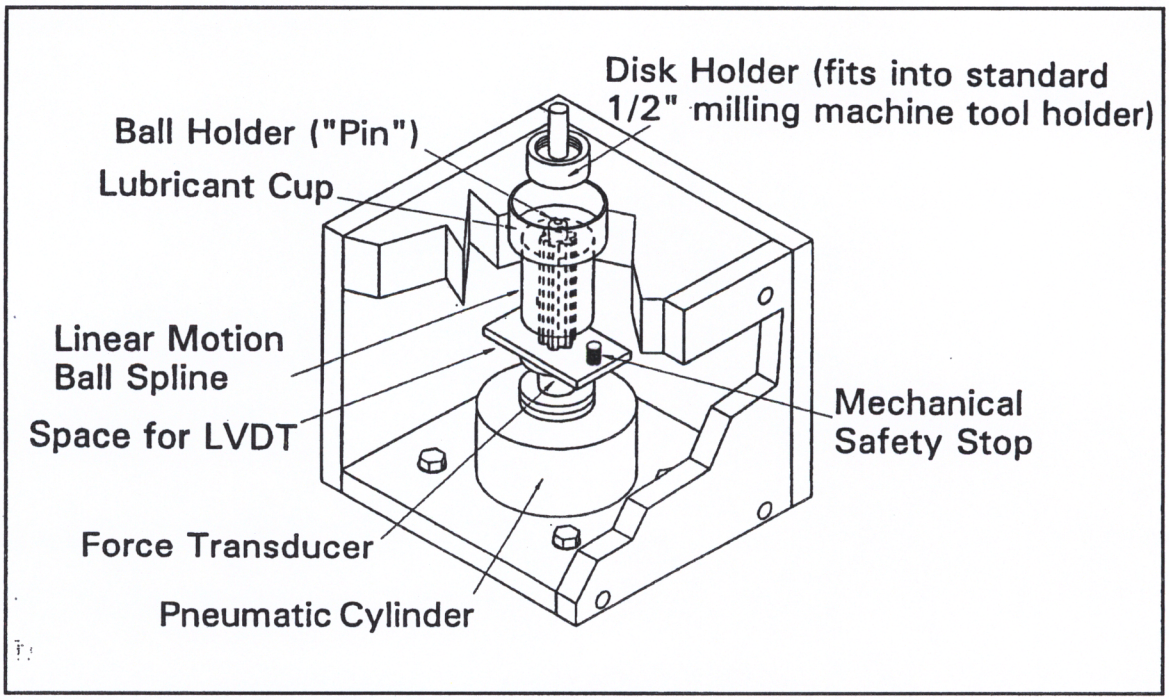

Figure 36 Design #3 - Isometric Cut Away View

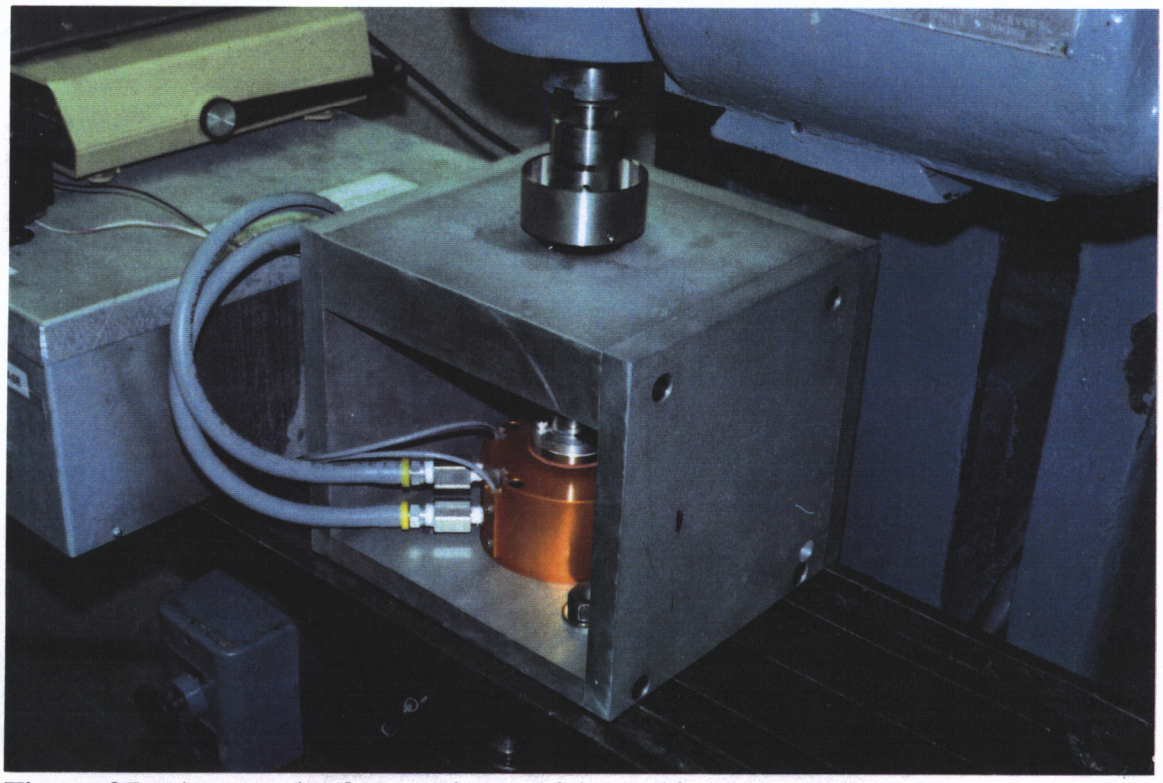

Figure 37 Photograph of New Pin-on-Disk Machine - Isometric

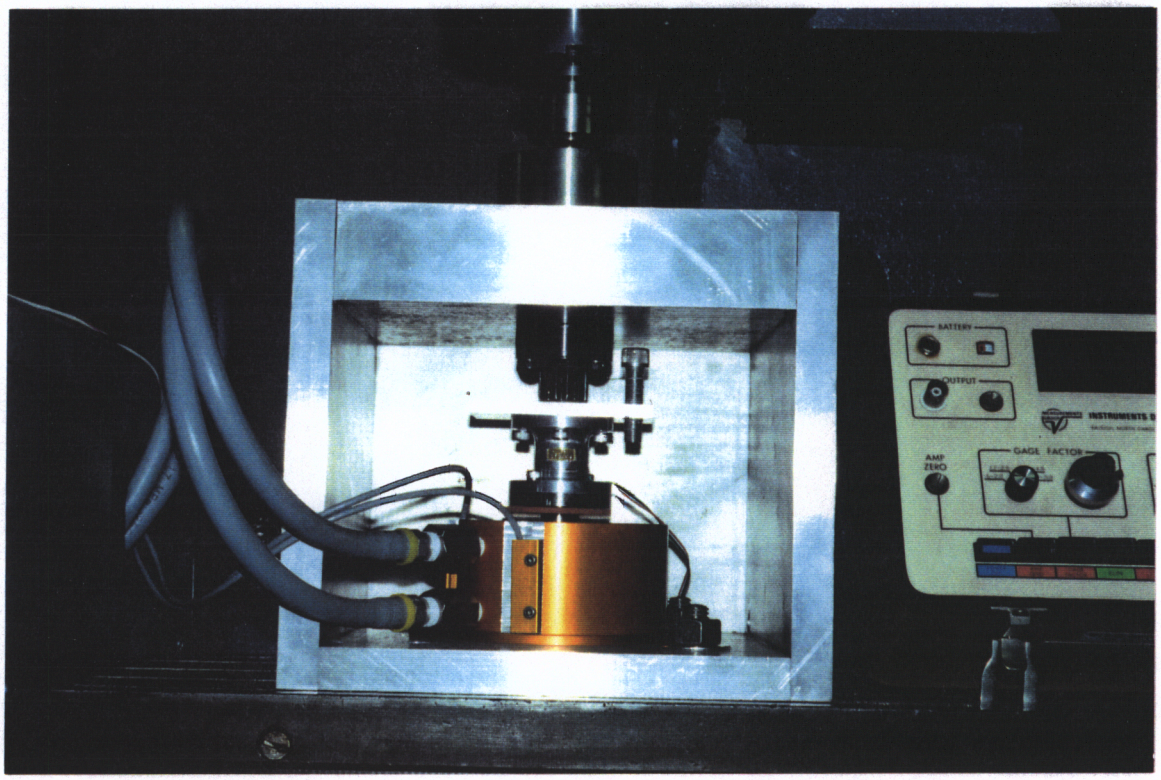

Figure 38 Photograph of New Pin-on-Disk Machine - Detail

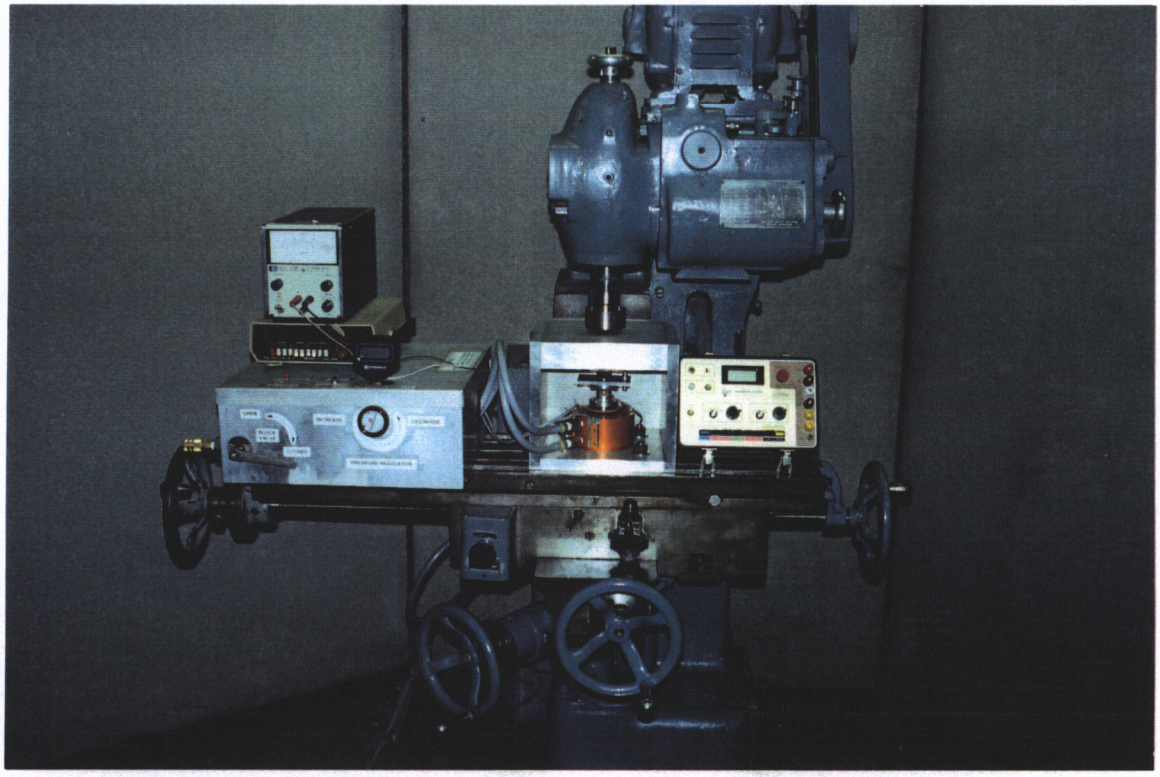

Figure 39 Photograph of New Pin-on-Disk Machine - Full View

lubricant is fixed to the rotating disk. In this new inverted high speed setup, the cup is fixed to the pin holder. This eliminates the need for any type of motion seal. The effects of centrifugal force are also eliminated through the upside-down geometry which allows a fixed lubricant holding cup to be used.

Moment arms, elastic elements, and inertial masses are all but eliminated in this design, effectively limiting all motions in the system to only those that the experimenter desires: disk rotation and load actuation. This stiffness drives natural frequencies higher than can be effectively measured or reached during operation, eliminating concerns of harmonic vibration.

The only "designed" elasticity is in the force transducer located between the actuator and the ball spline. The force transducer is a thin-walled aluminum cylinder with standard Measurements Group, Incorporated, N2A series, 350 ohm, constantan strain gages mounted in a full bridge configuration on the outer wall. An Instron machine was used to calibrate the transducer. The transducer was loaded and data on load, strain, and strain gage voltage output was acquired. The acquired data was used to plot load (N) versus bridge output voltage (V). These calibration curves are shown in Appendix F.

The ball spline has a very low coefficient of friction (0.007) and allows linear motion only. Low friction in the spline facilitates accurate measurement of load. Alignment is all but guaranteed with this geometry. The detailed specifications for this device are given in Table VI.

Table VI Specifications of New Pin-on-Disk Machine

System:	Solid A-on Solid A or B
Geometry:	Sphere-on-Flat (Fixed Ball on Rotating Disk)
Specimen Size:	1/4 in. Ball on 1 in. Diameter Disk
Specimen Materials:	Alloy Steels etc.; High Temperature Materials (Ceramics)
Applied Load:	1 N to 4500 N (= 1000 lbf.) (Maximum Pneumatic Loading Capability with 150 psi Air)
Sliding Velocity:	Variable: 0.1 m/s to 2.66 m/s (2.66 m/s at 4000 r.p.m. max. with a 12.7 mm diameter disk wear scar)
Sliding Distance:	Variable (500 m, 10,000 m, etc.)
Measurements:	Ball and Disk Wear, Load, Easily Modified to Measure Wear Rate
Specimen Temperature:	20°C - 150°C (Using Available Resistance Heater)
Environment:	Atmosphere - Design Easily Enclosed for More Control

An added advantage to this design is the inclusion of a mechanical safety system and an automatic shut-down system. The mechanical system consists of a single bolt, used as a mechanical stop, that can be adjusted to prevent the destruction of the ball holder due to excessive ball wear. The automatic system employs a magnetic piston head in the actuator, two LED indicator Hall effect switches, and a solenoid control valve. The first Hall effect switch simply marks the starting position of the piston head for a

test. As wear occurs, the head of the piston will travel upward. After the piston has traveled a defined distance, the magnetic field created by the piston head will trip the second Hall effect switch which in turn activates the solenoid control valve. The solenoid provides a power return stroke to the actuator pulling the pin away from a danger.

The automatic control system also employs a user operated kill switch. It is intended that this will be used by a researcher in the event of a system failure or for the intentional abortion of an experiment.

Initial tests with steel-on-steel systems have proven very successful. The configuration of this apparatus has come about through trial and lessons learned. Though it is very possible that other geometries may perform with equivalent success and that basic design modifications may improve the performance of this design, the present configuration operates better than expected. Basic design changes and configuration modifications are therefore not recommended. Detailed plans for the machine and all of the associated parts are given in Appendix G.

In contrast to the older pin-on-disk apparatus, this new design has expanded the range of speed, load, and frictional heat generation rates available. Maximum sliding speed has been increased by a factor of over 10 from 0.25 m/s to 2.66 m/s. Maximum loads have been expanded by a factor of 110 from 40 N to over 4500 N. Realistically, loads of 4500 N will never be used and maximum load will depend on the mechanical limitations of the material being tested.

Frictional heat generation is given by the equation:

$$\dot{Q} = \mu \cdot W \cdot V$$

Where:

Q	=	Frictional Heat Generation (Watts),
μ	=	Coefficient of Friction,
W	=	Normal Load (Newtons), and
V	=	Sliding Speed or Velocity (meters/second)

The coefficient of friction for alumina-on-alumina under hexadecane lubricated conditions is in general about 0.1 (estimate from experience). Under these conditions, the maximum frictional heat generation of the older machine under 40 N load and 0.25 m/s sliding speed is 1.0 W.

For alumina ceramics, a maximum 150 N load is realistic and higher loads may be attainable. This is a load increase by a factor of over 3.5. Broadly, however, the machine's estimated capabilities can be summarized as in Table VII.

Table VII New Pin-on-Disk Machine Potential Capabilities

	Maximums (Lubricated Conditions)	Steel-on-Steel	Ceramic-on-Ceramic
Estimated Coefficient of Friction	>0.1	0.1	0.1
Load (N)	4500	375	150
Maximum Sliding Speed (m/s)	2.66	2.66	2.66
Frictional Heat Generation (W)	>1200	100	40

This machine is capable of testing many different materials under high speed, high load, and high frictional heat generation contacts more likely to be seen in practical applications. It will also aid continued research on tribopolymerization where high contact temperature may be an important parameter for wear reduction.

8.0 CONCLUSIONS: PIN-ON-DISK MACHINE

1. A fully operational, well controlled, high load, high speed pin-on-disk machine for use in dry, vapor phase, and liquid lubricated contacts has been designed and constructed.

2. Loads from 0 to 4500 N are possible using a pneumatic cylinder. Realistically, this means that the maximum possible test loads, will be a function of material property limitations and will not be limited by the capability of the machine.

3. Sliding speeds up to 2.66 m/s can be reached with available milling machines.

4. The new pin-on-disk machine is theoretically capable of frictional heat generation rates of over 1200 W. Realistically, due to material load bearing limitations, maximum rates of frictional heat generation will be over 40 W for ceramic-on-ceramic systems and over 100 W for steel-on-steel systems.

5. The design minimizes moving parts in the contact region and can therefore be easily enclosed for environmental control, vapor phase experiments, and bulk heating (possibly 500°C, or more) of the materials being tested.

9.0 RECOMMENDATIONS: PIN-ON-DISK MACHINE

1. The original purpose behind modifying a milling machine was to take advantage of its robust features for high load experiments. For ceramics, this may be unrealistic since most are too brittle to withstand excessively high loads. It is recommended that the use of a smaller milling machine with higher rotational speeds be explored.

2. Since this design limits moving parts in the contact region, it lends itself to enclosure for atmospheric control. This would provide a means for continued research on vapor phase tribopolymerization under higher speed and higher load conditions.

3. Bulk temperature control of material specimens is also easily found with the addition of the enclosed environment. Proper insulation and use of radiative heaters will provide high temperature (500°C or more) environments.

4. Lubricant temperature should be monitored since exploratory tests have shown that lubricant temperature rises rapidly due to high frictional heat generation. Ideally, a standard chromel/alumel thermocouple may be used.

5. Direct heating of the lubricant using conductive heaters attached to the lubricant cup may also be explored.

6. A method of measuring friction in this geometry is also desirable. A force transducer of sorts may be incorporated underneath the pin and lubricant cup but in the interest of eliminating moment arms and elastic elements, this may not be the best alternative. Ideally, a torque transducer attached to the shaft of the rotating disk holder could be employed.

7. A Linear Voltage Displacement Transducer (LVDT) can easily be attached to the force transducer support structure. It is highly recommended that this piece of instrumentation be included for the measurement of actual wear rates as they are occurring during an experiment.

8. Vibrations occurring during sliding normal to the contact should be measured with an accelerometer mounted on the force transducer support structure.

9. Metallic-on-metallic contact measurements could easily be made with the addition of a slip-ring on the disk holder shaft. If good electrical contact can be made between the steel holders and electrically conductive specimens, electric potential across the interface could be measured.

10. Electronic data acquisition for all of these features should be pursued. Load, friction, vibration, bulk temperature, lubricant frictional heating temperature rise, wear rate, and metallic contact all provide possibilities for electronic data analysis techniques; especially measurements of correlation.

11. Initial tests need to be performed such that wear rate comparisons can be made between the new and old pin-on-disk machines. This will facilitate the correlation of future data with past results.

12. New fixtures for different size and shape test specimens should be constructed since the design is easily adaptable to different configurations (i.e., different ball sizes, flat-on-flat tests, etc.)

13. Since load is not measured directly from the contact, % error in the load measured by the force transducer below the ball spline shaft versus actual load above the ball spline shaft (at the point of contact) should be determined.

14. The solenoid valve safety system operates on a DC power source and is in its present state "unprotected" from a voltage supply opposite that which is needed for proper operation. Electronic protection should be built into the circuit in order to prevent destruction of the system. Battery operation may also be an option.

REFERENCES

1. Furey, M. J., Tribology. In *Encyclopedia of Materials Science and Engineering*, Editor-in-Chief M. B. Bever, Pergamon Press, Oxford, 1986, pp. 5145-5157.

2. "Ceramic Lubrication by Tribopolymerization: A Proposal for Research and Industrial Development," Proposal Submitted to the United States Department of Energy, Principal Investigators: M. J. Furey and C. Kajdas, November 1991.

3. Furey., M. J., and Kajdas, C., "Tribopolymerization as a Novel Approach to Ceramic Lubrication," *4th International Symposium on Ceramic Materials and Components for Engines*, June 10-12, 1991, Goteborg, Sweden.

4. Furey, M. J., "The Formation of Polymeric Films Directly on Rubbing Surfaces to Reduce Wear", *Wear*, 1973, 26, pp. 369-392.

5. Furey, M. J., "The in situ Formation of Polymeric Films on Rubbing Surfaces," *Proc. International Collog. Polymers and Lubrication*, Brest, Centre National de la Recherche Scientifique, Paris, No. 233, 1975, pp. 393-404.

6. Furey, M. J., Kajdas, C., Ward, T. C. and Hellgeth, J. W., "Thermal and Catalytic Effects on Tribopolymerization as a New Boundary Lubrication Mechanism," Plenary Lecture (MJF), *5th International Congress on Tribology*, Helsinki, Finland, June 12-15, 1989; also published in *Wear*, 1990, 136, pp. 85-97.

7. Furey, M. J., and Kajdas, C., "Tribopolymerization as an Antiwear Mechanism," *Symposium on Surface Science Applications and Advances in Tribology*, Division of Colloid and Surface Chemistry, 201st National Meeting, American Chemical Society, Atlanta, GA, April 14-19, 1991.

8. Furey, M. J., and Kajdas, C., "Models of Tribopolymerization as an Anti-Wear Mechanism," *Proceedings of the Japan International Tribology Conference*, 1990, Nagoya, Japan.

9. Furey, M. J., Kajdas, C., Kempinski, R. and Tripathy, B. S., "Tribology of Ceramics: Antiwear Action of Vinyl Monomers," *Annual Meeting of the Society of Tribologists and Lubrication Engineers*, Pittsburgh, PA, 1994.

10. Furey, M. J., Kajdas, C., Kempinski, R. and Tripathy, B. S., "Tribopolymerization and the Behavior of Oxygen-Containing Monomers in

Reducing Ceramic Wear," Paper, EUROTRIB '93 Congress, Budapest, Hungry, Aug. 30 - Sept. 2, 1993, *Proceedings*, Vol. 2, pp. 477-484.

11. Furey, M. J., "The Formation of Polymeric Films Directly on Rubbing Surfaces to Reduce Wear," *Wear*, 1973, 26, pp. 369-392.

12. Final Report to National Science Foundation on "The Role of Temperatures in Tribopolymerization as a Mechanism of Boundary Lubrication," by M. J. Furey, C. Kajdas, and T. C. Ward, Virginia Polytechnic Institute and State University, Blacksburg, VA, 1989.

13. "A New Approach to Ceramic Lubrication: Tribopolymerization," Proposal Submitted to the National Science Foundation, Principal Investigators: M. J. Furey and C. Kajdas.

14. Nakayama, K., Fujiwara, T. and Hashimoto, H., "Exoelectron Measurement Apparatus Incorporated in a Scanning Electron Microscope," *The Institute of Physics*, 1984, pp. 1199-1203.

15. Nakayama, K., Hashimoto, H., and Fukuda, Y., "Triboemission from Aluminum Oxide Film in Atmosphere," *Proc. Japan International Tribology Conference*, Nagoya, 1990, pp. 1411-1146.

16. Nakayama, K., Suzuki, N., and Hashimoto, H., "Triboemission of Charged Particles and Photons from Solid Surfaces During Frictional Damage," 1991.

17. Nakayama, K., and Hashimoto, H., "Triboemission from Various Materials in Atmosphere," *Wear*, 1991, 147, pp. 335-343.

18. Marin-Lefleche, P., "A Study of Tribopolymerization Under Fretting Conditions," Master of Science Thesis, Dept. of Mechanical Engineering, Virginia Polytechnic Institute and State University, Blacksburg, VA, May 1990.

19. Marin-Lafleche, P., Kajdas, C., Furey, M. J., Ward, T. C., and Hellgeth, J. W., "A Study of Tribopolymerization Under Fretting Contact Conditions," *8th International Colloq. Tribology "Tribology 2000"*, Esslingen, Germany, Jan. 14-16, 1992.

20. Fischer, T. E., and Tomizawa, H., "Interaction of Tribochemistry and Microstructure in the Friction and Wear of Silicon Nitride," *Wear*, 1985, 105, pp. 29-45.

21. Ishigaki, H., Kawaguchi, I., Iwasa, M., and Toibana, Y., "Friction and Wear of Hot Pressed Silicon Nitride, and Other Ceramics," *Wear of Materials*, 1985, K. C. Ludema (Ed.), ASME, New York, 1985, pp. 13-21.

22. Scott, H. G., "Friction and Wear of Zirconia at Very Low Sliding Speeds," *Wear of Materials*, 1985, K. C. Ludema (Ed.), ASME, New York, 1985, pp. 8-12.

23. Fischer, T. E., Anderson, M. P., Jahanmir, S., and Salher, R., "Friction and Wear of Tough and Brittle Zirconia in Nitrogen, Air, Water, Hexadecane, and Hexadecane Containing Stearic Acid" *Wear*, 1988, 124, pp. 133-148.

24. Sasaki, S., "The Effect of Surrounding Atmosphere on the Friction and Wear of Alumina, Zirconia, Silicon Carbide, and Silicon Nitride," *Wear of Materials*, 1989, K. Ludema (Ed.), ASME, New York, 1989, pp. 409-417; *Wear*, 1989, 134, pp. 185-200.

25. Graham, E. E. and Klaus, E. E., "Lubrication from the Vapor Phase at High Temperatures," *ASLE Transactions*, 1985, 29, 2, pp. 229-234.

26. Klaus, E. E., Jeng, G. S., and Duda, J. L., "A Study of Tricresyl Phosphate as a Vapor Delivered Lubricant," *Lubrication Engineering*, 45, 11, pp. 717-723.

27. Makki, J. F. and Graham, E. E., "Vapor Deposition on High Temperature Surfaces," *Tribology Transactions*, 1989, 33, 4, pp. 595-603.

28. Makki, J. and Graham, E. E., "Formation of Solid Films from the Vapor Phase on High Temperature Surfaces," *Lubrication Engineering*, 1990, 47, 3, pp. 199-206.

29. Hanyaloglu, B. and Graham, E. E., "Effect of Surface Condition on Formation of Solid Lubricating Films at High Temperatures," *Tribology Transactions*, 1991, 35, 1, pp. 77-82.

30. Hanyaloglu, B. and Graham, E. E., "Effect of Surface Temperature on Vapor Phase Lubrication," *Lubrication Engineering*, March 1993, 49, 3, pp. 227-232.

31. Lauer, J. L. and Dwyer, S. R., "Continuous High Temperature Lubrication of Ceramics by Carbon Generated Catalytically form Hydrocarbon Gases," *Tribology Transactions*, 1990, 33, 4, pp. 529-534.

32. Lauer, J. L. and Dwyer, S. R., "Lubrication of Ceramics by Surface-Generated Carbon form Gaseous Feed," *Proc. Japan International Tribology Conference*, Nagoya, Japan, 1990, pp. 989-994.

33. Gee, M. G., "Sliding Wear of Alumina," *Journal of Hard Materials*, Vol. 3 (3-4), 1992, pp. 363-377.

34. *CRC Handbook of Chemistry and Physics*, Robert C. Weast, Ed., CRC Press Inc., Florida, Vol. 67, 1986-1987.

35. Hokkirigawa, K., "Wear Mode Map of Ceramics," *Wear*, Vol. 151, 1991, pp. 219-228.

36. Buckley, D. H., and Miyoshi, K., "Tribological Properties of Structural Ceramics," *Structural Ceramics; Treatise on Materials Science and Technology*, Vol. 29, John B. Watchman, Ed., Academic Press, Inc., New York, 1989, pp. 293-365.

37. Vollhardt, K. P. C., *Organic Chemistry*, W. H. Freeman and Company, New York, 1987, pp. 441-442.

38. Hogmark, S., Olsson, M., and Blomberg, A., "Wear Mechanisms of Advanced Ceramic Materials," *Journal of Hard Materials*, Vol. 3 (2), 1992, pp. 153-167.

39. Schawartz, M., Editor in Chief, *Handbook of Structural Ceramics, McGraw-Hill Incorporated*, New York, 1992.

40. Cranmer, D. C., "Ceramic Tribology-Needs and Opportunities," *Tribology Transactions*, Vol. 31 (2), May 1987, pp. 164-173.

41. Kato, K.,"Tribology of Ceramics," *Wear*, Vol. 136, 1990, pp. 117-133.

42. Ott, L., *An Introduction to Statistical Methods and Data Analysis*, Third Edition, P. S. W. Kent Publishing Company, Boston, 1988.

43. Harris, C. M., and Crede, C. E., *Shock and Vibration Handbook, Second Edition*, McGraw-Hill Book Company, New York, 1976.

44. Firestone Company, *Firestone Airmount Actuators/Airmount Isolators Engineering Design Manual*, 1993.

APPENDIX A

Variable Voltage Transformer/Resistance Heater

Bulk Temperature Calibration

A variable voltage transformer or "Variac" was connected to a ring shaped resistance heater. The Variac itself employs a rotary dial coupled to a potentiometer. The face of this dial was divided into equal segments and then numbered. Figure 40 shows the heater positioned around the pin-on-disk contact region as it was to be used during a real experiment.

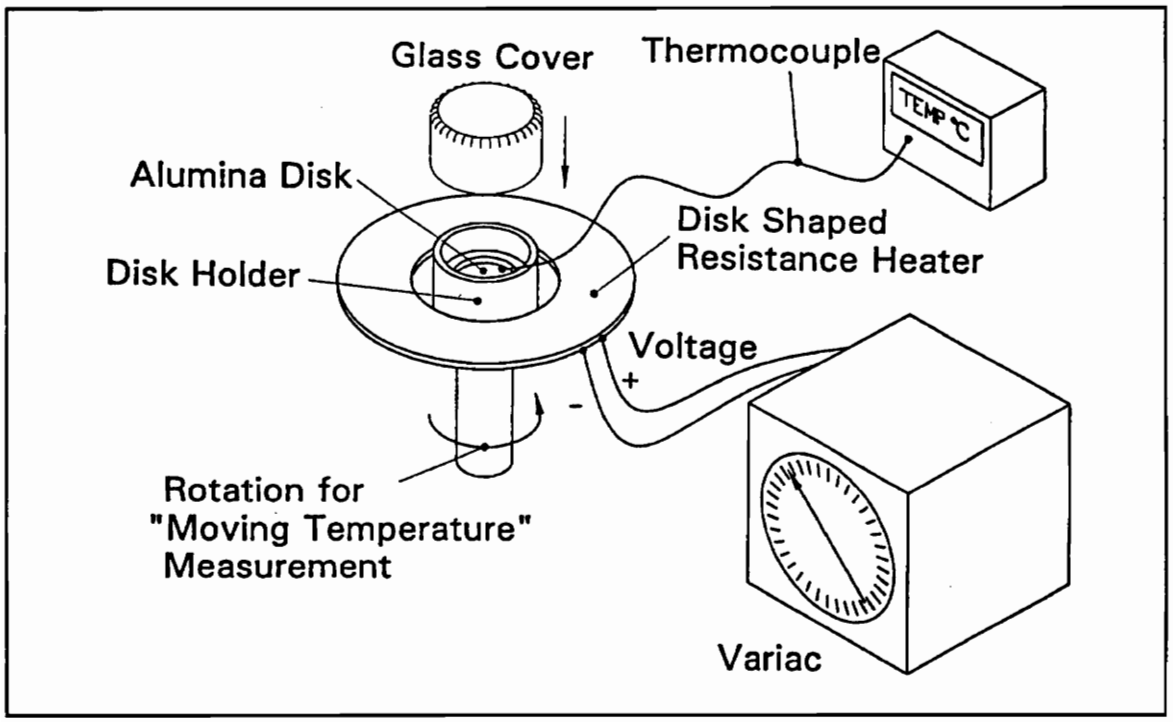

Figure 40 Configuration for Bulk Temperature Calibration

Bulk temperature was calibrated using a standard chromel/alumel thermocouple placed in contact with the surface of an alumina disk properly positioned with the glass cover secured over the region. A setting on the variac dial was selected and the region was allowed to heat. Temperature was checked every few minutes until it reached an equilibrium condition. At first, temperature was checked continuously for 20 minute periods. Bulk equilibrium was reached about 10-12 minutes after the heater itself reached its equilibrium temperature. These temperatures are recorded as "standing temperature" in Figure 41.

In the next step, the rotary motion of the disk was started. After 10 minutes, the disk was stopped and quickly, the thermocouple was brought into contact with the alumina disk surface. These temperatures are recorded as "moving temperature" in Figure 41 and are considered the bulk temperatures of the contact region during a sliding experiment when the variac was set to the corresponding position. Typically, all elevated bulk temperature experiments utilized the maximum variac setting, corresponding to a 145°C bulk temperature condition.

The following equations govern the regression line fit to the corresponding data points for both standing and moving temperatures. The letter "V" in these equations stands for the number on the variac dial to which the device was set to.

$$StandingTemperature\ (^{\circ}C) = 0.096\ V^2 + 2.094\ V + 16.482$$

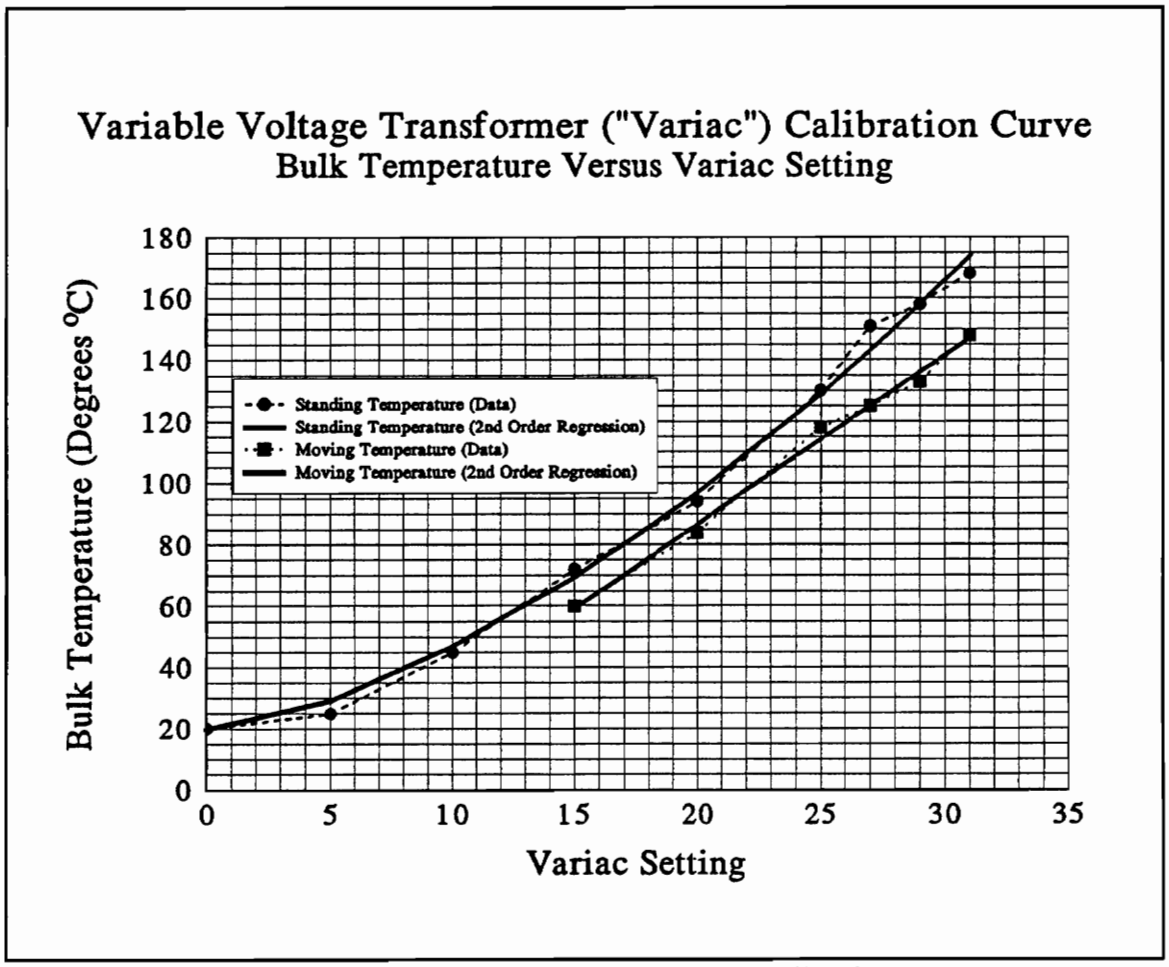

Figure 41 Variable Voltage Transformer Temperature Calibration Curve

$$MovingTemperature\ (°C) = -0.001\ V^2 + 5.521\ V - 23.394$$

Repeated tests of this procedure showed that this calibration of the variac and resistance heater was very repeatable.

APPENDIX B

Thermodynamic Vapor Mass Estimation

In order to estimate the mass of monomer that would be vaporized during an experiment, some straightforward thermodynamic relationships were considered. The goal was to conservatively estimate the mass of monomer that would be used during an experiment. Given that there was no method of measuring heat input into the system, certain assumptions were made to make the analysis possible:

1) **Adiabatic Monomer Heating System** - The heater itself is a well insulated device, and since its shape conforms to that of the boiling flask, an adiabatic wall around the flask is created in this configuration. In addition, though heat is being transferred to the system, the majority of the connecting tubes were short and made from materials whose materials do not readily transfer heat well, lending additional support to the validity of this assumption.

2) **Vinyl Acetate Vapor Mass** - Since vinyl acetate is the most volatile of the additives tested, an estimate of the mass of vapor formed under any given condition will be greater than the volume formed by any other monomer. This will provide an upper limit to mass of vapor that any of the additives would form under given conditions.

3) **Nitrogen Exiting the Flask is Saturated** - Since we are interested in an upper bound value of mass flow to insure that a test will run to completion, this assumption will provide an inflated estimate. This is a poor assumption for the reality of the situation, but rather, it serves the purpose at hand.

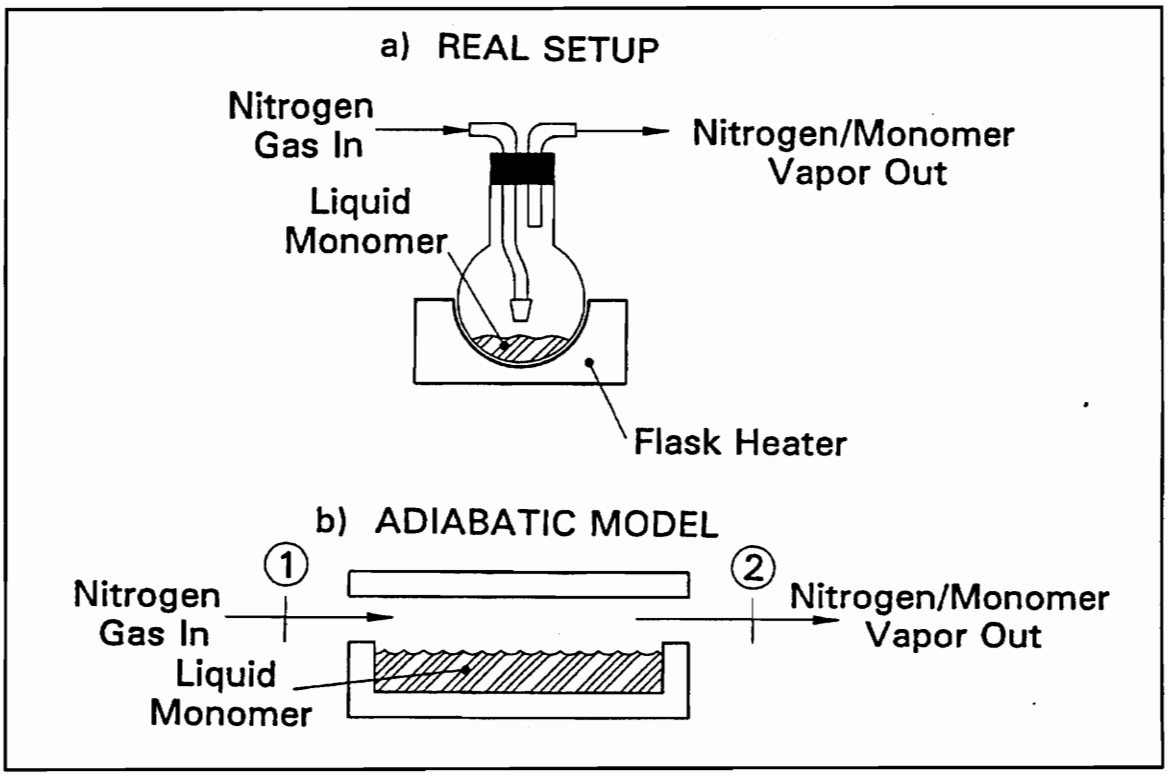

Figure 42 Comparison of Real and Thermodynamic Models

The real setup as used during experiments is shown in Figure 42a and the adiabatic model used to estimate the vapor mass to be consumed during a test is shown in Figure 42b. Table VIII contains vapor pressure data for vinyl acetate found in the CRC Handbook of Chemistry and Physics [34].

Table VIII Vinyl Acetate Vapor Pressures [34]

Vinyl Acetate Vapor Pressures
1 mmHg = 133.3 Pa

Vapor Pressure (mmHg)	1 mm	10 mm	40	100	400	760
Temperature (°C)	-48.0	-18.9	5.3	23.3	55.5	72.5

In the equations that follow, this notation is applies:

1 and 2 :	(Subscripts) refer to states at the inlet and exit of the flask as shown in Figure 42b;
C_p :	Constant Pressure Specific Heat;
T :	Temperature
N :	Nitrogen Gas;
V :	Monomer Vapor;
m :	Mass Flow;
h :	Enthalpy;
$fg_{monomer}$:	Refers to the change in state for the monomer between the liquid and vapor states;
R :	Gas Constant (for a particular substance)

Using the adiabatic assumption, the first law reduces to:

$$C_{pN}\,(T_2 - T_1) = \frac{m_{V2}}{m_{N2}}\,h_{fg_{monomer}}$$

Everything in this equation is known or can be measured except m_V and $h_{fg\text{-}monomer}$. Since a table of change in enthalpy for the selected monomers was not found readily available, the Clapeyron Equation was used to estimate $h_{fg\text{-}monomer}$ using the vapor pressure data found in the CRC Handbook. Manipulation of this equation gives:

$$\ln\left(\frac{P_2}{P_1}\right) = \frac{h_{fg\ Vinyl\ Acetate}}{R_{Vinyl\ Acetate}}\left(\frac{T_2 - T_1}{T_1 T_2}\right)$$

Substitution of 0.09688 kJ/kg·K for $R_{vinyl\ acetate}$ 40 mmHg for P_1, 278.3 K for T_1, 400 mmHg for P_2, and 328.5 K for T_2 gives:

$$h_{fg\ Vinyl\ Acetate} = 405.5\ \frac{kJ}{kg}$$

Returning next to the First Law and substituting 1.0416 kJ/kg·K for the C_p of Nitrogen at 300 K, 189.14 kg/m^3 for the density of Nitrogen at 300 K, 1 L/min for the volume flow of nitrogen, and a estimated 1°C for T_2-T_1, the mass of vinyl acetate monomer used per minute can be determined:

$$\left(1.0416\frac{kJ}{kg\cdot K}\right)(\ 1.0\ K\ ) = \frac{m_{Vinyl\ Acetate}}{\left(1\frac{L}{\min}\right)\left(0.001\frac{m^3}{L}\right)\left(189.14\frac{kg}{m^3}\right)}\left(405.5\frac{kJ}{kg}\right)$$

This yields:

$$_{Vinyl\ Acetate} = 0.486\ \frac{g}{\min}$$

Since one experiment requires 33⅓ minutes to reach the specified 500 meter sliding distance, this translates to:

$$m_{Vinyl\ Acetate} = 16.2\ \frac{grams}{experiment}$$

In addition to this analysis, a simple use of the ideal gas law was explored as an additional reference point. At room temperature, approximately 23.3°C, the CRC Handbook gives a value of 100 mmHg for the vapor pressure of vinyl acetate. Using the ideal gas law,

$$P \cdot V = m \cdot R \cdot T$$

substituting known values for P, R, and T, and selecting V = 1 Liter, we find that the mass of vinyl acetate vapor which will saturate 1 liter of nitrogen is:

$$m_{Vinyl\ Acetate} = 0.4653\ \frac{g}{L}$$

During one experiment (1 L/min for 33⅓ minutes) this translates to:

$$m_{Vinyl\ Acetate} = 15.4\ \frac{grams}{experiment}$$

This result corresponds well with the previous approach, as was expected due to the nature of the equations used. In reality, however, the gases exiting the flask heater were not expected to be saturated. Therefore, the results of this analysis were believed to be inflated conservative estimates of the behavior that was expected. This lead to the trial of approximately 12 grams of monomer in the flask for initial tests. Indeed the results were grossly inflated and concentrations of vinyl acetate never exceeded 0.1 g/L. Given the volatility of vinyl acetate, all other monomers showed even lower concentrations.

APPENDIX C

Statistics

All of the data necessary to perform detailed statistics are presented and illustrative examples of pertinent calculations are shown. Tables IX and X present ball wear volumes for all of the low and high temperature experiments performed respectively.

These data were subjected to Fisher's Least Significant Difference (LSD) method of comparison. This is a common method of determining whether or not a number of population means are statistically equal or if there is a significant statistical probability that the population means are different. The following analysis is presented for the elevated (145°C) bulk temperature experiments; it is identical to the analysis performed on the ambient bulk temperature data. The reader may check these additional data if it

Table IX Ball Wear Data for Ambient (20°C) Bulk Temperature Experiments

		Treatment (Monomer Delivery Temperature °C)			
	Experiment Number	**Nitrogen**	**Vinyl Acetate (20)**	**Vinyl Acetate (60)**	**Diallyl Phthalate (100)**
Ball Wear Volumes from Individual Experiments (mm^3)	1	0.0097828	0.0101282	0.0062485	0.0133754
	2	0.0114287	0.0126704	0.0068862	0.0300206
	3	0.0239198	-	0.0028987	-

Table X Ball Wear Data for 145°C Bulk Temperature Experiments

		Treatment (Monomer Delivery Temperature °C)			
	Experiment Number	**Nitrogen**	**Diallyl Phthalate (135)**	**Diallyl Phthalate (165)**	**Lauryl Methacrylate (120)**
Ball Wear Volumes from Individual Experiments (mm^3)	1	0.180830	0.196500	0.0092048	0.0763800
	2	0.220686	0.0644900	0.0012946	0.1344000
	Experiment Number	**Lauryl Methacrylate (140)**	**Vinyl Octadecyl Ether (130)**	**Vinyl Octadecyl Ether (145)**	**Vinyl Octadecyl Ether (165)**
	1	0.0490956	0.077234	0.0247659	0.0044940
	2	0.0048482	0.145046	0.0852042	0.0015859
	3	0.0075162	-	-	-
	4	0.0023200	-	-	-
	5	0.0123519	-	-	-
	6	0.0014981	-	-	-

is felt necessary.

Fisher's LSD Procedure is described as follows by Ott [42]:

1. Perform an analysis of variance to test the null hypothesis that all of the treatment means are statistically equal: H_0: $\mu_1 = \mu_2 = \ldots = \mu_t$ against the alternative hypothesis, H_1, that at least one of the means differs from the rest.

2. If there is insufficient evidence to reject H_0 using the F and p statistics, stop and end the procedure. (The p statistic gives the statistical confidence level at which one can conclude that means are different.)

3. If H_0 is rejected in favor of H_1, define the least significant difference (LSD) to be the observed difference between two sample means necessary

to declare the corresponding population means different.

4. For a specified value of α, the least significant difference for comparing μ_i to μ_j is:

$$LSD = t_{\frac{\alpha}{2}} \sqrt{s_W^2 \left(\frac{1}{n_i} + \frac{1}{n_j} \right)}$$

where n_i and n_j are the respective sample sizes from population i and j and t is the critical t value for a = $\alpha/2$ and dof denoting the degrees of freedom for s_W^2 (these values can be easily found in any general statistics text).

5. All pairs of sample means are then compared. If $|\bar{y}_i - \bar{y}_j| \geq$ LSD, we declare the corresponding population means μ_i and μ_j different.

6. For each pairwise comparison of population means, the probability of a Type I error is fixed at the specified value of α.

Minitab 6.1 statistical data analysis software was used to perform the analysis of variance table shown in Table XI.

Table XI Analysis of Variance (ANOVA) Table for Elevated Bulk Temperature (145°C) Ball Wear Volumes

Source	Degrees of Freedom	Sum of Squares	Mean Square	F-Test	p Value
Between Samples	dof_1 = t - 1 = 7	SSB = 0.08424	s_B^2=SSB/(t-1)= 0.01203	s_B^2/s_W^2 = 8.50	0.001
Within Samples (or Error)	dof_2 = n - t = 12	SSW = 0.01700	s_W^2=SSW/(n-1)= 000142		
Totals	19	TSS = 0.10124			

Having performed the first part of the LSD procedure, the second requirement is to determine if the null hypothesis, H_0, that all of the ball wear volume means are equal, can be rejected in favor of H_1, that at least one of the ball wear volume means is different, greater than or less than, the rest. Indeed, an F-statistic of 8.61 is high for the data analyzed, and this is confirmed by the p-value corresponding to this F-statistic. The confidence level for rejecting H_0 and accepting H_1 is:

$$100\ (1 - p\ value) = \%\ Statistical\ Confidence\ for\ Rejecting\ H_0$$

$$100\ (1 - 0.001) = 99.9\%$$

In other words, we can say with 99.9% confidence that at least one of the ball wear volume means is statistically different from the rest. This fulfills the second of the LSD comparison method requirements.

Selecting a 95% level of confidence (or $1 - 0.95 = \alpha = 0.05$) for pairwise comparisons, the procedure continues as follows:

$$t_{\frac{\alpha}{2}} = t_{\frac{0.05}{2}} = t_{0.025}$$

With dof = 12, the appropriate table gives a value of $t_{0.025} = 2.179$. Next, in order to perform pairwise comparisons, two values of LSD are needed. For most procedures, in which the means being compared have only two samples in their populations:

$$LSD = 2.179\sqrt{0.00141\left(\frac{1}{2}+\frac{1}{2}\right)} = 0.08182$$

For comparisons with lauryl methacrylate treatment ball wear volumes, the following LSD is used (because this particular population has 6 samples):

$$LSD = 2.179\sqrt{0.00141\left(\frac{1}{6}+\frac{1}{2}\right)} = 0.06681$$

Using the calculated LSD's and the average wear volumes in Table XII, the

Table XII Average Ball Wear Volumes for Individual Monomer Treatments at 145°C Bulk Temperature

		Average Ball Wear Volumes (mm^3)
Monomer Treatments Arranged in Order of Least Wear to Highest Wear Volume: Monomer (Delivery Temperature °C)	Diallyl Phthalate (165)	0.00111
	Vinyl Octadecyl Ether (165)	0.00304
	Lauryl Methacrylate (140)	0.01294
	Vinyl Octadecyl Ether (145)	0.05499
	Lauryl Methacrylate (120)	0.10539
	Vinyl Octadecyl Ether (130)	0.11140
	Diallyl Phthalate (135)	0.13050
	Nitrogen Standard	0.20076

pairwise comparisons proceed as follows:

$\bar{y}_{largest} - \bar{y}_{smallest} = 0.20076 - 0.00111 = 0.19968 > LSD$ *CONTINUE*

$\bar{y}_{2^{nd}\ largest} - \bar{y}_{smallest} = 0.12939 > LSD$ *CONTINUE*

$\bar{y}_{3^{rd}\ largest} - \bar{y}_{smallest} = 0.11029 > LSD$ *CONTINUE*

$\bar{y}_{4^{th}\ largest} - \bar{y}_{smallest} = 0.10431 > LSD$ *CONTINUE*

$\bar{y}_{5^{th}\ largest} - \bar{y}_{smallest} = 0.05388 < LSD$ *STOP !!!!*

Calculations are terminated at the point were the LSD is greater that the difference between the two treatments being compared (i.e. there is no longer a "significant difference" between the remaining means).

What these comparisons determine is that at the 95% confidence level, the treatment whose conditions resulted in the smallest wear volume, $\bar{y}_{smallest}$ (diallyl phthalate vapor delivered at 165°C), is statistically less than all of those for which the comparison yielded values > LSD. In other words, there is a 95% confidence, that the average ball wear volume observed for the diallyl phthalate 165°C vapor treatment is statistically less than that for the nitrogen standard (largest), diallyl phthalate 135°C (2nd largest), vinyl

octadecyl ether 130°C (3rd largest), and lauryl methacrylate 120°C (4th largest). This procedure also determines that the wear volumes observed for the other treatments, vinyl octadecyl ether 145°C (5th largest), lauryl methacrylate 140°C (6th largest), and vinyl octadecyl ether 165°C, are all statistically equal at the 95% confidence level to that of the diallyl phthalate 165°C treatment.

The next step in this procedure is exactly similar to the previous substituting the 2nd smallest average wear volume (vinyl octadecyl ether 165°C) for the smallest wear volume (diallyl phthalate 165°C). This is summarized as follows:

$$\bar{y}_{largest} - \bar{y}_{2^{nd}\ smallest}$$

$$\bar{y}_{2^{nd}\ largest} - \bar{y}_{2^{nd}\ smallest} \qquad etc.$$

This is done until the difference being compared is less than or equal to the previously determined LSD. The next step is of course:

$$\bar{y}_{largest} - \bar{y}_{3^{rd}\ smallest}$$

$$\bar{y}_{2^{nd}\ largest} - \bar{y}_{3^{rd}\ smallest} \qquad etc.$$

These procedures are continued until all possibilities are exhausted. As shown in the body of this paper, the results of the above analysis determine that at the 95% confidence level the following are true with respect to ball wear volumes (and thus the effectiveness of the treatment in reducing wear):

a) Nitrogen Standard	>	All other treatments (i.e., all monomer additives show a statistically significant reduction in wear at the 95% confidence level)
b) Diallyl Phthalate 135°C	>	Diallyl Phthalate 165°C
c) Lauryl Methacrylate 120°C	>	Lauryl Methacrylate 140°C
d) Vinyl Octadecyl Ether 130°C	=	Vinyl Octadecyl Ether 145°C
e) Vinyl Octadecyl Ether 145°C	=	Vinyl Octadecyl Ether 165°C
f) Vinyl Octadecyl Ether 130°C	>	Vinyl Octadecyl Ether 165°C

As can be seen, it appears that all of the monomer treatments used reduce wear and that each becomes statistically more effective with increases in monomer delivery temperatures. Statistical differences between the different monomer treatments is more difficult to determine. The following are also true at the 95% confidence level:

f) DP 135°C = LM 120°C = VOE 130°C = VOE 145°C

g) DP 165°C = LM 140°C = VOE 145°C = VOE 165°C

The following Figure 43 summarizes all of this statistical data. Populations not underlined by a common line are declared to have significantly different values of wear at the 95% confidence level as determined by Fisher's least significant difference method. All treatments underlined by a common line are statistically equivalent.

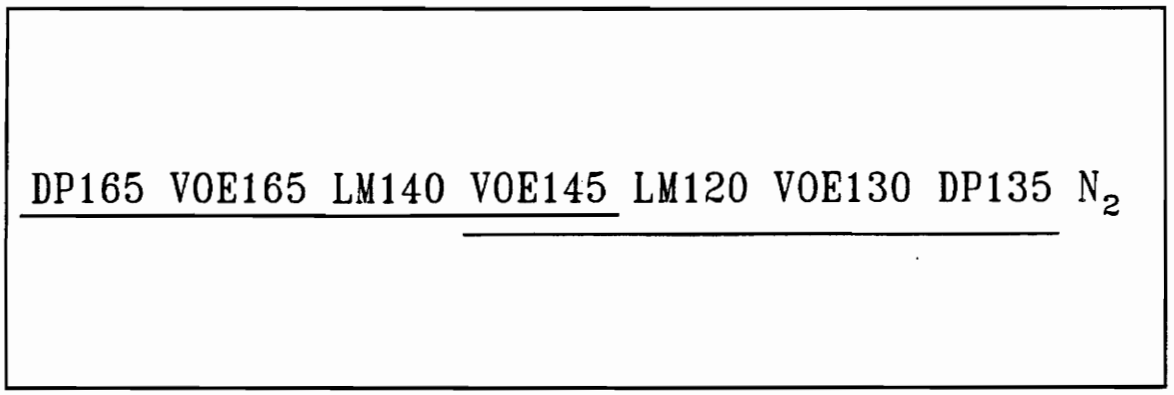

Figure 43 Summary of High Bulk Temperature Statistics

A summary of the statistical results for the ambient bulk temperature results are shown in Figure 44. These results were found at the 80% confidence level.

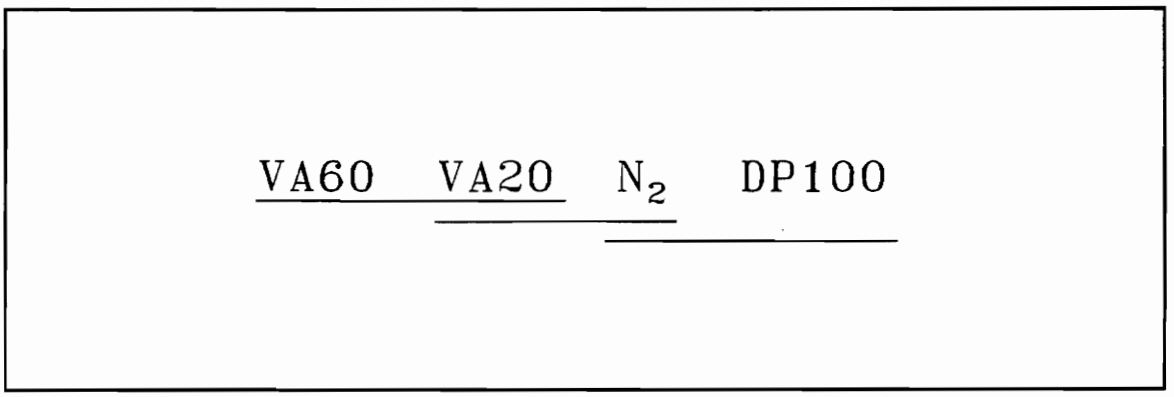

Figure 44 Summary of Ambient (20°C) Bulk Temperature Experiments

APPENDIX D

Wear Volume and Concentration Data

The data presented in the following tables can be found in the notebook labeled "Vapor Phase Tribopolymerization Research". Test numbers indicate the experiment from which these data were obtained. Friction strip charts and Talysurf traces of disk surfaces are also on the pages that correspond to the test number. Tables XIII and XIV show data for 20°C bulk temperature tests and 145°C bulk temperature tests respectively.

Table XIII Ambient Bulk Temperature (20°C) Test Results

Ambient Bulk Temperature (20°C) Test Results					
Treatment (Monomer Delivery Temperature)	**Test #**	**Average Vapor Concentration (g/l)**	**Ball Wear Volume (mm^3)**	**Disk Wear Volume (mm^3)**	**Average Total Wear Volume (mm^3)**
Nitrogen Standard	2 V	-	0.0098	0.5431	0.6270
	3 V	-	0.0114	0.2067	
	27 V	-	0.0239	1.1313	
Vinyl Acetate (Ambient - 20°C)	4 V	???	0.0101	-	-
	6 V	0.0156	0.0127	-	
Vinyl Acetate (60°C)	7 V	0.0789	0.0062	0.0518	0.0422
	9 V	0.0676	0.0069	0.0395	
	10 V	0.0936	0.0029	0.0192	
Diallyl Phthalate (100°C)	11 V	0.0046	0.0134	-	-
	12 V	0.0017	0.0300	-	

Table XIV Elevated Bulk Temperature (145°C) Test Results

Elevated Bulk Temperature (145°C) Test Results					
Treatment (Monomer Delivery Temperature)	**Test #**	**Average Vapor Concentration (g/l)**	**Ball Wear Volume (mm^3)**	**Disk Wear Volume (mm^3)**	**Average Total Wear Volume (mm^3)**
Nitrogen Standard	37 V	-	0.1808	0.5326	0.8653
	38 V	-	0.2207	0.7965	
Diallyl Phthalate (135°C)	28 V	0.0066	0.1965	-	-
	30 V	0.0065	0.0644	-	
Diallyl Phthalate (165°C)	16 V	0.0143	0.0009	0.0290	0.2236
	17 V	0.0065	0.0013	0.0135	
Lauryl Methacrylate (120°C)	31 V	0.0050	0.0764	-	-
	32 V	0.0055	0.1344	-	
Lauryl Methacrylate (140°C)	18 V	0.0186	0.0491	-	-
	20 V	0.0051	0.0048	-	
	21 V	0.0085	0.0075	-	
	22 V	0.0126	0.0023	-	
	33 V	0.0100	0.0124	-	
	34 V	0.0071	0.0015	-	
Vinyl Octadecyl Ether (130°C)	25 V	0.0009	0.0772	-	-
	26 V	0.0010	0.1450	-	
Vinyl Octadecyl Ether (145°C)	35 V	0.0042	0.0248	-	-
	36 V	0.0042	0.0852	-	
Vinyl Octadecyl Ether (130°C)	23 V	0.0045	0.0045	0.0195	0.2270
	24 V	0.0092	0.0016	0.0253	

APPENDIX E

Vibrational Characteristics

The bounce and wobble vibrations of concern were illustrated in Figure 33 and the modeling of this system is shown in Figure 45. The analysis of these characteristics is presented here.

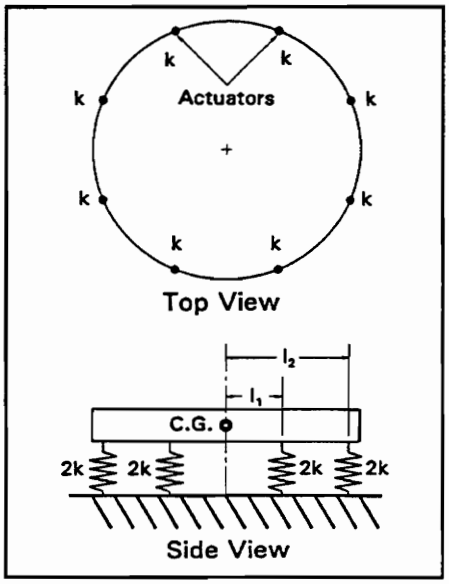

Figure 45 Vibration Analysis Model

The analysis of this system is analogous to the classic two-dimensional automobile problem where these are the two primary vibrational characteristics of concern. Though this system is in reality a three-dimensional system, the two-dimensional model fits the problem well.

The root of the bounce vibration concern is obvious. The wobble vibrations, on the other hand, were expected to be caused by the rotating off center loading of the pin-on-disk contact. The analysis of this system and these vibrations preceded as follows.

Since a circular arrangement of pneumatic actuators was used, each was modeled as a single air spring. According to [43], the stiffness of an air spring, "k", can be modeled as:

$$k = \frac{n P_i S^2}{V_i}$$

Where: n = the ratio of specific heats for whatever gas is used (1.4 for air),

P_i = air pressure inside of the cylinder,

S = surface area of piston inside cylinder, and

V_i = the volume of the cylinder (or the system if the cylinder is interconnected with one).

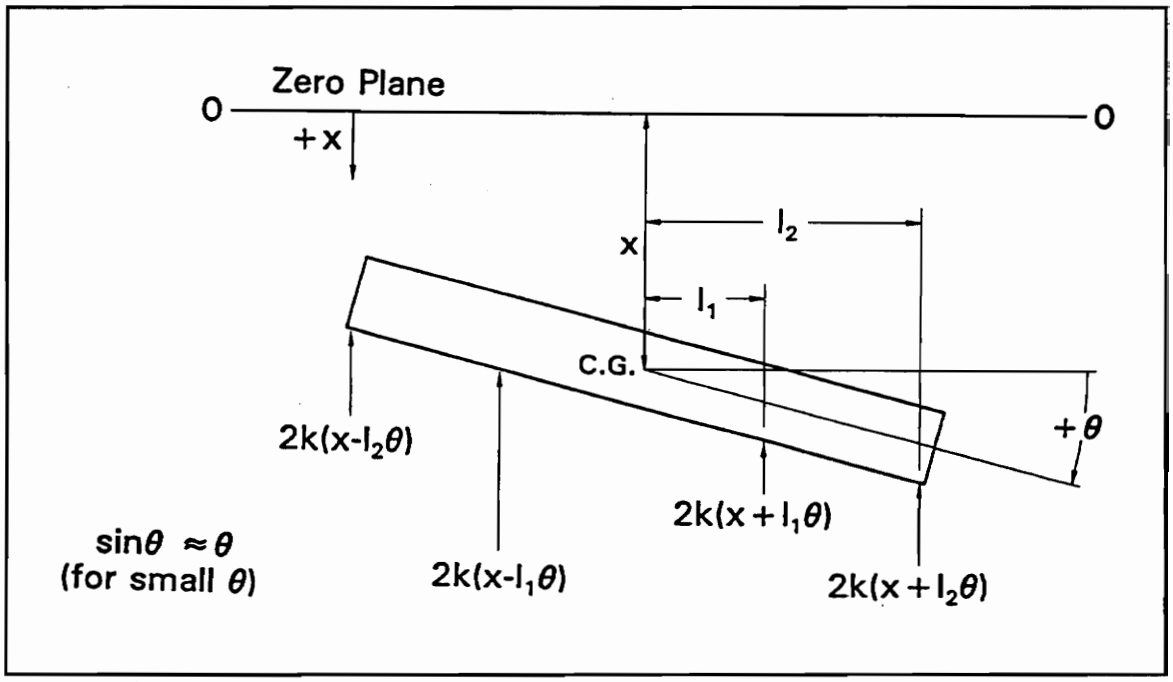

Figure 46 Model for Equations of Motion

Looking at Figure 46, the equations of motion can be easily written. Beginning with bounce vibrations:

$$\Sigma F = ma$$

and now avoiding the detailed mathematics, this reduces to:

$$m\ddot{x} + 8kx = 0$$

Turning to the wobble vibrations:

$$\Sigma M = J_o\ddot{\theta}$$

and again avoiding the detailed mathematics, this reduces to:

$$J_o\ddot{\theta} + 4k\theta\left(l_1^2 + l_2^2\right) = 0$$

Assuming the standard solutions of the equations and using a matrix format, these equations take the form:

$$\begin{bmatrix} (-\omega^2 m + 8k) & 0 \\ 0 & (-J_o\omega^2 + 4k\,(l_1^2 + l_2^2)) \end{bmatrix} \begin{bmatrix} X \\ \Theta \end{bmatrix} = \begin{bmatrix} 0 \\ 0 \end{bmatrix}$$

For the non-trivial solution to these equations, the determinant of the matrix must equal zero. Therefore, this operation was performed and with manipulations we have:

$$(J_o m)\,\omega^4 - \left[\,4km\,(l_1^2 + l_2^2) + 8J_o k\,\right]\omega^2 + 32k^2\left(l_1^2 + l_2^2\right) = 0$$

Using the quadratic equation this can be solved, and the resulting solutions define the bounce (ω_1) and wobble (ω_2) natural frequencies of the system:

$$\omega_1^2 = \frac{8k}{m} \qquad AND \qquad \omega_2^2 = \frac{4k\left(l_1^2 + l_2^2\right)}{J_o}$$

Having already given the relationship for the air spring stiffness and knowing the polar moment of inertia of a round plate:

$$J_o = \frac{md^2}{16}$$

where m = mass and d = diameter, substitution of these and the appropriate dimensions of the original machine design, the natural frequencies of the system took the values:

$$\omega_1 = 9.1\sqrt{\frac{P}{N}} \qquad AND \qquad \omega_2 = 12.9\sqrt{\frac{P}{N}}$$

where P = the pneumatic pressure in the system (psi) and N is a multiplication factor for the volume. For example, if the air cylinder was coupled with a air tank reservoir whose volume was 100 times that of the cylinder, N would equal 100. The option of adding some type of reservoir was considered since at moderate pressures (15-20 psi)

expected to be used during experiments, the natural frequencies of this system (between about 40 and 60 hertz) without a reservoir were found to be near the rotational frequency of the pin-on-disk contact (between about 25 and 60 hertz for 1500 and 4000 rpm respectively).

The Firestone Airspring analysis proved to be slightly more difficult to understand intuitively due to its unfamiliar nature. There was no method available for the analysis of the system's wobble characteristics but as already shown for the first system, the wobble natural frequency was relatively close to the bounce natural frequency. It was believed that this would also be the case for the Firestone Airspring and since bounce vibration characteristics were published for the device [44], this natural frequency could be determined. The data was presented in a tabular nature and according to this, the Model 110 was expected to have a bounce natural frequency of around 3.0 Hz. This was expected to be low enough below the rotational frequencies that excitation of bounce natural frequencies seemed unlikely. If the expectations concerning wobble natural frequencies was also true, the system would be well into a safe range of operation.

In reality, the expectations concerning wobble vibration were correct and at high rotational speeds, the off center loading did not cause a problem. Very unexpectedly, however, bounce vibrations did cause a problem and bounce natural frequencies were readily excited. The ball and disk bounced in and out of contact and the impact loading of the ceramic materials proved fatal causing test specimens to shatter.

The new system can not be readily analyzed due to its high stiffness. This design

approach was followed intentionally to insure that under the high speed and high load conditions, which had already proven to excite uncontrollable vibrations, that any and all motion could be controlled precisely. This desire has been realized, and though some very small vibrations are still evident in the system, they are all absorbed by the rigid body of the configuration.

The success of this design is due to primarily to the removal of elastic members, such as the Firestone Airspring or flimsy load arms, and the elimination of large masses in conjunction with these elastic members such as dead weights. Having eliminated these two sources of excessive and uncontrollable vibration, the new design provides for controlled and predictable dynamic operation.

APPENDIX F

Force Transducer Calibration

The force transducer is a thin-walled aluminum cylinder with four standard Measurements Group, Incorporated, N2A series, 350 ohm, constantan foil strain gages (2.11 nominal gage factor) mounted in a full bridge arrangement on the outer wall. Calibration was accomplished using a 1000 lb. load cell loaded into the Virginia Polytechnic Institute and State University Adhesive and Sealant Science Laboratory's Instron machine. Digital data was acquired during the calibration procedure corresponding to load versus bridge voltage output. Load data was acquired directly from the Instron and bridge output voltage was acquired from a Micro-Measurements P-3500 portable strain indicator used to power the bridge.

The P-3500 strain indicator gage factor was set to 2.110 to match the nominal gage factor of the foil gages as specified by the manufacturer. The "Amp Zero" setting was zeroed using the corresponding thumb screw. The analog output thumb screw was turned clockwise to its maximum voltage output position of 2.5 volts and the bridge itself was balanced (relatively high but still good -- near 4000 microstrain).

Increasing compressive loads were slowly applied and loads were allowed to "settle" on the transducer to minimize elastic hysteresis errors. After settling, strain output from the digital gage of the P-3500 strain indicator was manually recorded.

Four curves were created from this data as show in Figures 47-50. The first two

show the low load range for more accurate readings during lower load conditions. The second two show the full load range examined. Since excessive strain on the gages is not recommended, Figures 49 and 50 represent the maximum loading conditions for the force transducer. The equations governing the regression curve fits in these figures are given on page 133.

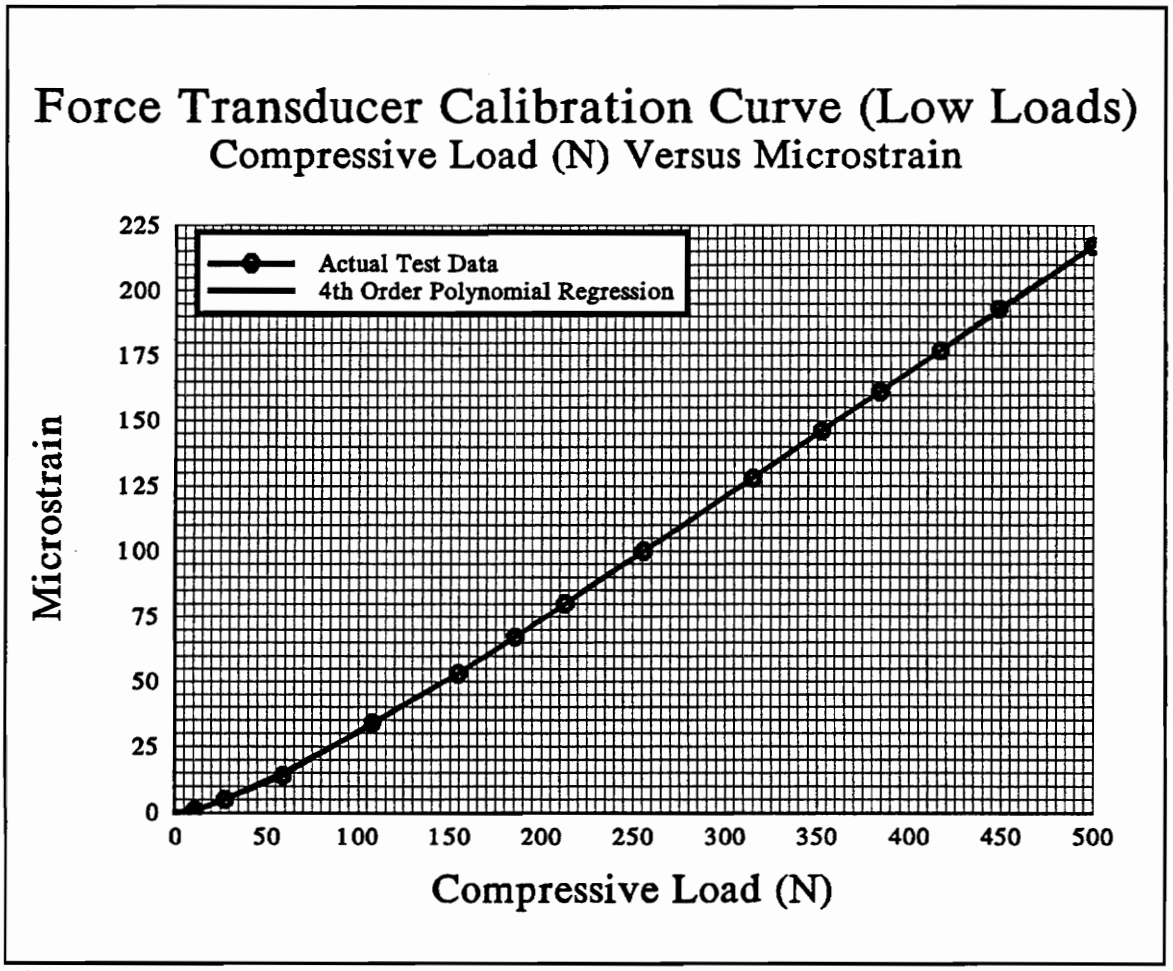

Figure 47 Force Transducer Calibration Curve (Low Loads) Load Versus Microstrain

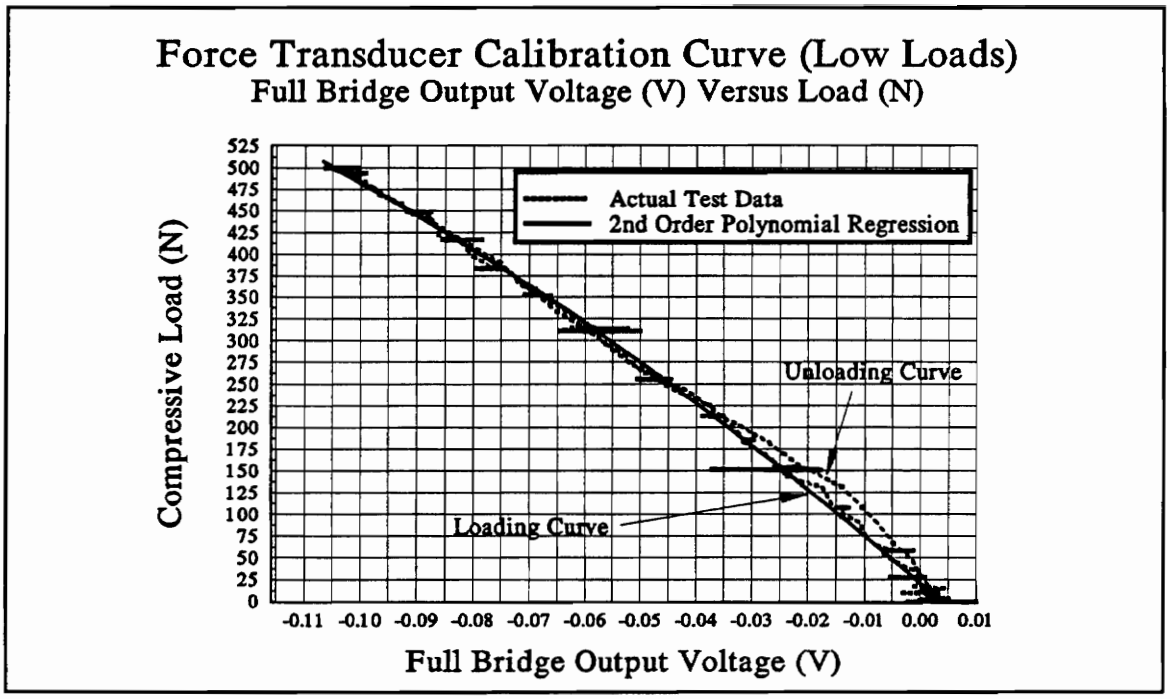

Figure 48 Force Transducer Calibration Curve (Low Loads) Voltage Versus Load

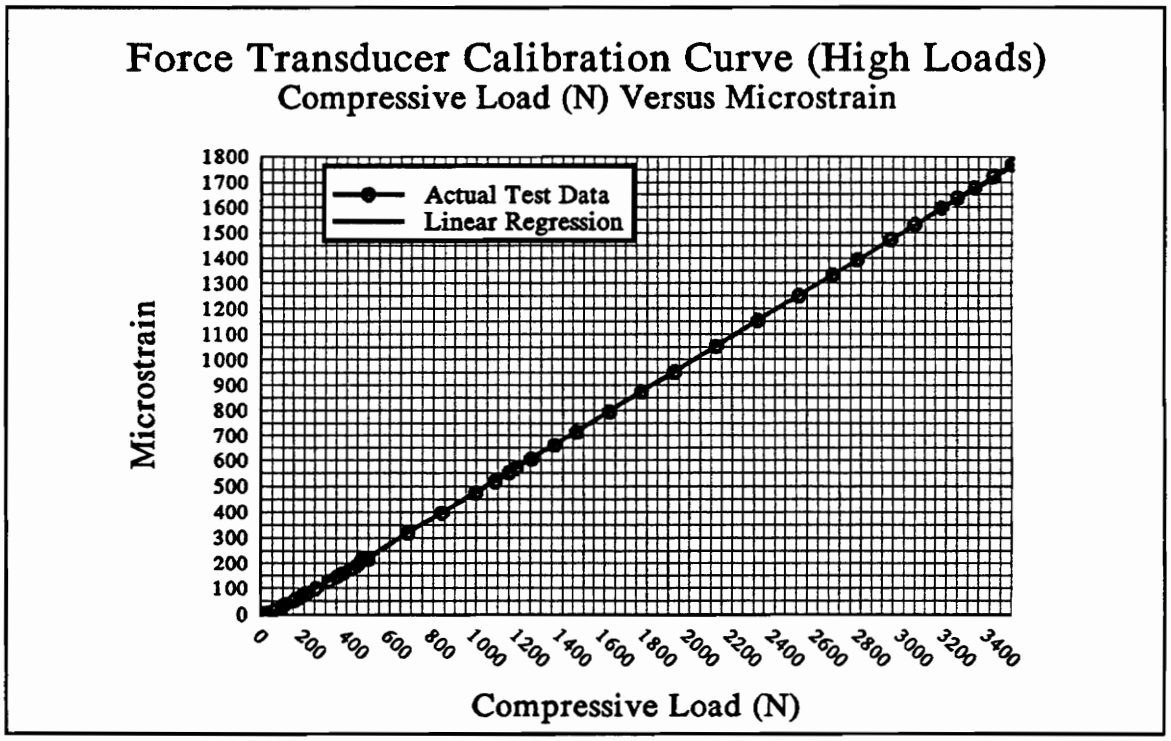

Figure 49 Force Transducer Calibration Curve (High Loads) Load Versus Microstrain

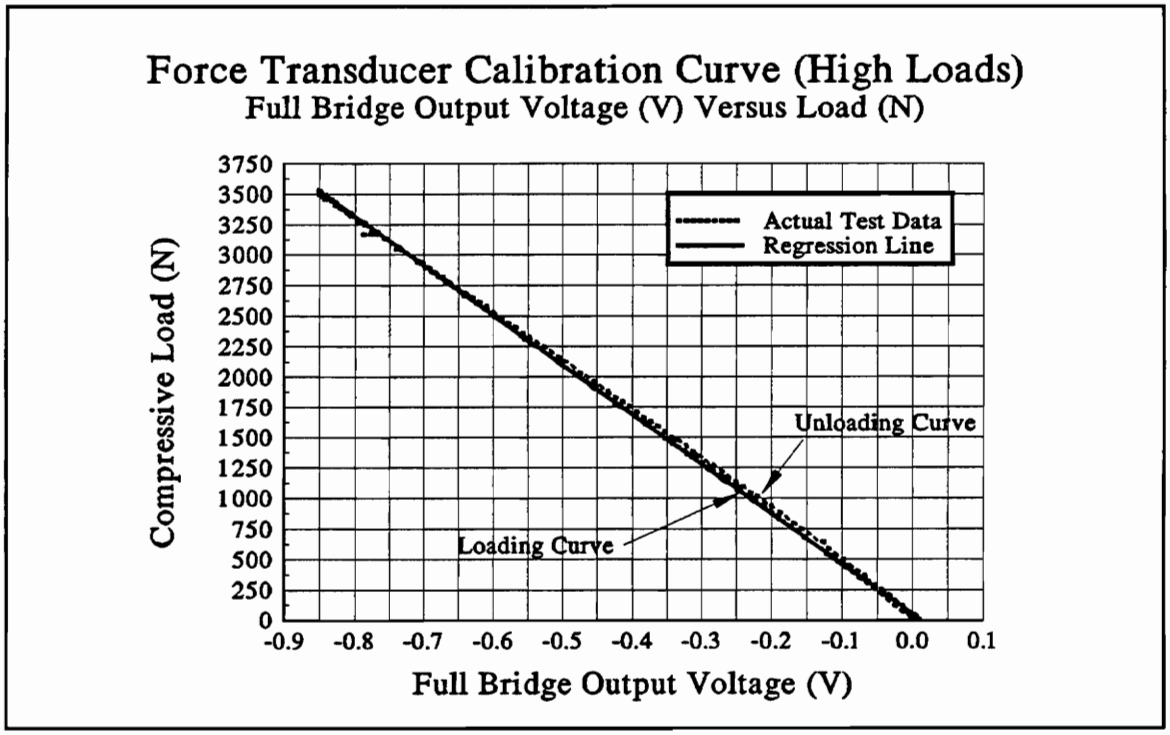

Figure 50 Force Transducer Calibration Curve (High Loads) Voltage Versus Load

For Figure 47:

$$MICROSTRAIN = (1.59\times10^{-9})(LOAD)^4 - (2.18\times10^{-6})(LOAD)^3 + (0.0011)(LOAD)^2 + (0.23)(LOAD) - 2.08$$

For Figure 48:

$$LOAD\ (N) = -9319.93\ (VOLTAGE)^2 - 5548.9\ (VOLTAGE) + 20.91$$

For Figure 49:

$$MICROSTRAIN = 0.51\ (LOAD) - 29.37$$

For Figure 50:

$$LOAD\ (N) = -4084.066\ (VOLTAGE) + 54.902$$

APPENDIX G

High Speed, High Load Pin-on-Disk Machine: Design Detail

The design of the high speed, high load pin-on-disk machine has been through several iterations and the final iteration as the machine is constructed is presented here. Figures 51 through 63 illustrate the basic construction dimensions of the design as well as the materials used for each part. Isometric views of the machine were shown previously in Figures 35 and 36.

In Figure 51, the 3.81 in. diameter bolt circle provides a mounting arrangement for the pneumatic loading cylinder. The four larger holes on this same face are spaced and sized so that the apparatus can be bolted to the currently available milling machine table. These may have to be re-machined if a different milling machine is used.

Figure 59 shows the bottom part of the ball or "pin" specimen holder. A standard 3/8 in. UNF threaded rod can be cut and re-machined to these specifications. Similarly, if a different geometry is desired (i.e., an 1/8 in. ball-on-flat etc.) it is suggested that a 3/8 in. UNF threaded rod be the starting material and re-tooled to meet the desired specifications.

Figure 60 shows the top part of the ball or "pin" holder. If these specifications are followed properly, the ball specimen will extend 0.05 in. ("50 thousandths") out of the holder. Stainless steel is recommended though several plain steel replicates of this part have also been made.

In Figure 61, a hole tapped 3/8-24 UNF is intended for use with the mechanical safety stop. A socket-head capscrew or other similar bolt is threaded into this hole and positioned by turning to a depth set by the experimenter. This bolt will limit the upward travel of the pin specimen during an experiment due to wear.

Figure 63 gives the dimensions of the force transducer. The transducer was made from 6061-T6 aluminum alloy for its high strength characteristics as well as its ability to deflect under load. As designed, the resolution of the transducer using standard foil strain gages (generally sensitive to about 1 microstrain) should be approximately 1 N. In reality, the machining process gave the critical center section of the gage dimensions of 1.063" O.D. (outside diameter) and 1.001 I.D. (inside diameter). With these dimensions the resolution of the transducer is about 4 N. With higher loads (i.e., over 100 N), this is acceptable corresponding to a less than 4% error in load measurement. At lower loads, however, the error becomes larger. If such loads are to be used with minimal percent error in measurement, a thinner walled transducer should be made specifically for low load experiments. If the existing transducer were re-tooled for the purpose of use under all load conditions, high load applications may endanger the gages or mechanical failure of the transducer's aluminum structure. It is therefore suggested that a new low load (< 100 N) force transducer be made (if desired) and that the existing transducer be retained for high load (> 100 N) experiments.

Figure 64 shows the standard electronic full bridge strain gage configuration in the upper left corner and the actual mounting of the gages on the transducer. Two 90°

rosettes were used to simplify installation and to insure that 90° angles were maintained between the gages themselves. The gages were purchased from Measurements Group, Inc., Micro-Measurements Division, model number N2A-13-SO53P-350. This is a standard open-faced constantan gage mounted on a laminated polyimide backing intended for precision transducer applications. The N2A Series of gages has an elongation capability of approximately ±3% and are intended for use under elastic strain conditions. The gages have a resistance of 350.0 ohms ± 0.2% and a nominal gage factor of 2.11, both at 24°C. Figure 65 was taken from the rosette packaging material and gives general gage characteristics as well a curve governing the thermal effects on gage output.

Gages were mounted and covered using standard Micro-Measurements adhesives and coating materials. M-Bond 610 strain gage adhesive was selected for exposure to high temperatures. Its allowable range of operation is -45°C to 205°C. M-Bond 610 is a solvent thinned epoxy-phenolic adhesive of tetrahydrofuran (64.4%), epoxy novolac (30.3%), and methyl ethyl ketone (5.3%) cured using tetrahydrofuran (THF) and 1,2,4,5-benzenetetracarboxylic anhydride.

Gages were covered for protection from laboratory elements, particularly from the oils and hydrocarbon monomers used in tribopolymerization research. First, a single coat of M-Coat C was applied as a base coat. This was followed by two outer coats of M-Coat B. M-Coat C is a solvent thinned (xylene 25% and naphtha 10%) air-drying RTV silicone rubber (trimethylated silica and methyltrimethoxysilane) and is used as a general gage protection. M-Coat B is an air drying, solvent-thinned (MEK) nitrile rubber

selected for its excellent resistance to commercial oils and other hydrocarbons such as gasoline and kerosene.

In the final construction, the force transducer and the associated strain gages are bolted to the bottom of a Nook Industries, Inc. ball spline similar to the cut away view illustrated in Figure 66 (Nook Industries - PowerTrax Catalogue). The device consists of a 1.906 in. diameter outer race containing six sets of recirculating ball bearings and a 1.000 in. nominal 0.800 in. root diameter spline inner race (a case hardened steel shaft grooved for ball bearings). The spline has a coefficient of friction of 0.007, minimizing any effects it may have on load measurement.

The outer race was mounted in a slightly oversized hole in the machine's top plate (Figure 55) giving an minimal press fit and then glued into place using Loctite Quick Set 404 cyanoacrylate adhesive. Having fixed the outer race and eliminating rotation, the spline shaft is limited to linear motion only. In addition, ball bearings were specially fit to the races to minimize rotational backlash to 0.003 in.. The outer race carries the Nook model number SOR 8944. The spline shaft was specially cut to a length of 3.5 in. and drilled and tapped on both ends for 3/8-24 UNF threads. The bottom end bolts to the force transducer and the top end bolts to the ball holder or "pin".

The pneumatic actuation system is shown in Figure 67. This outlines air flow through the internal workings of the system. The inlet on the left shows a maximum pressure rating of 150 psi and a minimum of 20 psi. All of the major components of the system (the pressure regulator, the solenoid valve, and the pneumatic cylinder) have

maximum pressure ratings of 150 psi. The minimum is determined by the minimum 20 psi pilot pressure necessary to operate the solenoid control valve.

The block valve at the inlet is normally closed when pressurized air connected to the system. This prevents a high pressure surge from damaging the diaphragm of the pressure regulator. After pressure lines are connected, the block valve is slowly opened.

The 40 micron paper air filter (ARO Air Filter) is necessary to allow for a wide range of air pressure sources. Although the ideal source of air pressure is a clean supply such as that found in a pressurized tank, the filter allows air pressure from the Virginia Tech Power Plant (a not so clean source--i.e., rust, dirt, etc.) to be used as well. Air pressure from the power plant is typically around 80 psi.

The pipe cross sends high pressure air (80 psi when the power plant supply is used) to the necessary connection points of the system. Two lines connect to the pilot supplies of the control valve. A third line connects high pressure air to the pressure regulator.

The regulator is a Fairchild Model 81 multistage pneumatic pressure regulator designed for precision operation with a fluctuating upstream supply. It has a minimum recommended operating supply of 20 psi. Its maximum output is 100 psi. The device is designed for accurate control of output pressure over a wide range of inlet pressures.

A regulated air pressure leaves the regulator and enters the housing of a Fabco-Air Inc. solenoid controlled, pilot operated, air valve (model 18-GG-4-X 12V DC). Minimum pilot supply is rated at 20 psi although a maximum of 150 psi may be used.

Supply to the inlet (and consequently to the pneumatic loading cylinder) may be in the range of 0-150 psi. This control valve controls air flow into the loading cylinder; a 3" diameter bore Fabco-Air "Pancake" model U-C-721-X-J. During an experiment, flow enters the air cylinder below the piston forcing the shaft upward and loading a test specimen ball against the rotating disk. When the automatic safety system is employed or when the experiment is aborted by the operator, the solenoid trips and the control valve reverses the flow of air to the cylinder. Pressurized air enters the cylinder *above* the piston forcing the piston head down (while air beneath the piston is exhausted to the atmosphere) removing the pin from contact with the disk.

The air cylinder itself employs U cups of Trox™, which replace the standard O-ring on the piston head. This gives the system a lower breakaway friction (2.0 psi) than standard O-rings (3.0 psi). In addition, the piston head itself is magnetic. The Hall effect sensors of the automatic control system detect the magnetic field of the piston and thus the position of the piston head.

The electronics of the automatic shutdown and control system are shown in Figure 68. Although protection is provided under normal operating conditions for reversed current flow from the inductive solenoids, note that there is no protection built into the circuit for reversed current flow if the +10 V and -10 V potentials are reversed. If this mistake is made, the Hall effect sensors (small transistors) may be destroyed.

Briefly, under normal conditions, current flows from red to blue throughout the system and the PE 10 LED sensor lights when next to the magnetic piston head. If,

however, the PE 25 Hall effect sensor trips (due to sensing the magnetic piston head), current is sent from red to green in the left hand portion of the circuit, closing the circuit across the solenoid control valve and reversing the flow of air into the pneumatic cylinder. This can also be accomplished by flipping the "kill" switch (3-way normally closed momentary switch in Figure 68). To reset the system, and again direct pressurized air beneath the piston head for loading, the reset switch (normally open momentary switch) is tripped by the operator.

The procedure for running an experiment is rather simple. First, after having the desired samples properly cleaned and loaded into their holders, the holders are loaded into the machine. The disk holder shaft fits directly into a 1/2" tool holder in the head of the milling machine. The ball holder is then threaded through the bottom of the lubricant cup as far as possible. The part of the threaded rod that extends below the bottom of the lubricant cup is then threaded into the top of the spline shaft. The lubricant cup itself is used as the "lock nut" and when the ball holder is threaded as far as possible into the spline shaft, the lubricant cup is tightened against the shaft locking it and the pin specimen into place.

Air pressure lines should be attached with the block valve and pressure regulator closed. The block valve is then slowly opened. The power source to the automatic control system should be turned on and monitored. The sliding speed for the experiment and radius of contact should be selected. These are obviously related. Speed is selected by setting the milling machine gearing (or dial on a variable speed machine) and the

radius of contact is selected by positioning the x-y-z table.

Having set these positions, the mechanical safety stop should be turned to an appropriate position limiting the upward travel of the piston head due to wear. Similarly the Hall effect switches need to be positioned properly as well, with the PE 25 tripping the solenoid control valve at the same position that the mechanical safety stop contacts the top plate limiting upward motion.

Having set all necessary measurement recording equipment properly (note particularly the settings described for the P-3500 strain indicator in Appendix F) the desired lubricant should be added to the lubricant cup, the milling machine and disk rotation turned on, and the pressure regulator opened loading the ball against the spinning disk. Load may be determined by viewing the LCD window on the strain indicator and familiarity with the calibration curve.

Tests should be timed with a stopwatch to insure that desired sliding distances are accomplished. Upon completion of an the experiment, the kill switch may be used to end the test at the proper time. Holders and the lubricant cup should be properly cleaned and stored for future use.

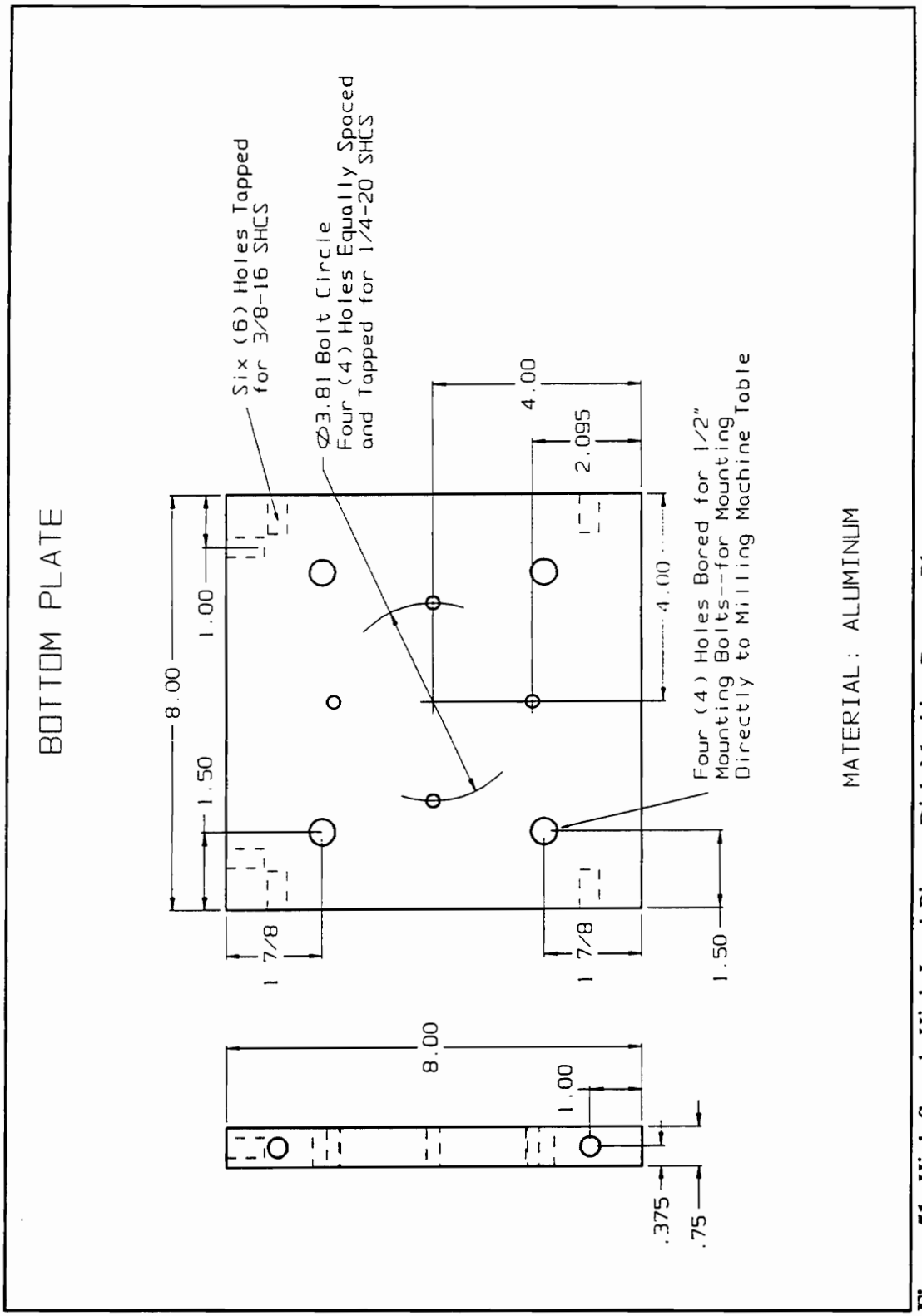

Figure 51 High Speed, High Load Pin-on-Disk Machine Bottom Plate

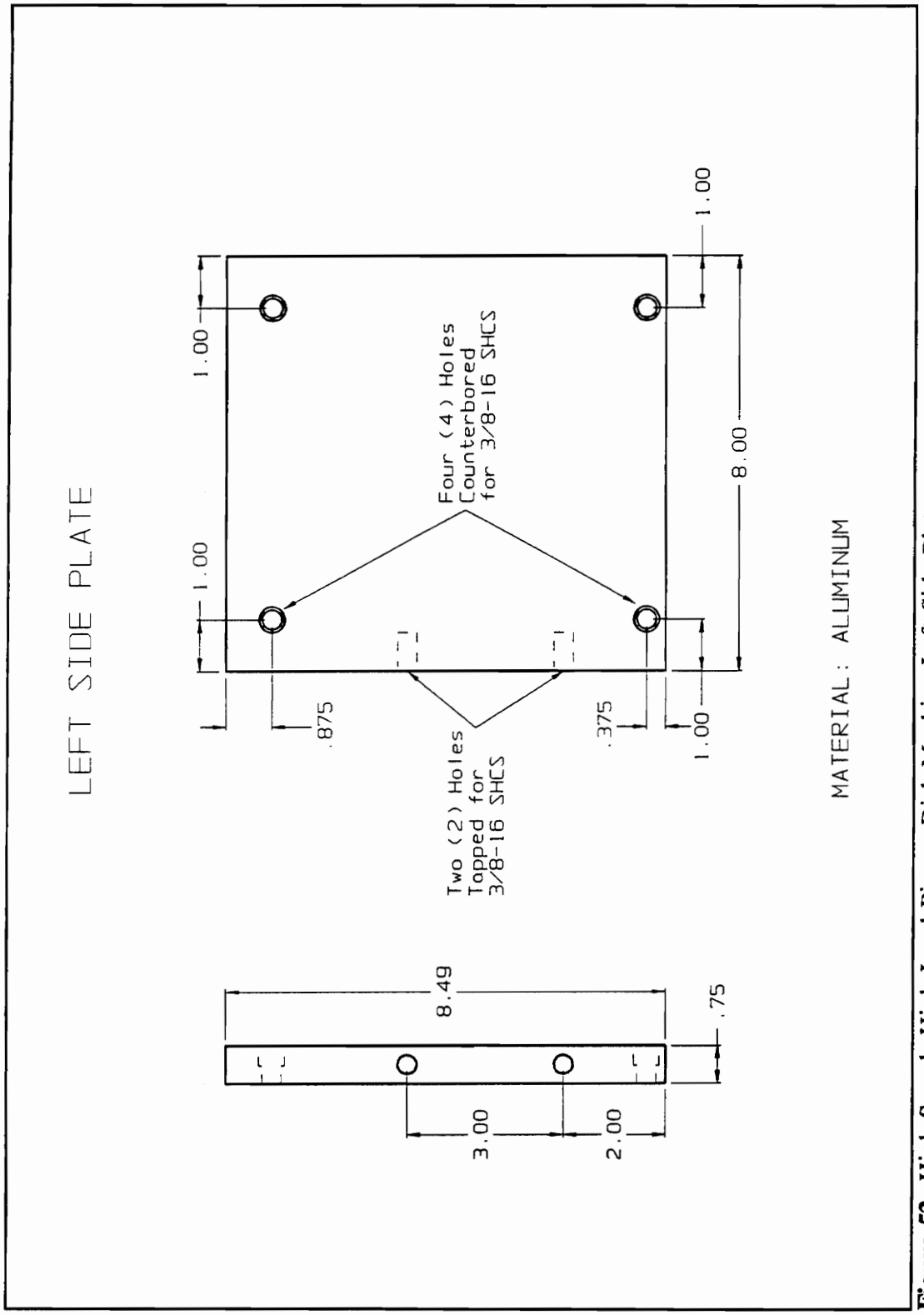

Figure 52 High Speed, High Load Pin-on-Disk Machine Left Side Plate

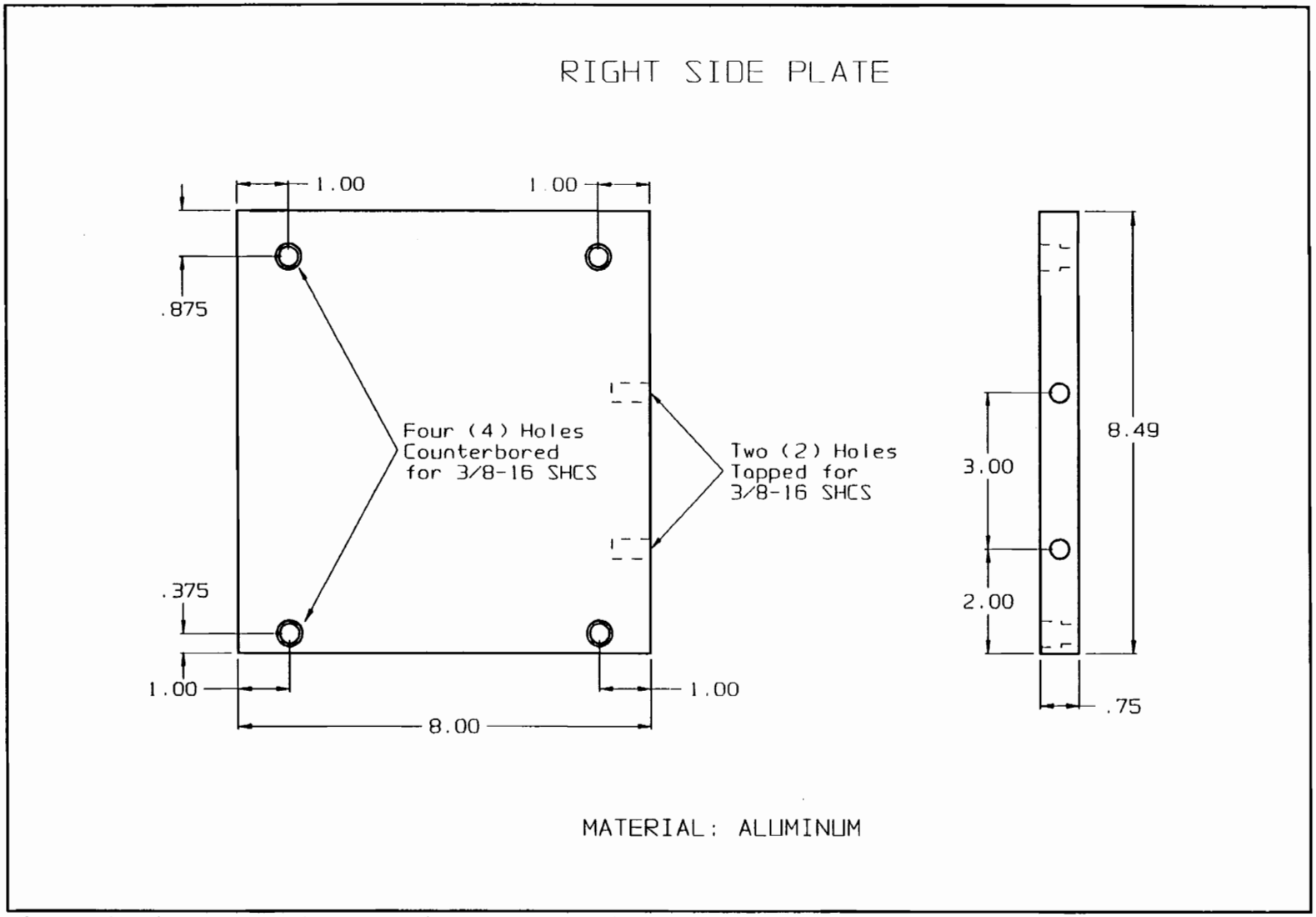

Figure 53 High Speed, High Load Pin-on-Disk Machine Right Side Plate

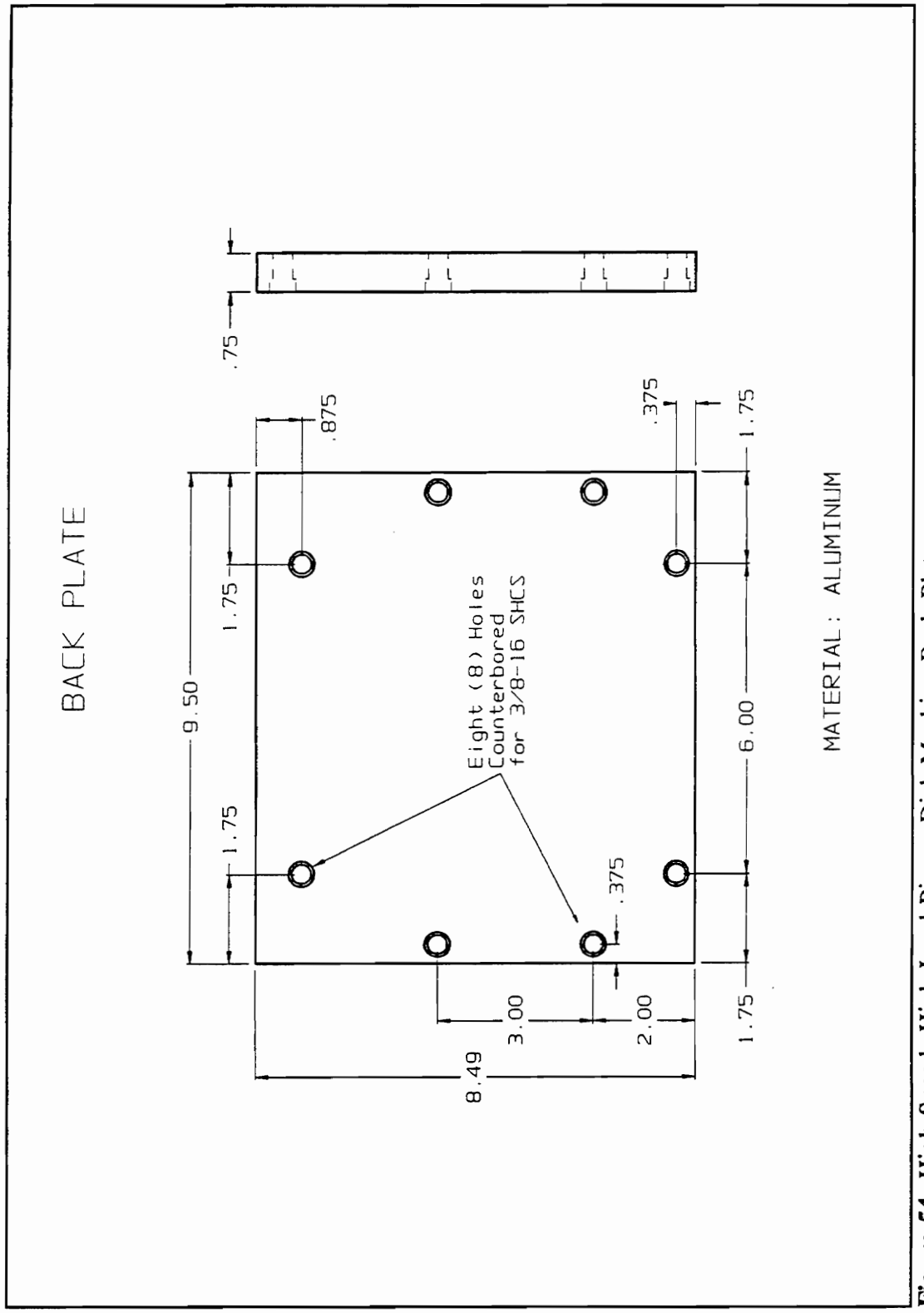

Figure 54 High Speed, High Load Pin-on-Disk Machine Back Plate

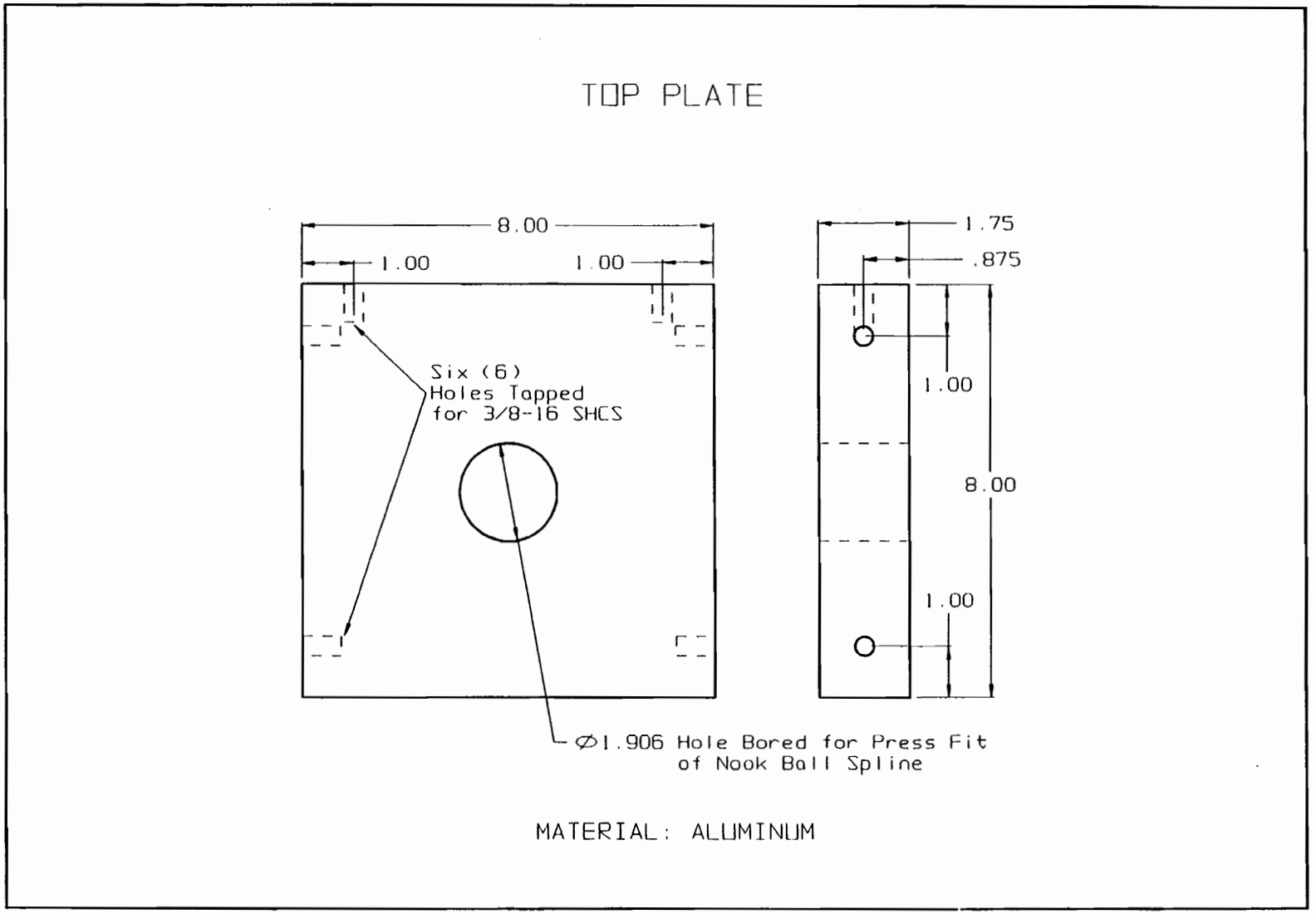

Figure 55 High Speed, High Load Pin-on-Disk Machine Top Plate

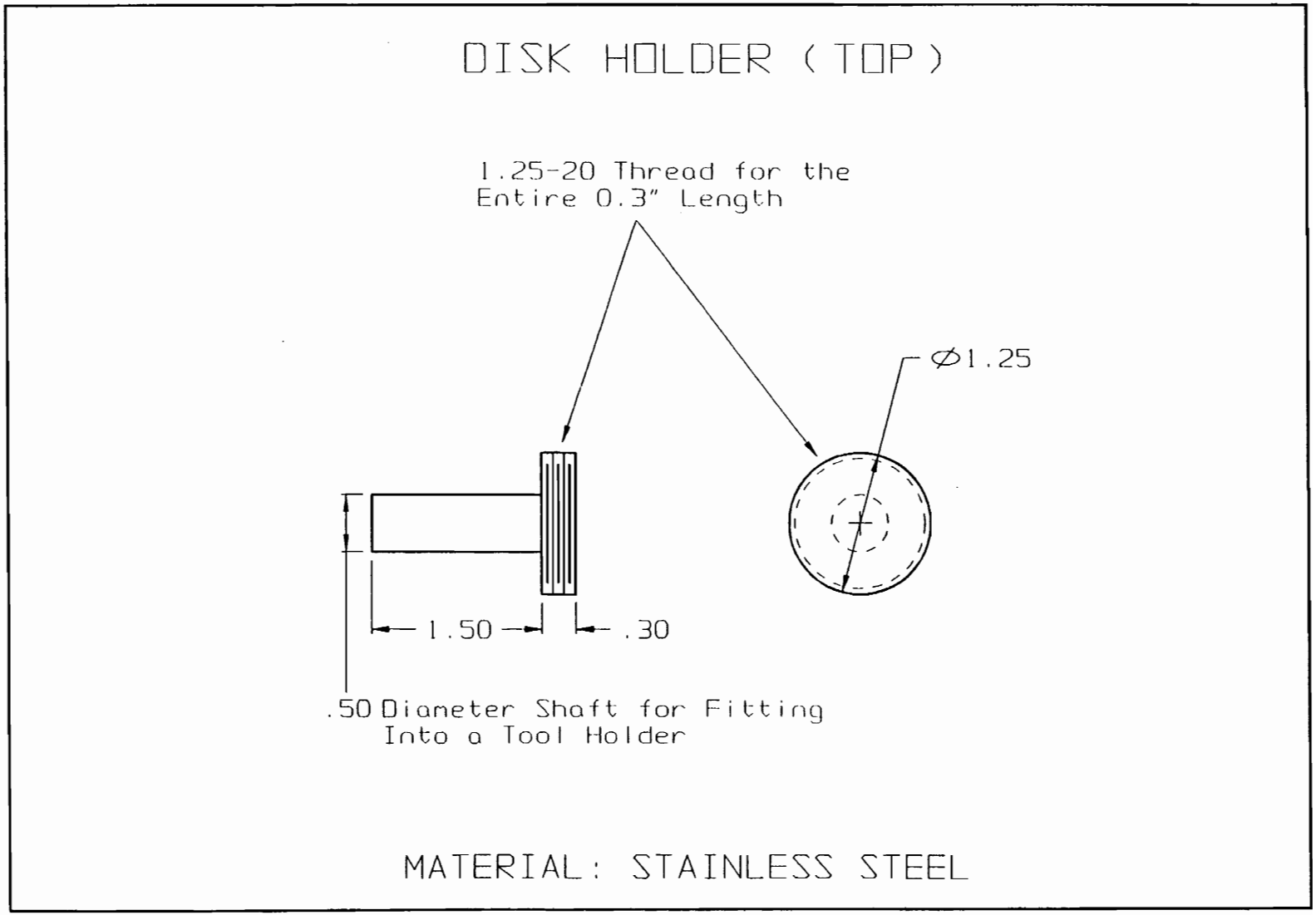

Figure 56 High Speed, High Load Pin-on-Disk Machine Disk Holder (Top)

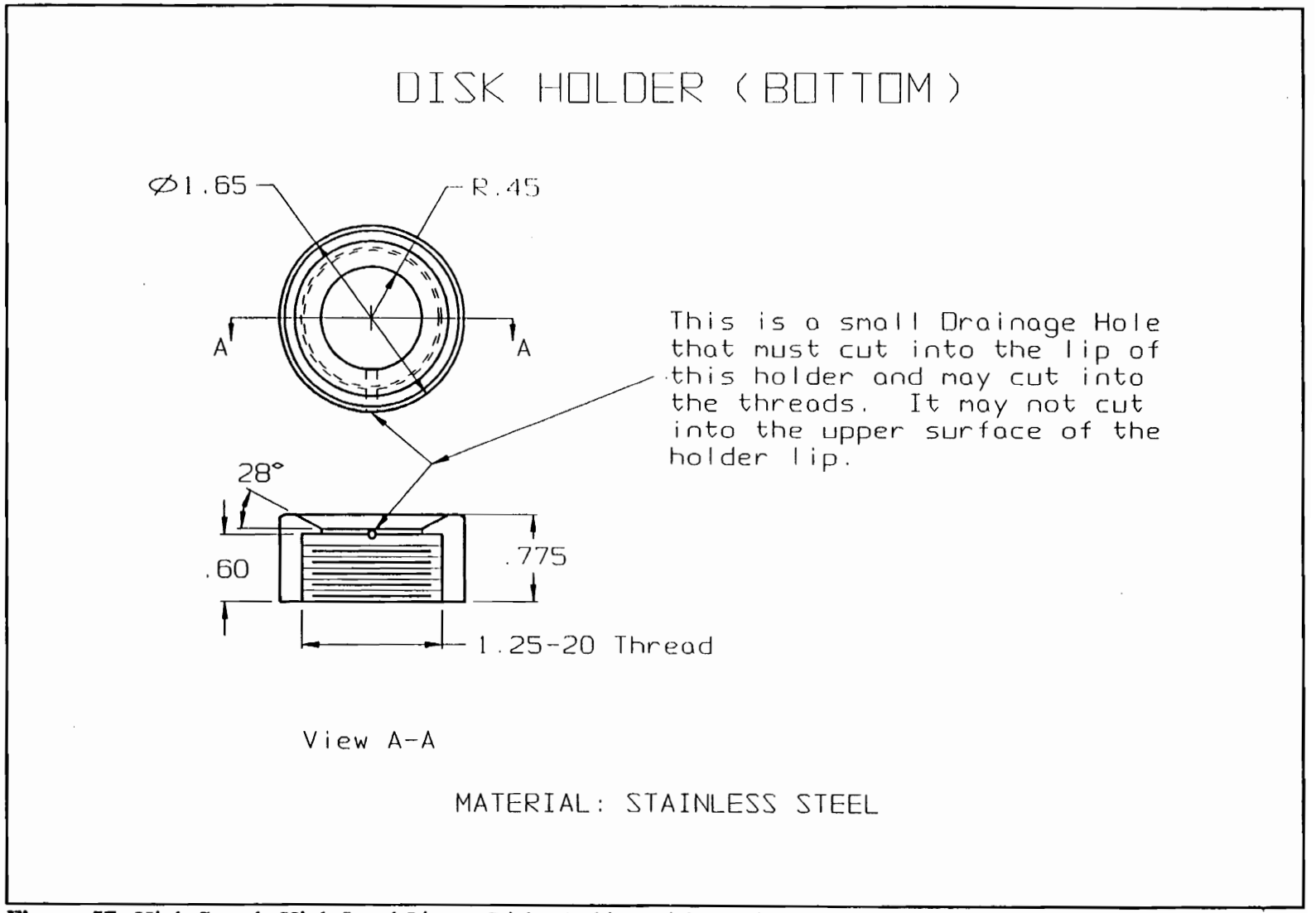

Figure 57 High Speed, High Load Pin-on-Disk Machine Disk Holder (Bottom)

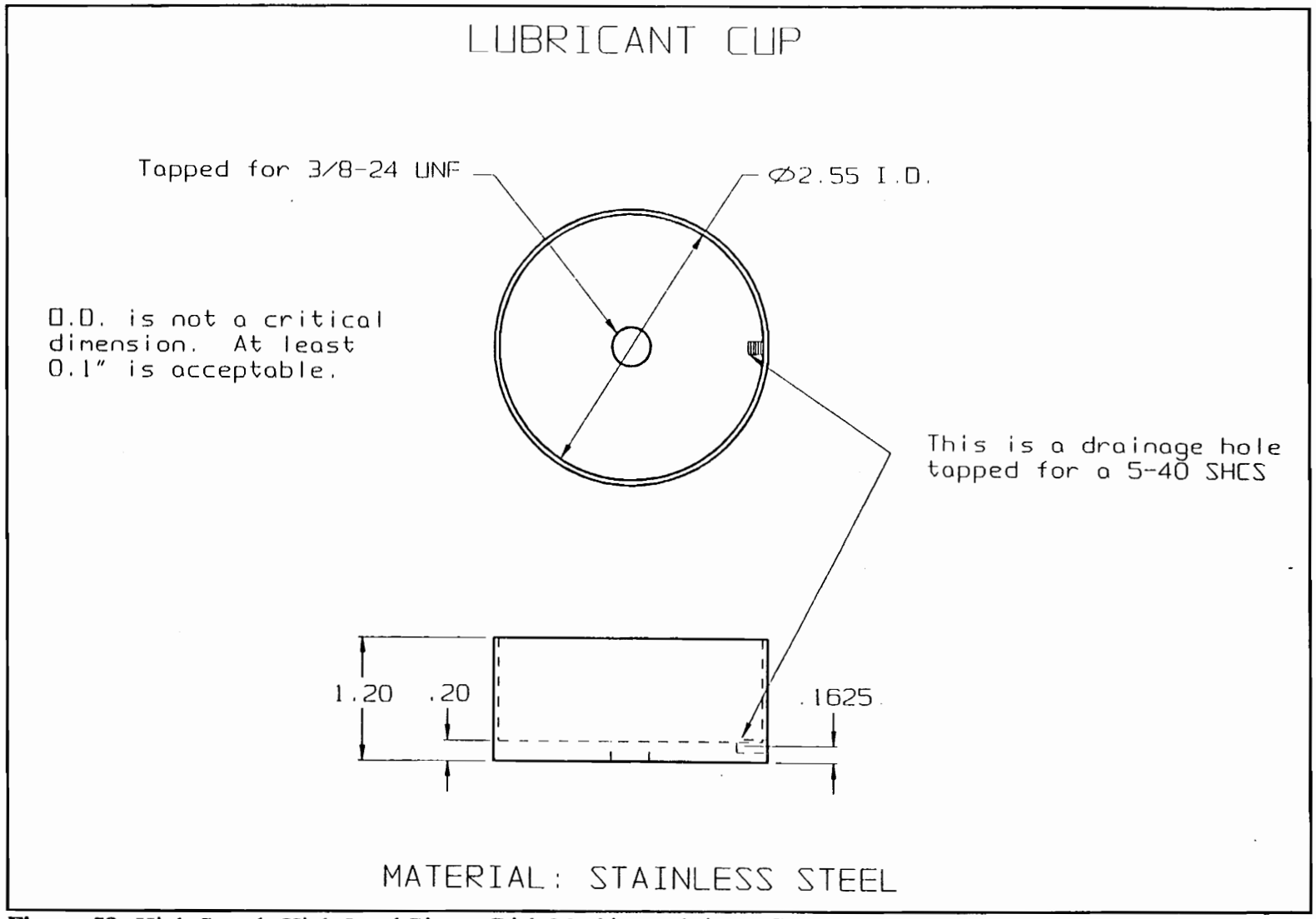

Figure 58 High Speed, High Load Pin-on-Disk Machine Lubricant Cup

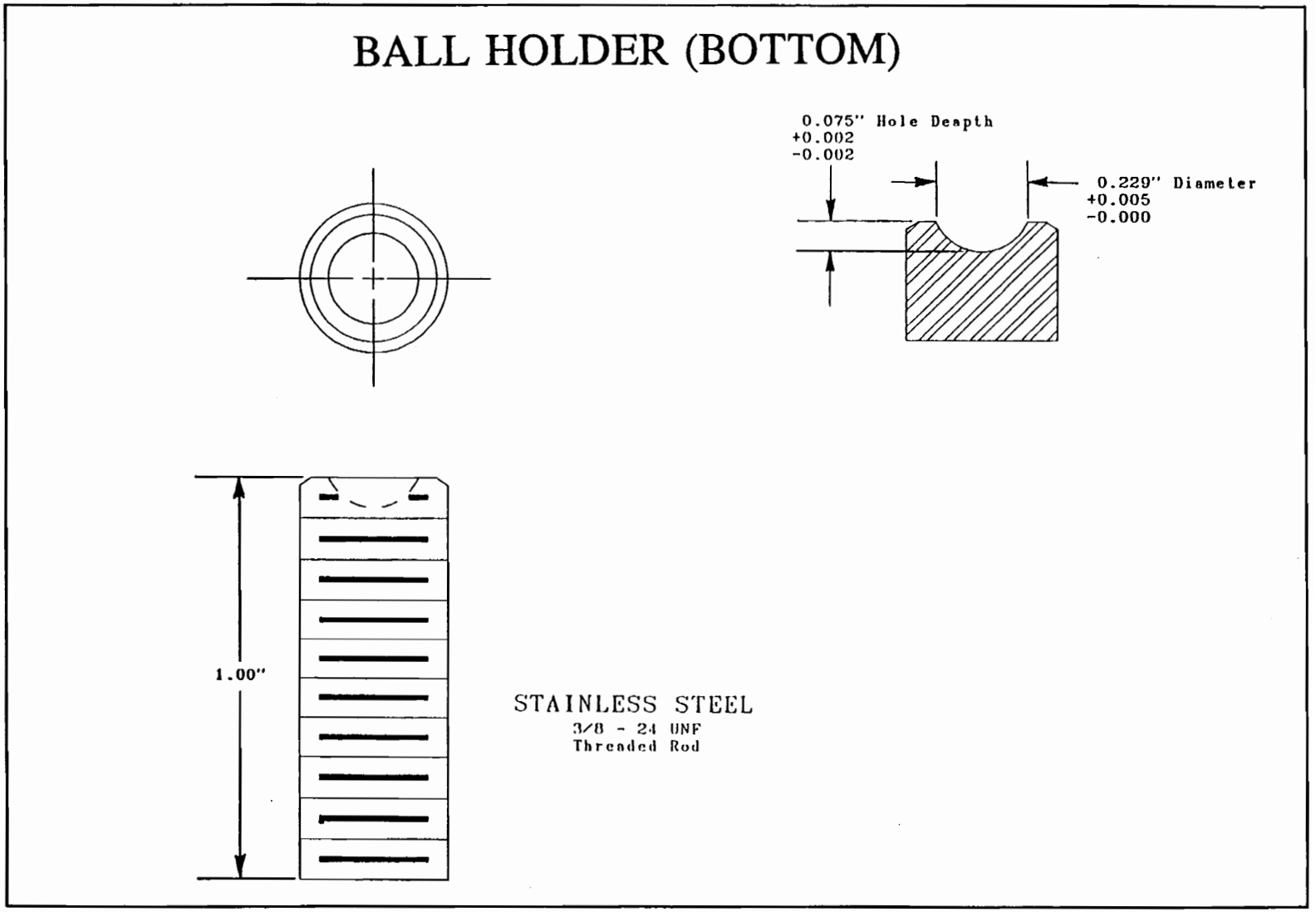

Figure 59 High Speed, High Load Pin-on-Disk Machine Ball Holder (Bottom)

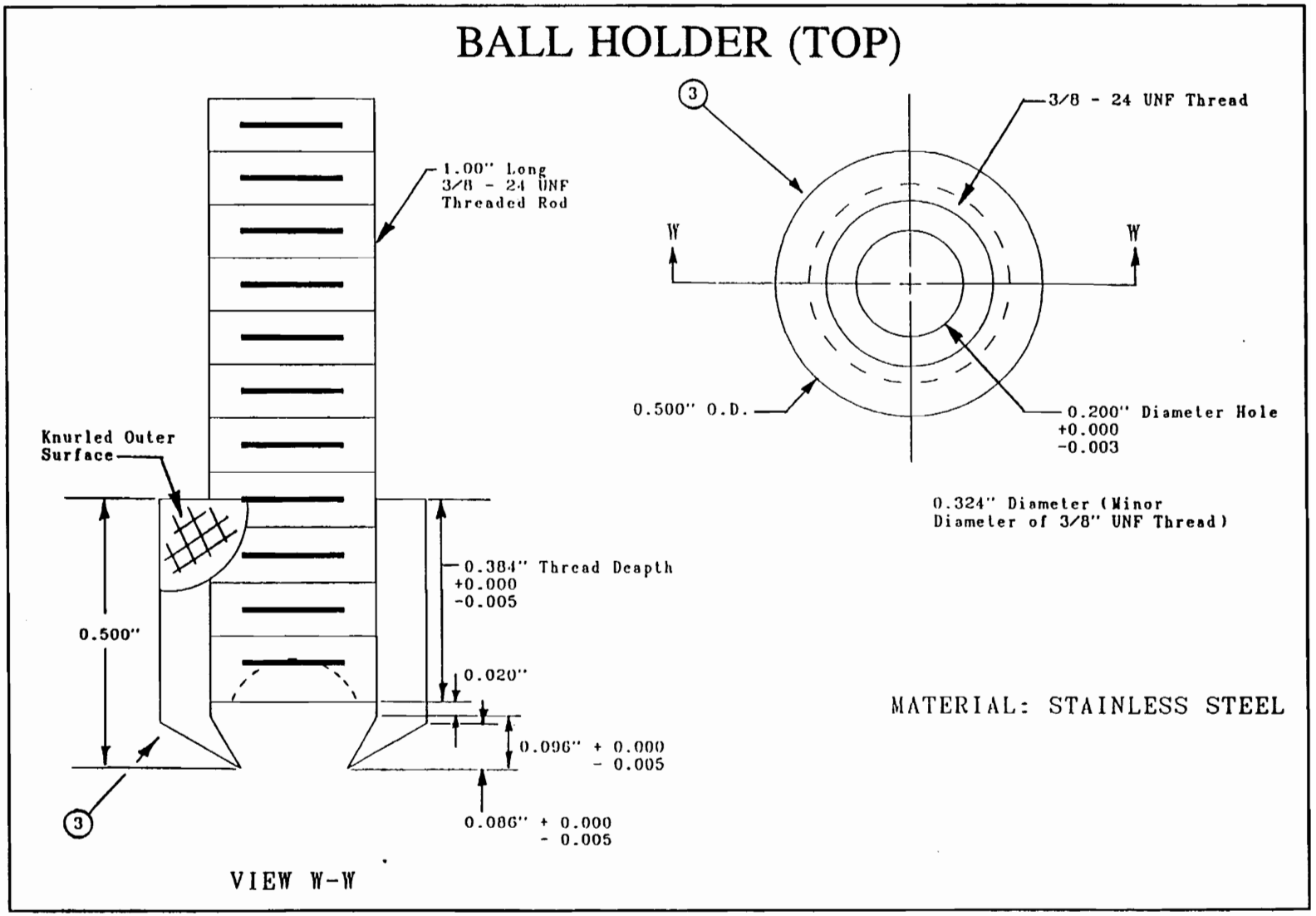

Figure 60 High Speed, High Load Pin-on-Disk Machine Ball Holder (Top)

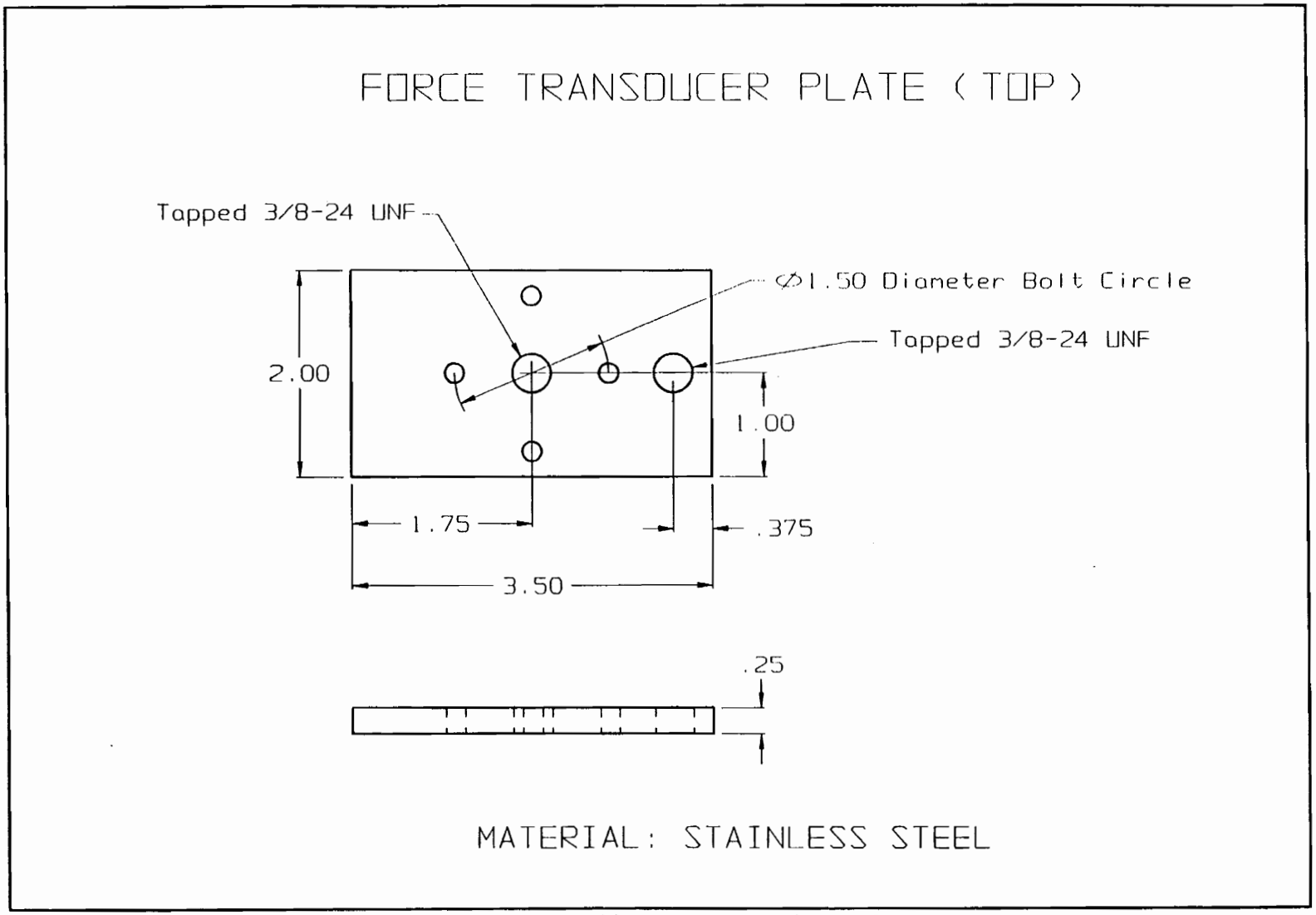

Figure 61 High Speed, High Load Pin-on-Disk Machine Force Transducer Plate (Top)

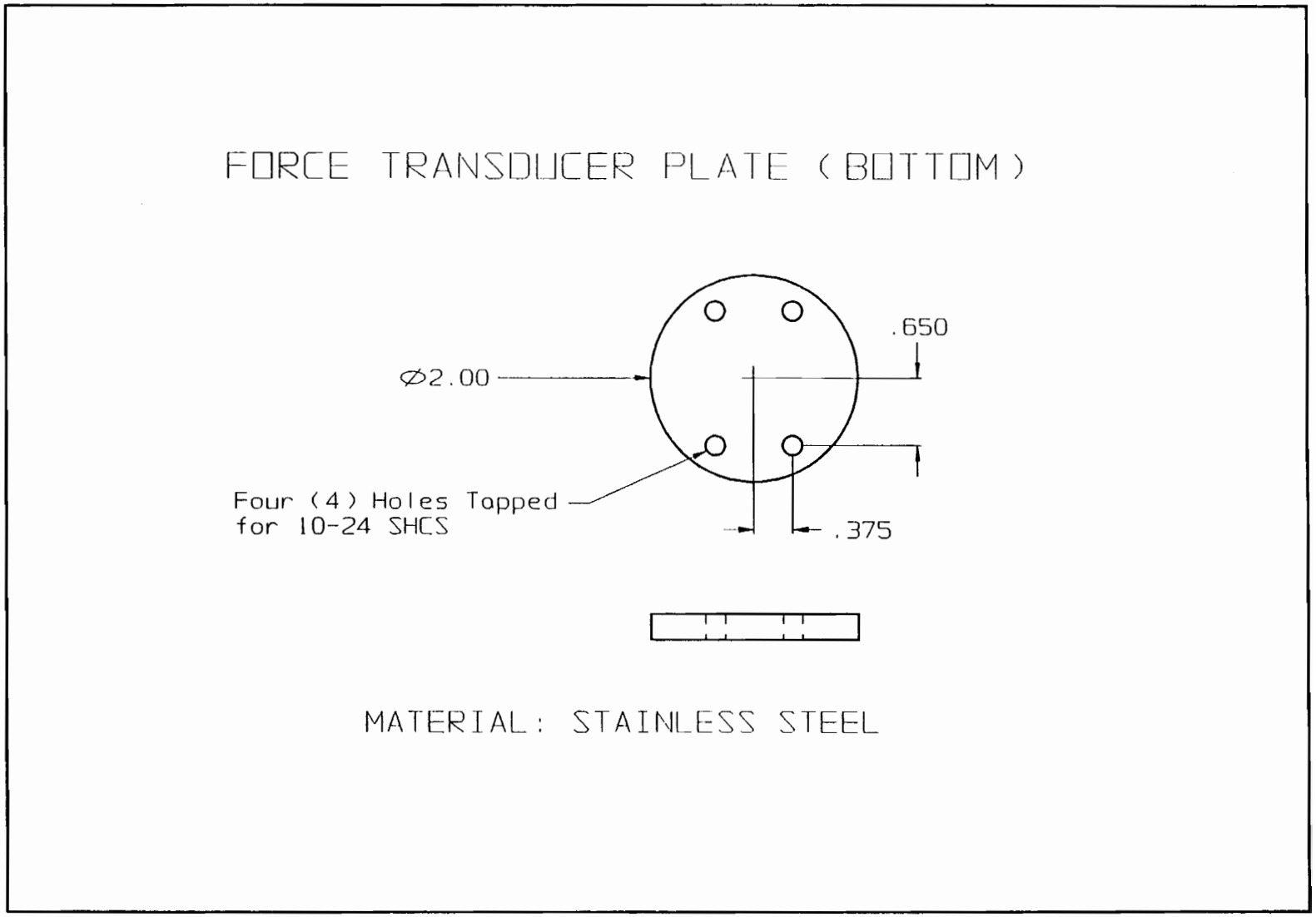

Figure 62 High Speed, High Load Pin-on-Disk Machine Force Transducer Plate (Bottom)

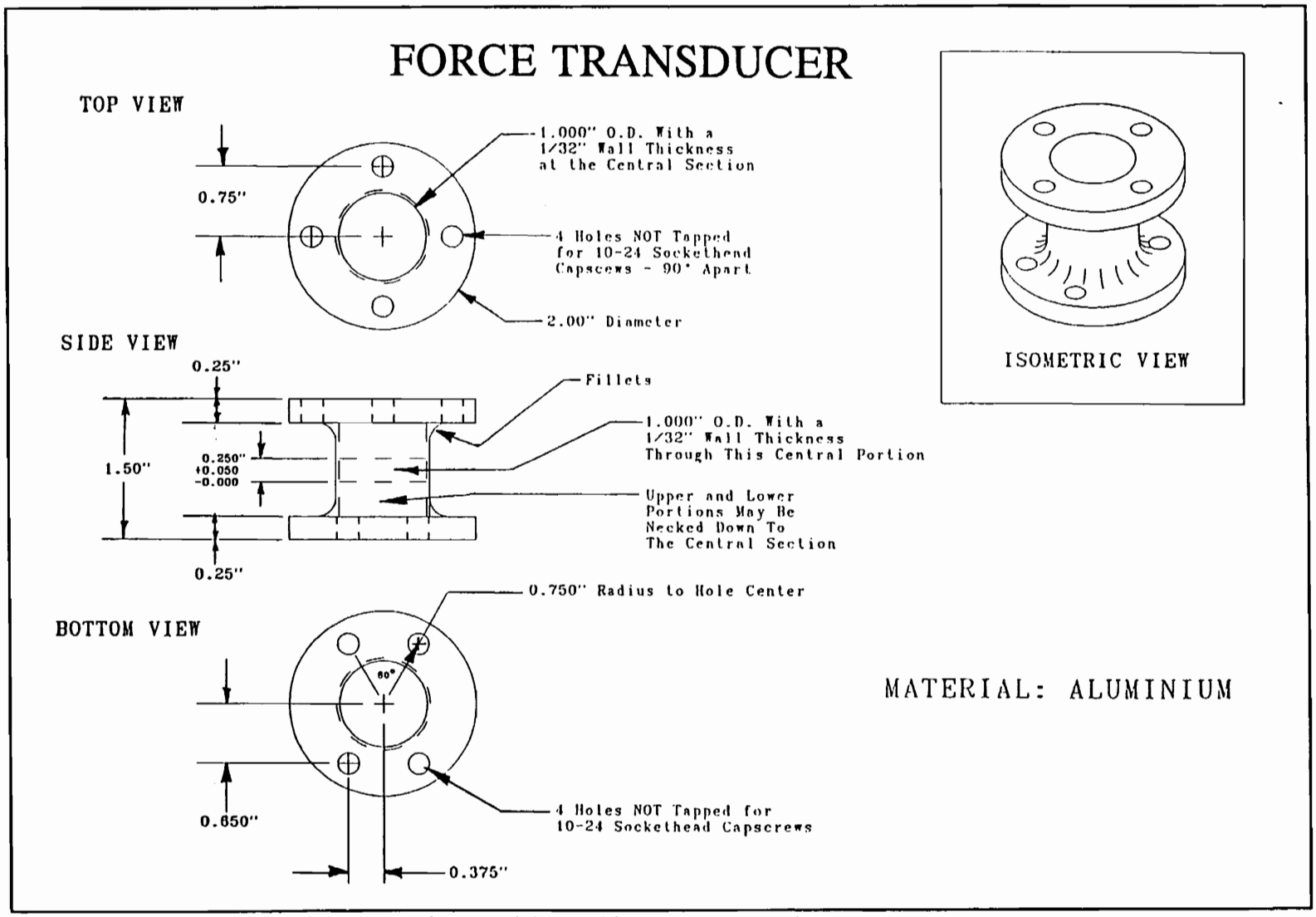

Figure 63 High Speed, High Load Pin-on-Disk Machine Force Transducer

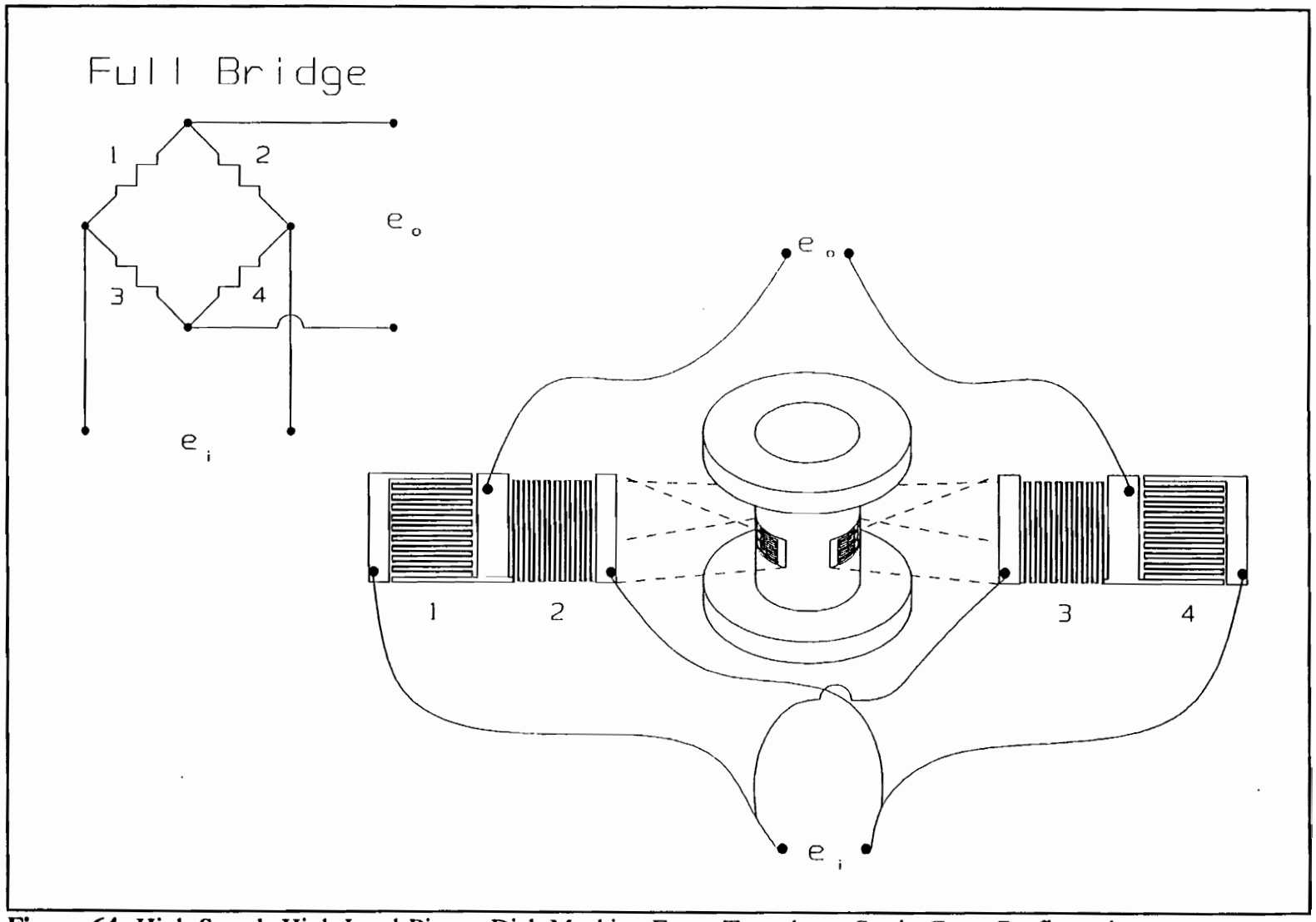

Figure 64 High Speed, High Load Pin-on-Disk Machine Force Transducer Strain Gage Configuration

GENERAL INFORMATION: N2A-SERIES STRAIN GAGES

GENERAL DESCRIPTION: N2A-Series gages are a family of constantan strain gages preferred for precision transducer applications within their normal operating range. The gage is open-faced construction on a tough, flexible polyimide backing.

TEMPERATURE RANGE: -100° to +200° F (-75° to +95° C) for precision static transducer service.

SELF-TEMPERATURE COMPENSATION: See data curve below.

STRAIN LIMITS: Approximately ±3%; should not exceed ±0.2% for precision transducer work.

FATIGUE LIFE: 10^7 cycles at ±1500μin/in (μm/m); 10^6 cycles at ±1700μin/in (μm/m); 10^5 cycles at ±3000μin/in (μm/m) for uni-directional tension or compression only. Longer gage lengths and lower resistances show greater endurance and less scatter in fatigue life.

CEMENTS: M-Bond 43-B or M-Bond 610 is recommended for N2A-Series gages in transducer service. M-Bond 600 also provides good performance. M-Bond 200 can be used for general-purpose applications. Refer to Micro-Measurements Catalog A-110 for information on bonding agents and Bulletin B-130 for installation procedures.

SOLDER: M-Line 361 (63-37) tin-lead solder is recommended for lead attachment. Refer to Micro-Measurements Catalog A-110 for further information on solders.

PROTECTIVE COATINGS: N2A-Series open-faced gages should always be protected with a suitable coating that is applied as soon as possible after gage installation. Refer to Micro-Measurements Catalog A-110 for information on Strain Gage Protective Coatings.

BACKING: The backing of N2A-Series gages has been specially treated for optimum bond formation with all appropriate strain gage adhesives. No further cleaning is necessary if contamination of the prepared surface is avoided during handling.

G028

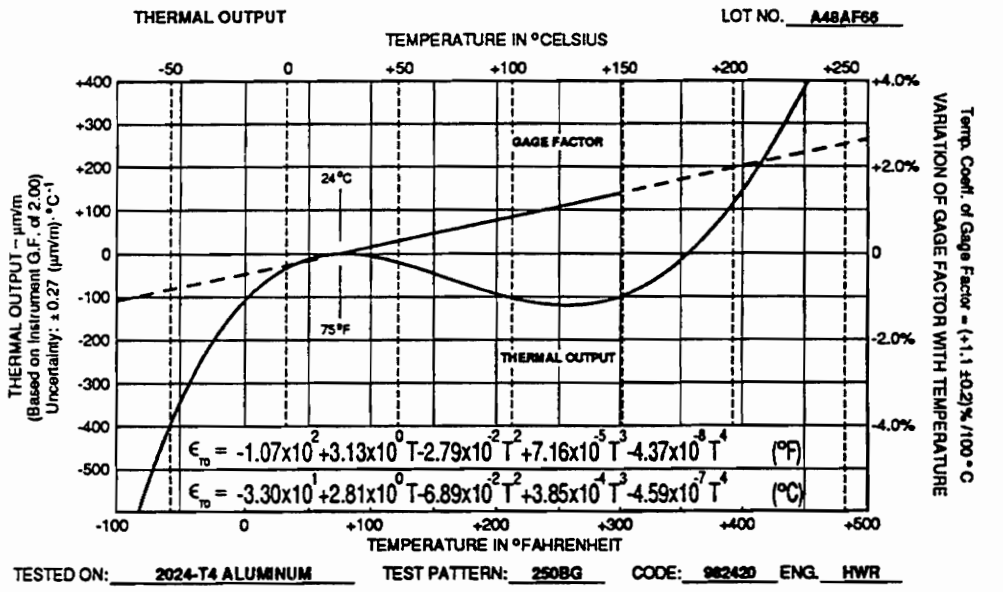

Figure 65 High Speed, High Load Pin-on-Disk Machine General Strain Gage Characteristics [Measurements Group, Incorporated - Gage Package]

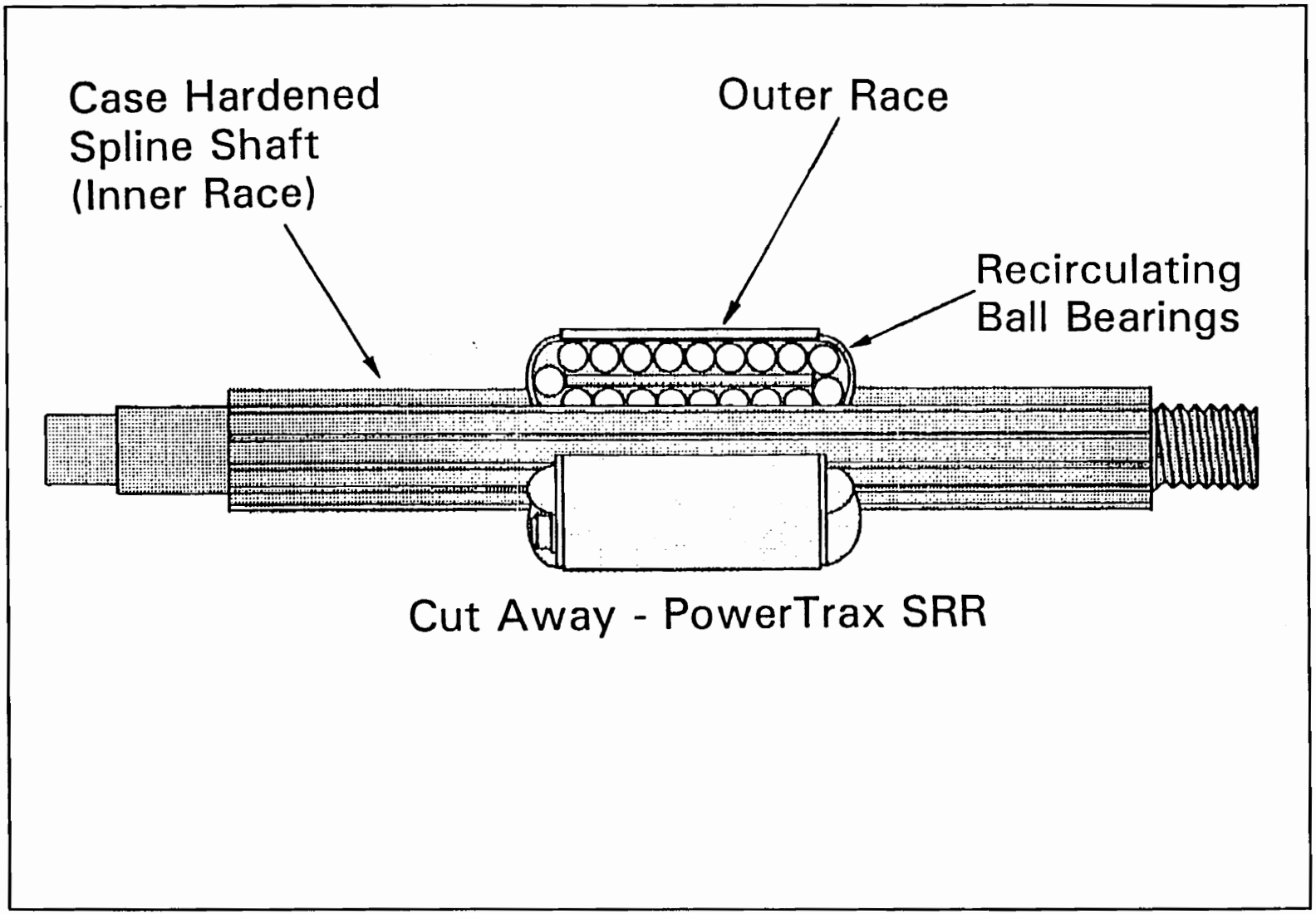

Figure 66 High Speed, High Load Pin-on-Disk Machine Nook Industries Ball Spline [Nook PowerTrax Catalogue]

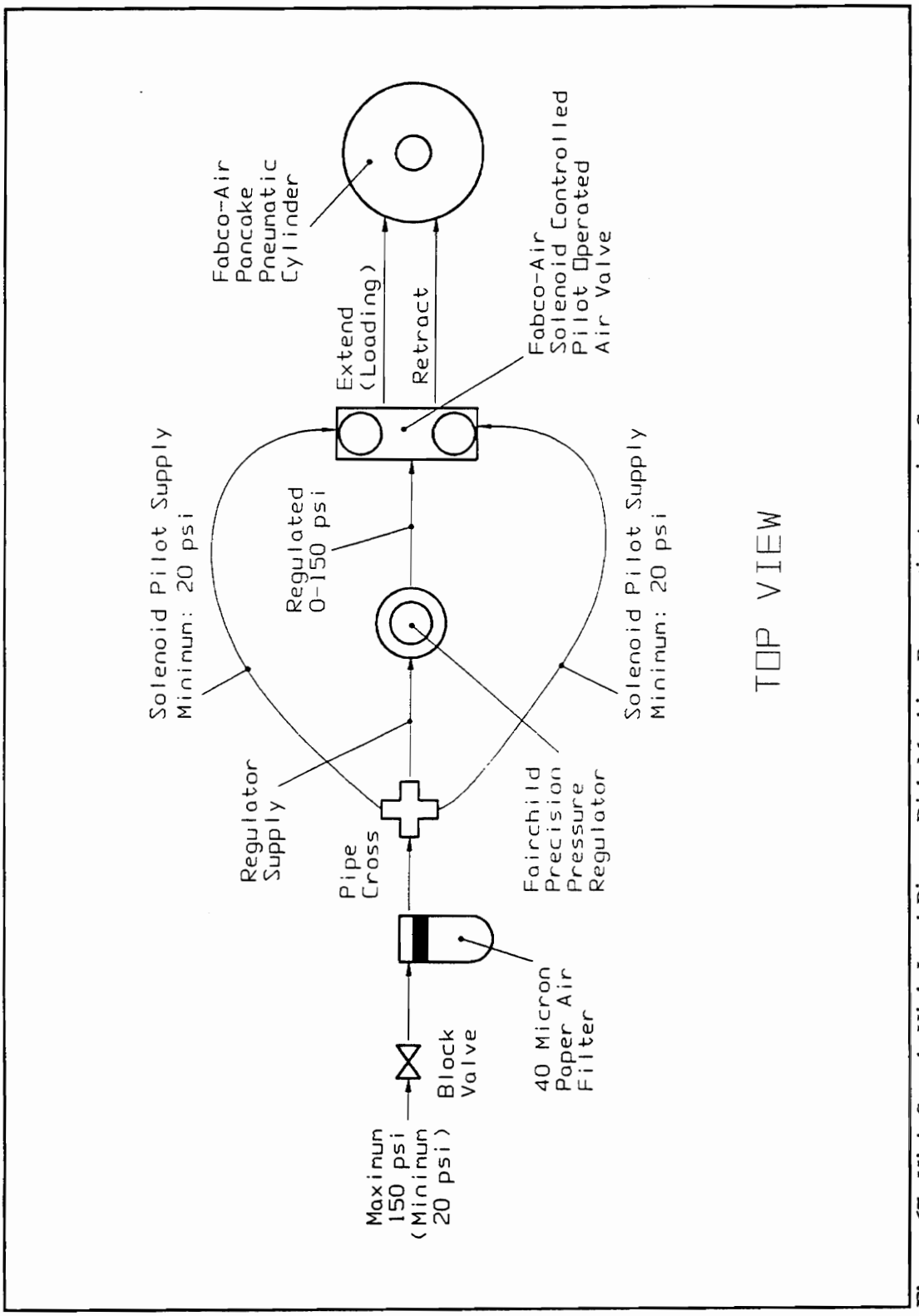

Figure 67 High Speed, High Load Pin-on-Disk Machine Pneumatic Actuation System

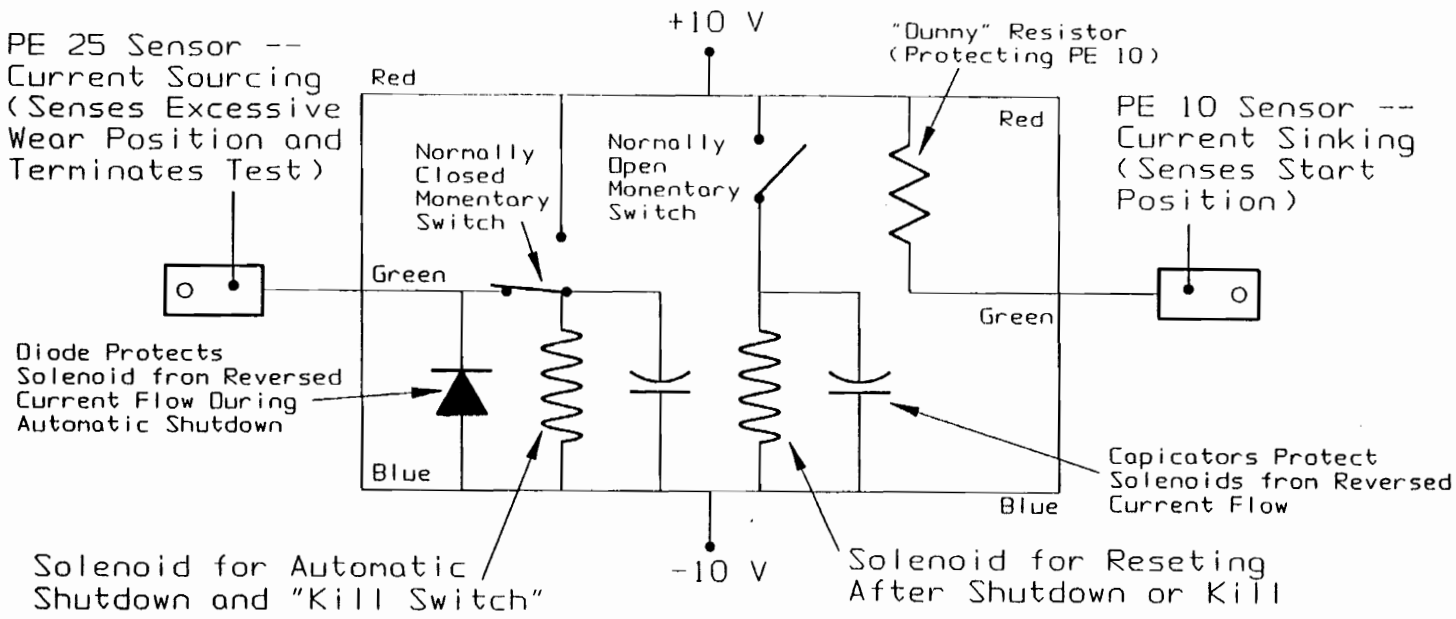

Figure 68 High Speed, High Load Pin-on-Disk Machine Automatic Shutdown and Control System Electronics

VITA

The author was born on July 27, 1970 in Marietta, Ohio to Mr. James Edward Smith and Mrs. Carolyn A. Hammer Smith. He received his Bachelor of Science degree with Honors in Mechanical Engineering from Virginia Polytechnic Institute and State University in July 1992. He began work toward the Master of Science degree in Mechanical Engineering at Virginia Polytechnic Institute and State University in August 1992. The author is actively seeking employment in an area where his new basic knowledge of tribology, polymers, and ceramics will serve him well.